THE
PHYSICAL REVIEW
A journal of experimental and theoretical physics established by E. L. Nichols in 1893

SECOND SERIES, VOL. 67, NOS. 5 AND 6 MARCH 1 AND 15, 1945

Neutron-Proton Scattering and the Meson Theory of Nuclear Forces

J. M. JAUCH
Palmer Physical Laboratory, Princeton University, Princeton, New Jersey
(Received November 6, 1944)

The angular dependence of the scattering of 14-Mev neutrons on protons is calculated with an interaction derived from Schwinger's mixed meson theory. The scattering shows a slight predominance for the backwards direction in the center of mass system. This result is in contradiction with the experimental results. The conclusion is drawn that the charge symmetrical theories cannot give the correct angular dependence of the scattering cross section.

1. INTRODUCTION

THE recent experiments by Amaldi and coworkers[1] on neutron-proton scattering indicate that for a neutron energy of 14 Mev the angular dependence of the scattered neutrons shows a marked preference for the scattering in the forward direction. It has already been pointed out by Wick[2] that an investigation of the angular distribution of the neutron-proton scattering will furnish a crucial test on the type of exchange forces. For the 14-Mev neutrons the angular dependence is mainly determined by the interaction in P states. In the so-called symmetrical meson theory, which makes use of both charged and neutral mesons in a symmetrical way, the potential is usually positive for P states, thus leading to a repulsive force. The symmetrical theory is the only existing satisfactory meson theory of nuclear forces which takes account of the existence of charged mesons in cosmic rays and the charge independence of nuclear forces.

A theoretical investigation of the angular dependence in the neutron-proton scattering has recently been published by Hulthén.[3] He uses for his calculations the interaction scheme proposed by Møller and Rosenfeld.[4] These authors use two different kinds of mesons, of spin zero and one, respectively, symmetrical with respect to the charge. The advantages of doing this are stated in the paper quoted above[4] and will not be repeated here. Møller and Rosenfeld chose the coupling constants of the two mesons with the nucleons equal, and as a consequence of this the tensor force vanishes. This is at variance with the known fact of the electric quadrupole moment of the deuteron. Attempts to explain this quadrupole moment with the non-static part of the forces have so far not met with success.[5] The result of Hulthén's calculations with this theory does not reproduce the experimentally observed angular dependence, the scattering being more backwards in this theory.

[1] Amaldi *et al.*, Naturwiss. **30**, 582 (1942); these results were recently confirmed by F. C. Champion and C. F. Powell, Proc. Roy. Soc. **183**, 64 (1944).
[2] G. Wick, Zeits. f. Physik **84**, 799 (1933).
[3] L. Hulthén, Arkiv. f. Mat. Astronom. Fys. **29**, No. 33 (1943); also B. Ferreti, Nuovo Cimento **XXI**, No. 1, 25 (1943).
[4] C. Møller and Rosenfeld, Kgl. Danske Vid. Sels. Math.-Fys. Medd. **XVII**, No. 8 (1940).
[5] C. Møller, Danske Vid. Sels. Math.-Fys. Medd. **XVIII**, No. 7 (1941).

The present investigation deals with the calculation of the angular dependence of the scattering with a modification of the Møller-Rosenfeld theory proposed by Schwinger.[6] In this theory we still have the two kinds of mesons, but the vector meson (spin one) is assumed to have a rest mass somewhat larger than that of the scalar meson (spin zero). This modification leads to a tensor force which has the correct sign in the static approximation (nucleons at rest). The question which we shall investigate in this paper is whether the tensor force modifies the scattering of 14-Mev electrons in such a way as to give the correct angular dependence.

A similar problem was treated recently by Rarita and Schwinger.[7] They use, however, square well potentials with range and depth so adjusted as to give correct values of deuteron binding energy and quadrupole moment. Their method for the calculation of the scattering is very convenient for the states of lowest value of the orbital angular momentum quantum number, but it becomes increasingly cumbersome for the higher states. We shall develop, therefore, the scattering theory with a tensor force in a more general way. It is to be expected that the result will not depend very much on the actual shape of the potential function. This expectation is borne out by the result of our calculation which differs very little from Rarita and Schwinger's result. In view of the importance of the conclusions which can be drawn from this result, it seemed to us worthwhile to carry out the numerical calculation for the meson potential of Schwinger's mixed theory.

For the numerical evaluation of the scattering cross section and the angular dependence, we use the values of the coupling constants and the masses of the two mesons which have been recently determined from the deuteron problem and the scattering of slow neutrons on protons.[8] These constants have been calculated from the theory in the so-called weak coupling approximation, where the force between nucleons is obtained as a first approximation of a development in rising powers of the coupling constant. Recently it has been doubted whether this is a sufficiently good approximation.[9] This doubt is justified if we use the extended source for the heavy particle in the interaction operator. In that case the condition for validity of the weak coupling theory is

$$(f\kappa)^2 \ll (a\kappa)^3,$$

where f is the coupling constant of the dimension of a length; κ is the reciprocal Compton wavelength of the meson; and a is the size of the source. Now from our determination of the coupling constant we find $(f\kappa)^2 \sim 0.05$, while $a\kappa \sim 0.1$, because the range of the nuclear forces should be determined by the mass and not by the size of the source. The perturbation treatment of the weak coupling theory is, therefore, hardly justified.

The situation is, however, quite different if we use the point source model together with the λ limiting process.[10] The condition for the validity of the perturbation treatment is then[11]

$$f\kappa \ll 1, \quad r \gg f$$

and we are well within the region of the weak coupling case.

2. THE NUCLEAR FORCES IN THE MIXED SYMMETRICAL THEORY

We consider two nuclear particles situated at positions $\mathbf{y}_1$ and $\mathbf{y}_2$ respectively. A pseudoscalar meson field ψ_α of mass κ and a vector field $\psi_{\alpha\nu}$ of mass μ will interact with these particles. The index α distinguishes the three components in isotopic spin space and ν is the vector index. The fields ψ_α and $\psi_{\alpha\nu}$ are Hermitian operators.

The Hamiltonian for the field plus the interaction term is then,

$$H = H_f + H_{\text{int}},$$

with,

$$H_f = \frac{1}{2}\sum_\alpha \int \{\pi_\alpha^2 + (\nabla\psi_\alpha)^2 + \kappa^2\psi_\alpha^2\} d^3x + \frac{1}{2}\sum_\alpha \int \left\{\pi_\alpha^2 + \frac{1}{\mu^2}(\nabla\cdot\pi_\alpha)^2 + (\nabla\times\psi_\alpha)^2 + \mu^2\psi_\alpha^2\right\} d^3x,$$

[6] J. Schwinger, Phys. Rev. **61**, 387 (1942).
[7] W. Rarita and J. Schwinger, Phys. Rev. **59**, 556 (1941), also C. Kittel and G. Breit, Phys. Rev. **56**, 744 (1939).
[8] J. M. Jauch and Ning Hu, Phys. Rev. **65**, 289 (1944).
[9] G. Wentzel, Helv. Phys. Acta **13**, 269 (1940); J. R. Oppenheimer and J. Schwinger, Phys. Rev. **60**, 150 (1940).
[10] P. A. M. Dirac, Inst. H. Poincaré Ann. **9**, 13 (1939); W. Pauli, Rev. Mod. Phys. **15**, 175 (1943).
[11] W. Pauli, Phys. Rev. **64**, 332 (1943).

$$H_{\text{int}}=(4\pi)^{\frac{1}{2}}f\sum_{\alpha,r}\tau_\alpha^{(r)}(\boldsymbol{\sigma}^{(r)}\cdot\nabla)\psi_\alpha(\mathbf{y}_r)$$
$$+4\pi f\sum_{\alpha,r}\tau_\alpha^{(r)}(\boldsymbol{\sigma}^{(r)}\cdot[\nabla\times\psi_\alpha(\mathbf{y}_r)])$$

where $\boldsymbol{\sigma}$ and τ_α are the operators of spin and isotopic spin.

The first-order term of the interaction between two nuclear particles situated at positions $\mathbf{y}_1$ and $\mathbf{y}_2$ is then,[12]

$$V_{\text{int}}=\tfrac{1}{3}f^2T\{\Lambda J+SK\},$$

with,

$$T=\sum_\alpha\tau_\alpha^{(1)}\tau_\alpha^{(2)}\quad S=3\Sigma-\Lambda,$$

$$\Lambda=\boldsymbol{\sigma}^{(1)}\cdot\boldsymbol{\sigma}^{(2)},$$

$$\Sigma=\frac{1}{r^2}(\boldsymbol{\sigma}^{(1)}\cdot\mathbf{y})(\boldsymbol{\sigma}^{(2)}\cdot\mathbf{y})\quad\mathbf{y}=\mathbf{y}_1-\mathbf{y}_2,$$

$$J=\kappa^2\frac{e^{-\kappa r}}{r}+2\mu^2\frac{e^{-\mu r}}{r}.$$

$$K=\frac{1}{r^3}\{(3+3\kappa r+\kappa^2r^2)e^{-\kappa r}-(3+3\mu r+\mu^2r^2)e^{-\mu r}\}.$$

The Schrödinger equation for the scattering problem is

$$-\frac{1}{M}\nabla^2\psi+V_{\text{int}}\psi=\epsilon\psi,\qquad(1)$$

where M is the mass of one nuclear particle[13] and ϵ is the energy in the center of mass system. The latter is half the energy in the laboratory system. The singularity of the function $K(r)$ near the origin is of the form $1/r$. The solutions of the two-body problem are, therefore, well behaved and form a complete orthonormal system.

3. THE MATRIX ELEMENTS OF THE TENSOR FORCE OPERATOR

The term in the interaction operator which contains the factor S is usually called the tensor force. Since the angular momentum operator $\mathbf{L}$ does not commute with S, it follows that the angular momentum is no longer an integral of motion. The total angular momentum

$$J=L+\tfrac{1}{2}(\boldsymbol{\sigma}^{(1)}+\boldsymbol{\sigma}^{(2)}),$$

however, is still an integral, since it commutes with S. It is, therefore, still possible to classify the states according to their total angular momentum quantum number J, defined by the eigenvalues of the operator $\mathbf{J}^2$:

$$\mathbf{J}^2=J(J+1).$$

In order to write down the eigenfunctions which belong to these eigenvalues J, we denote with $Y_l^m(\vartheta,\varphi)$ the normalized spherical harmonics and with u_1^m, u_0 the normalized spin functions for triplet and singlet states, respectively. The triplet and singlet functions which belong to a given value of J, normalized to unity, are then:

$$W_{J,J-1}^M=\frac{1}{[J(2J-1)]^{\frac{1}{2}}}\sum_{m+m'=M}C_{mm'}^J(J-1,1)Y_{J-1}^m u_1^{m'},$$
$$W_{J,J+1}^M=\frac{1}{[(J+1)(2J+3)]^{\frac{1}{2}}}\sum_{m+m'=M}C_{mm'}^J(J+1,1)Y_{J+1}^m u_1^{m'},\qquad(2)$$
$$W_{J,J}^M=\frac{1}{2[J(J+1)]^{\frac{1}{2}}}\sum_{m+m'=M}C_{mm'}^J(J,1)Y_J^m u_1^{m'},$$
$$V_J^M=Y_J^M u_0.$$

The coefficients $C_{mm'}(l,l')$ are the Clebsch-Gordon coefficients for the composition of two angular momenta l, l', to a resultant angular momentum J, which may assume the values $l+l'$, $l+l'-1$, $\cdots$, $|l-l'|$. They may be determined from group theoretical considerations alone. We do not give the explicit form of these coefficients.[14]

Since the operators Λ and Σ commute with the total angular momentum operator $\mathbf{J}$, these operators will have no matrix elements with respect

[12] For the derivation of this result cf. reference 4.

[13] We neglect the small difference between neutron and proton mass.

[14] Cf. B. L. van der Waerden, *Die gruppentheoretische Methode in der Quantenmechanik* (Springer, Berlin, 1932), p. 69 ff.

to states of different angular momentum. The four-dimensional submatrices of these operators in the space of the functions (W, V) belonging to a fixed value of J are easily evaluated by direct computation. A simplification is introduced by the fact that both the operators Λ and Σ commute with the permutation operator P, as well as with the total spin operator $\sigma^{(1)}+\sigma^{(2)}$. From these relations it follows immediately that the two functions $W_{J,J}$ and V are eigenfunctions of Λ and Σ. The other two functions, however, $W_{J,J-1}$ and $W_{J,J+1}$ are transformed into each other by the operator Σ. This is the characteristic property of the tensor force, which couples states of different orbital angular momentum, thus giving rise to the quadrupole moment in the deuteron ground state. The result of a straightforward calculation of these matrix elements may best be written in the matrix notation. If we order the states as indicated above [Eq. (2)], we find for these matrices

$$\Sigma=\begin{pmatrix} \frac{1}{2J+1} & \frac{2}{2J+1}[J(J+1)]^{\frac{1}{2}} & 0 & 0 \\ \frac{2}{2J+1}[J,J+1]^{\frac{1}{2}} & -\frac{1}{2J+1} & 0 & 0 \\ 0 & 0 & 1 & 0 \\ 0 & 0 & 0 & -1 \end{pmatrix},$$

$$\Lambda=\begin{pmatrix} 1 & 0 & 0 & 0 \\ 0 & 1 & 0 & 0 \\ 0 & 0 & 1 & 0 \\ 0 & 0 & 0 & -3 \end{pmatrix}.$$

The eigenvalues of Σ follow immediately from the relation $\Sigma^2=1$ and $tr\Sigma=0$. The first relation implies that the eigenvalues of Σ are all ± 1. From the second we find that the sum of these eigenvalues is zero and therefore both values occur as eigenvalues twice. The operator S for the tensor force is then in this notation

$$S=3\Sigma-\Lambda$$

$$=\begin{pmatrix} -2\frac{J-1}{2J+1} & \frac{6}{2J+1}[J(J+1)]^{\frac{1}{2}} & 0 & 0 \\ \frac{6}{2J+1}[J(J+1)]^{\frac{1}{2}} & -\frac{2(J+2)}{2J+1} & 0 & 0 \\ 0 & 0 & 2 & 0 \\ 0 & 0 & 0 & 0 \end{pmatrix}$$

and its eigenvalues are 2, 2, -4, 0. This follows from the fact that $\Sigma\Lambda=\Lambda\Sigma$ and Λ and Σ may therefore be transformed simultaneously into the diagonal form.

The matrices given above degenerate if $J=0$ since for this case $W_{J,J-1}=W_{J,J}=0$, as may be seen from an inspection of the Gordon coefficients. We are then left with the two states $^1S_0$ and $^3P_0$ only.

4. THE RADIAL EQUATIONS

We are now in a position to derive the radial differential equations. For that purpose it is necessary to remember that the functions (W, V) form an orthonormal set of functions in the space of the spin functions and on the surface of the unit sphere. If there were no coupling of the states through the tensor force, we would obtain for each value of $J>0$ four independent radial equations. With the tensor force, however, we find instead two equations and a coupled system of two equations. The number of independent solutions is of course four again, for each value of $J>0$, because the system allows two linearly independent solutions which satisfy the boundary conditions of the problem, which we distinguish by an index $+$ or $-$.

In order to write down the radial equations we need to know the value of the operator $T=\sum_\alpha \tau_\alpha^{(1)}\tau_\alpha^{(2)}$ for the different states. For the neutron-proton scattering problem we have a system that consists of a neutron and a proton. Such a system may be either in a triplet or a singlet state in isotopic spin space, for which T has the eigenvalues $+1$ and -3, respectively. The system as a whole, including space, spin, and isotopic spin degrees of freedom, must be in an antisymmetrical state according to the exclusion principle. Since the singlet states are symmetrical and the triplets antisymmetrical it follows that

$$T=\begin{cases} -1+2(-1)^l & \text{for singlet} \\ -1-2(-1)^l & \text{for triplet} \end{cases} \Big\} \text{states in spin space.}$$

The complete solution may be written in the form $\frac{1}{r}\omega_{J,S}^{M}, \frac{1}{r}\chi_J^M$ with

$$\begin{aligned} \omega_{J,\pm}^{M} &= a_\pm(r)W_{J,J-1}^{M}+b_\pm(r)W_{J,J+1}^{M}, \\ \omega_{J,0}^{M} &= c(r)W_{J,J}^{M}, \\ \chi_J^M &= d(r)V_J^M. \end{aligned} \tag{3}$$

Inserting these expressions into the Schrödinger equation (1) and using the matrix form of S we find, by equating the coefficients of each W and V to zero, the following radial equations for the functions a, b, c and d.

$$a''-\frac{J(J-1)}{r^2}a+(1+2(-1)^{J-1})\frac{Mf^2}{3}\left[Ja+K\left(-\frac{2(J-1)}{2J+1}a+\frac{6}{2J+1}[J(J+1)]^{\frac{1}{2}}b\right)\right]+k^2a=0,$$

$$b''-\frac{(J+1)(J+2)}{r^2}b+(1+2(-1)^{J+1})\frac{Mf^2}{3}\left[Jb+K\left(\frac{6}{2J+1}[J(J+1)]^{\frac{1}{2}}a-\frac{2(J+2)}{2J+1}b\right)\right]+k^2b=0, \quad (4)$$

$$c''-\frac{J(J+1)}{r^2}c+(1+2(-1)^{J})\frac{Mf^2}{3}[J+2K]c+k^2c=0,$$

$$d''-\frac{J(J+1)}{r^2}d-(1-2(-1)^{J})Mf^2Jd+k^2d=0.$$

In these equations we have introduced the wave number $k'=(M\epsilon)^{\frac{1}{2}}$. Some special cases are of interest for our problem. We write them down explicitly:

(a) Triplet States

$$\begin{aligned}
&{}^3S_1+{}^3D_1: && a''+Mf^2Ja+2\sqrt{2}Mf^2Kb+k^2a=0,\\
&&& b''-\frac{6}{r^2}b+Mf^2(J-2K)b+2\sqrt{2}Mf^2Ka+k^2b=0,\\
&{}^3P_0: && b''-\frac{2}{r^2}b-\frac{Mf^2}{3}[J-4K]b+k^2b=0,\\
&{}^3P_1: && c''-\frac{2}{r^2}c-\frac{Mf^2}{3}[J+2K]c+k^2c=0, \quad (5)\\
&{}^3P_2+{}^3F_2: && a''-\frac{2}{r^2}a-\frac{Mf^2}{3}\left[Ja+K\left(-\frac{2}{5}a+\frac{6\sqrt{6}}{5}b\right)\right]+k^2a=0,\\
&&& b''-\frac{12}{r^2}b-\frac{Mf^2}{3}\left[Jb+K\left(\frac{6\sqrt{6}}{5}a-\frac{8}{5}b\right)\right]+k^2b=0.
\end{aligned}$$

(b) Singlet States

$$\begin{aligned}
&{}^1S_0: && d''+Mf^2Jd+k^2d=0,\\
&{}^1P_1: && d''-\frac{2}{r^2}d-3Mf^2Jd+k^2d=0, \quad (6)\\
&{}^1D_2: && d''-\frac{6}{r^2}d+Mf^2Jd+k^2d=0.
\end{aligned}$$

5. THE SCATTERING PROBLEM

The asymptotic behavior of the solutions of these equations determines the scattering cross section. In order to determine the connection between this cross section and the phase shifts at infinity we write down first the asymptotic form of the stationary state wave function appropriate for the scattering problem.

$$\psi_1{}^m\sim e^{ikz}u_1{}^m+\sum_{m'}f_{mm'}(\vartheta)u_1{}^{m'}\frac{e^{ikr}}{r} \quad (7)$$

for triplet states and

$$\psi\sim e^{ikz}u_0+f(\theta)u_0\frac{e^{ikr}}{r} \quad (8)$$

for singlet states.

The differential scattering cross section is obtained by averaging the square of the amplitude of the scattered wave over the most general linear superposition of these four states.

$$\sigma(\theta)=|\sum_{m,m'}\lambda_1{}^mf_{mm'}u_1{}^{m'}+\lambda_0fu_0|_{Av}=\tfrac{1}{4}\{\sum_{m,m'}|f_{mm'}|^2+|f|^2\}. \quad (9)$$

The next step is to find the connection of the phase shifts at infinity with the quantities f, $f_{mm'}$. Let the functions at infinity be denoted with

$$a_{J,\pm}=(2/\pi)^{\frac{1}{2}}\alpha_{J,\pm}\sin\left(kr-\frac{J-1}{2}\pi+\xi_{J,\pm}\right),$$

$$b_{J,\pm}=(2/\pi)^{\frac{1}{2}}\beta_{J,\pm}\sin\left(kr-\frac{J+1}{2}\pi+\eta_{J,\pm}\right),$$

$$c_J=(2/\pi)^{\frac{1}{2}}\sin\left(kr-\frac{J}{2}\pi+\zeta_J\right),$$

$$d_J=(2/\pi)^{\frac{1}{2}}\sin\left(kr-\frac{J}{2}\pi+\delta_J\right).$$

This notation is convenient because in the absence of any interaction we have $\xi=\eta=\zeta=\delta=0$. We distinguish the two linearly independent but otherwise arbitrary solutions for the system with the index $+$ or $-$.

It is clear that, because of the linear independence of triplet and singlet spin functions, the amplitude f depends only on the phase shifts δ_J of the singlet states, while $f_{mm'}$ depends on the phases ξ_J, η_J, ζ_J of the triplet states. The connection between f and δ_J is given by the ordinary scattering theory of Faxén and Holtsmark and does not need to be derived here:[15]

$$f=\frac{1}{2ik}\sum_J (2J+1)^{iJ}(e^{2i\delta_J}-1)P_J(\cos\vartheta) \quad (10)$$

where $P_J(x)$ are the Legendre polynomials of order J.

In order to derive the connection between $f_{mm'}$ and the phase shifts ξ, η, ζ, we write the solution for triplet states as a linear combination of the solutions (3).

$$\psi_1{}^M=\frac{1}{kr}\sum_{J,S} {}^MC_{J,S}\overset{M}{\omega}_{J,S}$$
$$=e^{ikz}u_1{}^M+\text{scattered wave.} \quad (11)$$

The plane wave part will be a superposition of solutions of the force-free equation for which we have

$$\overset{0M}{\omega}_{J,-}=(kr)^{\frac{1}{2}}J_{J-1/2}(kr)W_{J,J-1},$$
$$\overset{0M}{\omega}_{J,+}=(kr)^{\frac{1}{2}}J_{J+3/2}(kr)W_{J,J+1},$$
$$\overset{0M}{\omega}_{J,0}=(kr)^{\frac{1}{2}}J_{J+1/2}(kr)W_{J,J},$$

$$e^{ikz}u_1{}^M=\frac{1}{kr}\sum_{J,S} {}^MB_{J,S}\overset{0M}{\omega}_{J,S}.$$

The coefficients in this series may be evaluated in terms of the well known series[15]

$$e^{ikz}u_1{}^M=\sum A_J Y_J{}^0(\vartheta,\varphi)\frac{1}{\sqrt{kr}}J_{J+1/2}(kr)u_1{}^M,$$

$$A_J=2\pi i^J(2J+1)^{\frac{1}{2}},$$

by identifying the coefficients of the linearly independent functions $Y_J{}^0(1/(ur)^{\frac{1}{2}})J_{J+1}(kr)u_1{}^M$. For each value of J and M we obtain then a set of three linear equations for the three unknown coefficients ${}^MB_{J+1,-}$, ${}^MB_{J-1,+}$, ${}^MB_{J,0}$ which may be expressed in terms of the A_J. The result of a straightforward calculation along these lines is the following:

$${}^{-1}B_{J,-}=\left[\frac{J+1}{2(2J-1)}\right]^{\frac{1}{2}}A_{J-1},$$
$${}^{-1}B_{J,+}=\left[\frac{J}{2(2J+3)}\right]^{\frac{1}{2}}A_{J+1},$$
$${}^{-1}B_{J,0}=A_J,$$
$${}^{+1}B_{J,-}=\left[\frac{J+1}{2(2J-1)}\right]^{\frac{1}{2}}A_{J-1},$$
$${}^{+1}B_{J,+}=\left[\frac{J}{2(2J+3)}\right]^{\frac{1}{2}}A_{J+1},$$
$${}^{+1}B_{J,0}=-A_J,$$
$${}^{0}B_{J,-}=\left[\frac{J}{2J-1}\right]^{\frac{1}{2}}A_{J-1},$$
$${}^{0}B_{J,+}=\left[\frac{J+1}{2J+3}\right]^{\frac{1}{2}}A_{J+1},$$
$${}^{0}B_{J,0}=0.$$

From the condition that the scattered wave contains only outgoing spherical waves, we obtain

$$\sum_{J,S}({}^MC_{J,S}\overset{M}{\omega}_{J,S}-{}^MB_{J,S}\overset{0M}{\omega}_{J,S})\sim\sum_{M'} f_{MM'}u_1{}^{M'}\frac{e^{ikr}}{r}. \quad (12)$$

In order to get the expression for ${}^MC_{J,S}$ into a convenient form, we write by suppressing the indices J and M

$$\begin{aligned} C_+\alpha_+e^{-i\xi+}+C_-\alpha_-e^{-i\xi-}&=C\alpha e^{-i\xi},\\ C_+\beta_+e^{-i\eta+}+C_-\beta_-e^{-i\eta-}&=C\beta e^{-i\eta},\\ C_+\alpha_+e^{i\xi+}+C_-\alpha_-e^{i\xi-}&=C\alpha e^{i\xi},\\ C_+\beta_+e^{i\eta+}+C_-\beta_-e^{i\eta-}&=C\beta e^{i\eta}, \end{aligned} \quad (13)$$

or shorter

$$C_+\omega_++C_-\omega_-=C\omega\equiv C(aW_{J,J-1}+bW_{J,J+1}),$$

where a and b behave asymptotically like

$$a\sim(2/\pi)^{\frac{1}{2}}\alpha\sin\left(kr-\frac{J-1}{2}\pi+\xi\right),$$

$$b\sim(2/\pi)^{\frac{1}{2}}\beta\sin\left(kr-\frac{J+1}{2}\pi+\eta\right).$$

[15] Cf. N. F. Mott and H. S. W. Massey, *Theory of Atomic Collisions* (Oxford University Press, 1933).

Taking suitable linear combinations of the Eqs. (13), we have

$$C_+\alpha_+ \sin\xi_+ + C_-\alpha_- \sin\xi_- = C\alpha \sin\xi,$$
$$C_+\alpha_+ \cos\xi_+ + C_-\alpha_- \cos\xi_- = C\alpha \cos\xi,$$
$$C_+\beta_+ \sin\eta_+ + C_-\beta_- \sin\eta_- = C\beta \sin\eta,$$
$$C_+\beta_+ \cos\eta_+ + C_-\beta_- \cos\eta_- = C\beta \cos\eta.$$

From this we get

$$\operatorname{tg}\xi = \frac{\alpha_+ \sin\xi_+ + \lambda\alpha_- \sin\xi_-}{\alpha_+ \cos\xi_+ + \lambda\alpha_- \cos\xi_-},$$
$$\lambda = \frac{C_-}{C_+} \qquad (14)$$
$$\operatorname{tg}\eta = \frac{\beta_+ \sin\eta_+ + \lambda\beta_- \sin\eta_-}{\beta_+ \cos\eta_+ + \lambda\beta_- \cos\eta_-}.$$

These formulae enable us to calculate ξ and η for each value of J, M in terms of ξ_+, ξ_-, η_+, η_-, α_+, α_-, β_+, β_- and $\lambda = C_-/C_+$. The phases and amplitudes are determined from the integration of the systems of Eqs. (4). The only quantity which is not yet determined is λ. In order to find λ we must make use of the boundary condition (7), which requires that the scattered wave contains only outgoing waves. If we put the coefficients of the incoming waves in (2) equal to zero, we obtain for each value of J and M three equations of the form

$$\alpha C e^{-i\xi} = B_-,$$
$$\beta C e^{-i\eta} = B_+, \qquad (15)$$
$$C_0 e^{-i\xi} = B_0.$$

The first two of these equations are only compatible if

$$\sigma = \frac{B_-}{B_+} = \frac{\alpha}{\beta} e^{i(\eta-\xi)} = \frac{\alpha_+ e^{-i\xi_+} + \lambda\alpha_- e^{-i\xi_-}}{\beta_+ e^{-i\eta_+} + \lambda\beta_- e^{-i\eta_-}}.$$

Solving this equation for λ we obtain

$$\lambda = -\frac{\alpha_+ e^{-i\xi_+} - \sigma\beta_+ e^{-i\eta_+}}{\alpha_- e^{-i\xi_-} - \sigma\beta_- e^{-i\eta_-}}. \qquad (16)$$

For each value of J and M we can therefore determine λ from (16) and then ξ and η with the help of (14). Inserting the values of (15) for C and C_0 in the expression (12) we find for the coefficients of the outgoing spherical waves

$${}^M R_{J,-} = (2/\pi)^{\frac{1}{2}}(e^{2i\xi_J{}^M} - 1)e^{-i(J-1/2)\pi}\, {}^M B_{J,-},$$
$${}^M R_{J,+} = (2/\pi)^{\frac{1}{2}}(e^{2i\eta_J{}^M} - 1)e^{-i(J+1/2)\pi}\, {}^M B_{J,+},$$
$${}^M R_{J,0} = (2/\pi)^{\frac{1}{2}}(e^{2i\xi_J} - 1)e^{-i(J/2)\pi}\, {}^M B_{J,0}$$

Finally we obtain for the scattering matrix $f_{MM'}$ from (7) and (2)

$$f_{MM'} = \frac{1}{2ik}\sum_J \left\{ {}^M R_{J,-} \frac{1}{[J_1(2J-1)]^{\frac{1}{2}}} C^J_{M-M',M}(J-1,1)\, Y^{M-M'}_{J-1} \right.$$
$$\left. + \frac{1}{[(J+1)(2J+3)]^{\frac{1}{2}}} {}^M R_{J,+} C^J_{M-M',M'}(J+1,1)\, Y^{M-M'}_{J+1} + \frac{1}{[(J+1)J]^{\frac{1}{2}}} {}^M R_{J,0} C^J_{M-M',M'}(J,1)\, Y^{M-M'}_J \right\}. \qquad (17)$$

Inserting this expression in the formula (9) gives the desired connection between the scattering cross section and the phase shifts.

6. NUMERICAL EVALUATION

For the numerical computation of the phase shifts we must integrate the Eqs. (5) and (6) for triplet and singlet states. The following procedure was adopted: the equations were first made dimensionless by introducing the new variable $x = \kappa r$. The functions $j(x) = \lambda J$, $k(x) = \lambda K$, with $\lambda = (M/\kappa)(\kappa f)^2 = 0.532$ were then[8] calculated and tabulated. The energy E was assumed to be 14 Mev which gives for $k/\kappa = 0.6165$. The differential equation was then replaced by a difference equation with the differences in x chosen sufficiently small so as to keep the error in the final result of the order of five percent at most. It was found that a difference in x of $\Delta x = x_n - x_{n-1} = 0.2$ was sufficient for this accuracy. This was tested by carrying out sample integrations with the difference $\Delta x = 0.1$. The deviation from the result for $\Delta x = 0.2$ was taken as an approximate value of the error. This test was used both for an ordinary equation and a system. The integration was then carried out from $x = 0$ to $x = 4$. At $x = 4$ the potential functions are very small, less than $\frac{1}{10}$ percent of the value at $x = 1$. We have therefore neglected the potential functions for values of $x > 4$. The solutions for the region $4 < x < \infty$ are then the known functions of the force-free case. These functions are then pieced together at the

point $x=4$ with the solutions obtained from the numerical integration of the differential equation in such a way that the function itself, as well as its derivative, is continuous. For the two systems which must be integrated, we obtained two linearly independent solutions a_+, b_+ and a_-, b_- by assuming the two different boundary conditions: $a_+(0.2)=1$, $b_+(0.2)=0$ and $a_-(0.2)=0$, $b_-(0.2)=1$, in addition to $a_\pm(0)=b_\pm(0)=0$.

The result of this calculation of the phase shifts is summarized in the following table:

$^3S_1+{}^3D_1$:

$$\xi_{1+}=+1.829$$
$$\eta_{1+}=\ 0.0068 \quad \beta_+/\alpha_+=18.96,$$
$$\xi_{1-}=\ 1.764$$
$$\eta_{1-}=\ 0.0073 \quad \beta_-/\alpha_-=22.84,$$

$^3P_2+{}^3F_2$:

$$\xi_{2+}=-0.0930$$
$$\eta_{2+}=+0.0655 \quad \beta_+/\alpha_+=6.95,$$
$$\xi_{2-}=-0.588$$
$$\eta_{2-}=+0.0641 \quad \beta_-/\alpha_-=118,$$

$^3P_1$: $\zeta_1=-0.501$ $^1S_0$: $\delta_0=+1.516$,
$^3P_0$: $\eta_0=-0.0293$ $^1P_1$: $\delta_1=-0.156$,
$^1D_2$: $\delta_2=+0.00453$.

The next step is to determine the correct linear combination of the two solutions of the systems. For this we apply formula (16). Formula (14) will give us then the values of $\xi^{M}{}_{J}$ and $\eta^{M}{}_{J}$. Since λ is in general a complex number we have also for ξ and η in general complex numbers. The result is as follows:

$^3S_1+{}^3D_1$: $\xi_1\pm=1.679-0.0009i$
$\xi_1{}^0=1.679-0.0018i$,
$\eta_1\pm=0.00267+0.0257i$
$\eta_1{}^0=0.00583+0.0124i$,
$\xi_2\pm=-0.0618+0.00035i$
$\xi_2{}^0=-0.0602+0.0005i$,
$\eta_2\pm=0.0521+0.0012i$
$\eta_2{}^0=0.0554-0.0009i$.

These quantities we must insert in formulae (17) and (9) to obtain the scattering cross section. We calculated only the ratio R of the cross section at $\vartheta=\pi$ and $\vartheta=\pi/2$. The result is:

$$R=\frac{\sigma(\pi)}{\sigma(\pi/2)}=1.1.$$

7. CONCLUSION

From the result of our calculation it can be seen that the symmetrical mixed theory gives an angular distribution in the center of mass system which is in contradiction with the experimental result which is $R=0.52\pm0.03$ for 14-Mev neutrons. Our result differs very little from the result of Schwinger and Rarita ($R=1.16$, $E=15.3$ Mev) which indicates that the preferential backwards scattering is virtually independent of the shape of the potential curve. This gives a great deal of generality to the conclusion which we want to draw from these calculations. *This conclusion is that the charge symmetrical meson theories lead to the wrong angular dependence for high energy neutron-proton scattering.*

We suggest therefore that, in the light of this result, the so-called meson pair theory of nuclear forces should be re-examined. They are known to give the same exchange operators in the nuclear force as the neutral theory.[16] But they lead to creation and absorption of charged mesons, which thus may be connected with the penetrating particles of the cosmic rays.

It is a pleasure to acknowledge the stimulating interest of Professor W. Pauli of the Institute for Advanced Study in the progress of this work. I am indebted to Mr. O. Goldman for some help with the numerical work.

[16] R. E. Marshak, Phys. Rev. **57**, 1101 (1940); Spin-dependent pair-interactions with mesons of integral spins were recently proposed by J. M. Jauch and J. L. Lopes, An. Acad. Bras. Ci. (in print); O. Klein, Arkiv f. Mat. Astronom. Fys. **30**, No. 3 (1944).

Heavy Particle Groups From the Neutron Disintegrations of Nitrogen and Neon†

HERBERT IVAN ZAGOR* AND FRANK A. VALENTE
Department of Physics, Washington Square College, New York University, New York, New York

(Received November 29, 1944)

Studies of the $_7N^{14}$ (n, a) $_5B^{11}$ reaction by the method of Wilhelmy seem to indicate the emission of heavy particle groups from nitrogen as a result of resonance transmutation by fast neutrons from a Ra+Be source. The total energy of the alpha-particle plus recoil nuclei lies at 1.33, 1.64, 1.94, 2.15, 2.64, 2.98, 3.82, 4.14, and 4.48 Mev. The data are in good agreement with those of other experimenters and it appears unlikely that the maxima in the distribution curve are caused by statistical fluctuations, but are intimately connected with nuclear transformations. Neon yields three alpha-particle groups at 0.85, 1.05, and 1.68 Mev in the energy range 0.25–2.5 Mev by a similar study. It appears probable that the reaction $_{10}Ne^{20}$ (n, a) $_8O^{17}$ is responsible for the 1.68-Mev group. The association of these groups with the intermediate nuclei Ne^{21} or Ne^{22} is not unique as long as it is not clear which excited states of the end nuclei can occur, and as long as accurate mass values of all the nuclei involved in these reactions are not known. Hydrogen gave a smooth distribution curve, as was expected.

I. INTRODUCTION

THE study of neutron disintegrations of nuclei with the emission of heavy particles is expected to yield data necessary for the development of an adequate theory of nuclear structure. There are several experimental methods which can be used for this purpose, among these being a promising method first proposed and tried by Wilhelmy.[1] This method consists of an ionization chamber coupled to a linear amplifier and recording oscillograph. The dimensions of the ionization chamber must be large enough to utilize the full range of the heavy particles resulting from the transformation. By means of this method, large amounts of statistical data can be collected and, even without direct knowledge of the actual neutron energies of individual processes, keys to transformations can be obtained.

Nuclear transformations by resonance penetration of the nuclear potential barrier by means of charged particles of discrete energies[2] have been known for some time. Prior to the work of Wilhelmy, resonances with fast neutrons had not been observed because of the difficulty of obtaining a homogeneous, step-wise source of fast neutrons. Wilhelmy, however, used a continuous source of fast neutrons and was able to obtain these resonances in the case of (n, a) and (n, p) processes.

In Wilhelmy's method, neutrons from a continuous source irradiate the target gas in the ionization chamber. If discrete groups are emitted, the energy distribution of the resulting particles, when measured, shows peaks. There is evidence that such emission resonance correlates with a penetration resonance of the neutrons,[3] and the energy of the incident neutron can be calculated from the energy balance of the reaction. With each resonance, there occurs an excited state of the intermediate nucleus, the energy of which can be measured.

II. FUNDAMENTAL ASSUMPTION

The range of nuclear particles is a function of the charge, gas pressure, and initial energy, whereas the total number of ions formed is only a function of the initial energy. Thus the average energy of ion pair formation in a given gas is nearly independent of the kind of ionizing particles and, approximately, of their velocities.

III. PURPOSE OF EXPERIMENTS

A. Nitrogen

Heretofore, the disintegration of nitrogen by neutrons has been studied from two points of

* Now at Camp Evans Signal Laboratory.

† Submitted by Herbert Ivan Zagor in partial fulfillment of the requirements for the degree of Doctor of Philosophy in the Graduate School of Arts and Science, New York University, New York, New York.

[1] E. Wilhelmy, Zeits. f. Physik **107**, 769 (1937).

[2] For example, see the work of W. Maurer, Zeits. f. Physik **107**, 721 (1937).

[3] W. Maurer, Zeits. f. Physik **107**, 721 (1937).

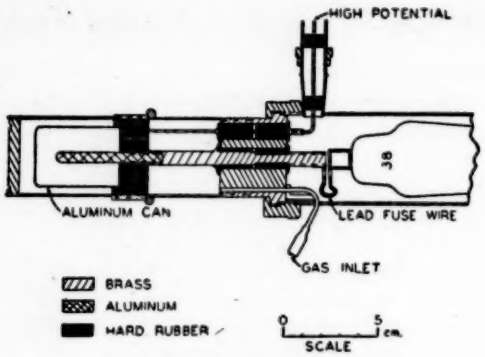

FIG. 1. Ionization chamber.

view: (1) reaction energies and kind of emitted particles; and (2) number, energy, and types of groups.

With respect to the second, Wilhelmy[1] has shown the existence of five energetically distinct groups. He used both Po+Be and Rn+Be neutron sources and apparently detected the alpha-particle groups from the reaction $_7N^{14}$ (n, a) $_5B^{11}$.

Comparat and Thibaud[4] using Rn+Be neutrons, repeated the work using greater resolving power, and made measurements at energies below the range of Wilhelmy's observations. Their statistics, however, are poor, leaving their data open to some question. Hansen,[5] in studying the range-velocity relation for boron, also investigated the reaction $_7N^{14}$ (n, a) $_5B^{11}$ with D+Be neutrons. In the overlapping energy region, their results are substantially in agreement.

Hansen questions whether the maxima he observed have physical meaning or are caused by statistical fluctuations. As a check, he applied the χ^2 test and found "that if the points were represented by the smooth curve, then the chance that the deviations were as large as those observed was about 3 in 10." He concludes that this does not prove that the smooth curves are not the best representations of the points. Hansen points out that although it is unlikely that an event which has 3 changes in 10 of happening should happen in six consecutive runs, a possible interpretation might be that all six runs are equally bad.

As a result of these data there was some doubt as to the reality of the groups, and the nitrogen work was repeated by a similar method, but with a 200 mC Ra+Be neutron source.

B. Neon

The disintegration of neon by neutrons has been studied by Jaeckel,[6] and Harkins, Gans, and Newson[7] with a cloud chamber and by Gailer,[8] using the method of Wilhelmy.[1] Jaeckel observed only 34 neon disintegration tracks in the Wilson chamber, with only one observed disintegration ascribed to the $_{10}Ne^{22}$ (n, a) $_8O^{19}$ process. The other tracks were ascribed to the $_{10}Ne^{20}$ (n, a) $_8O^{17}$ reaction, as were the eleven forks observed by Harkins, *et al.* Gailer observed five groups which he ascribed to alpha particles.

The statistics of the cloud chamber data are few and the results indicate (1) no proton reactions, and (2) no mutually consistent values of the energy of reaction of the transformation.

The five groups observed by Gailer in the 1–6 Mev energy region are produced by alpha-particles because protons of about 2 Mev, or greater, had too great a range to yield their total energy in his chamber and so produced no sharp maxima. At most, the first maximum, i.e., the 1.76 Mev group, if considered as a proton group, is in

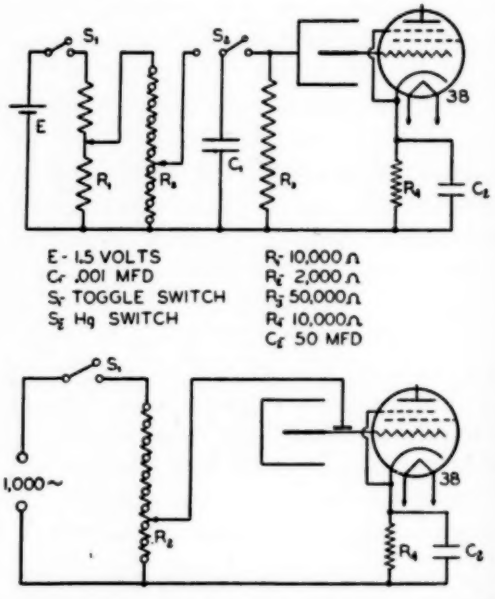

FIG. 2. Pulse generators for testing linearity of amplifier.

[4] P. Comparat and J. Thibaud, J. de phys. et rad. [7] 10, 161 (1939).
[5] W. Hansen, Ph.D. Thesis, Yale University (1941).
[6] R. Jaeckel, Zeits. f. Physik 96, 151 (1935).
[7] W. Harkins, D. Gans, and H. Newson, Phys. Rev. 47, 52 (1935).
[8] K. Gailer, Zeits. f. Physik 110, 605 (1938).

question. But, as Gailer states, this is highly improbable because no protons have been observed in the previous Wilson chamber experiments on neon.[6,7]

In view of this, it was thought desirable to repeat the work on neon in the 1–2.5 Mev energy region with Wilhelmy's method in order to check and clarify the work of the others, and to attempt to observe additional groups, if any.

IV. APPARATUS

The neutron source was a 200 mC radium bromide plus powdered beryllium mixture contained in a brass cylinder 2 cm in diameter and 4 cm high. A lead jacket 0.5 cm thick was placed around the brass cylinder to absorb the soft gamma-rays. The source and lead jacket were put in a cylindrical lead bucket of 5 cm wall thickness, and in addition, a lead block 5 cm thick was always kept between the source and ionization chamber. Thus there was always 10.5 cm of lead between the source and ionization chamber for the absorption of the gamma-rays.

The ionization chamber had the form of concentric cylinders, as shown in Fig. 1. The outer cylinder was an aluminum can which formerly had contained 35 mm film, the inner electrode was an aluminum rod, and both electrodes were inserted in a cylindrical block of hard rubber. This combination was encased in a brass tube which was screwed to a brass housing in which the first amplifying tube was placed. The tube and the housing were separated by a brass plug through which the insulated electrodes and gas inlet tube passed. The gas inlet tube had a needle valve and pressure gauge attached.

TABLE I. Comparison of proton recoil counts obtained with working chamber and calibration chamber.

Chamber 1	Chamber 2
2652 counts/5 minutes	2650 counts/5 minutes
2711	2600
2630	2686
2601	2643
2600	2700
2638	2636
2696	2621
2677	2634
2619	2676
2690	2642
2627	2691
2670	2603
31,811 Total	31,982 Total

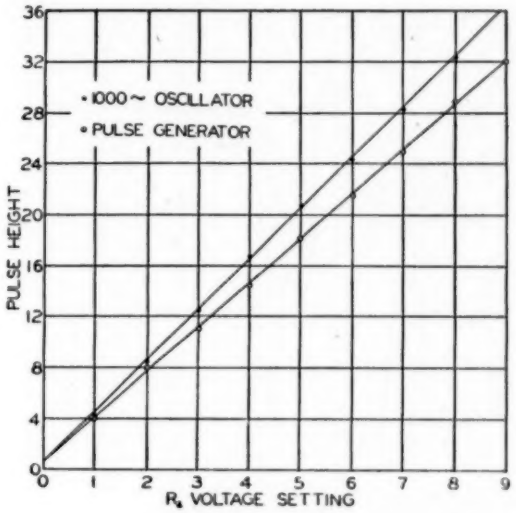

FIG. 3. Graph of oscilloscope pulse height against gang switch setting $R2$.

The experiments were performed with 2100 volts on the positive electrode of the ionization chamber. This high voltage was supplied by a separate power pack—a half-wave rectifier of conventional design.

A negative feed-back linear amplifier, developed by Waddel[9] was used. The Waddel circuit was modified slightly in the first amplification stage by (1) the introduction of degenerative feed-back and (2) having the control grid tied to ground by a 106,700 megohm resistor.

The recording by an oscillograph was made upon a continuously moving film. A Sept f:3.5 lens with Super XX 35 mm film was found satisfactory in conjunction with a Pl screen in a DuMont type 164 oscilloscope. The films were projected on a screen which had a fixed scale and counted visually. Electrical counting by means of photo-cell, biased thyratron, and scaling circuit was first tried, but was unsuccessful because the film density of the tracks was not uniform and the photo-cell circuit could only be adjusted for one particular film contrast at a time. In addition, pulses very close together could not be resolved and were recorded as a single count.

As it is important that the amplifier be linear, the response of the amplifier was tested by means of the pulse generators shown in Fig. 2. In the upper circuit of Fig. 2, condenser C_1 is charged

[9] R. Waddel, Rev. Sci. Inst. 10, 311 (1939).

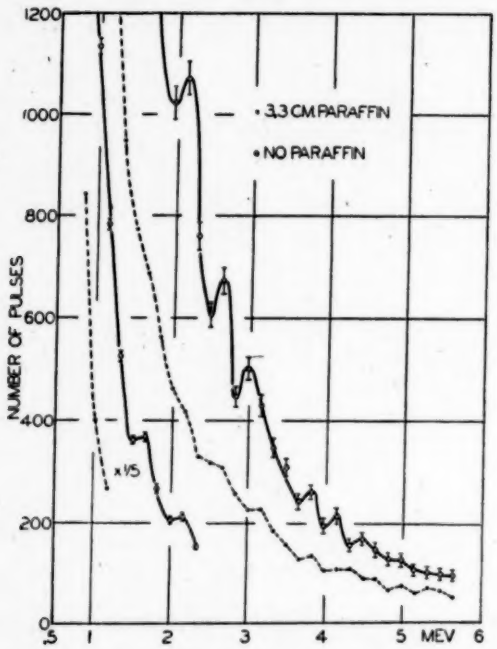

FIG. 4. Upper curve is a plot of number of pulses against $E_{\alpha+B}$ for $_7N^{14}(n, a)_5B^{11}$ reaction. Dotted lower curve is plot of number of pulses against pulse size, with 3.3 cm paraffin between source and detector. Nitrogen pressure is 336 cm Hg.

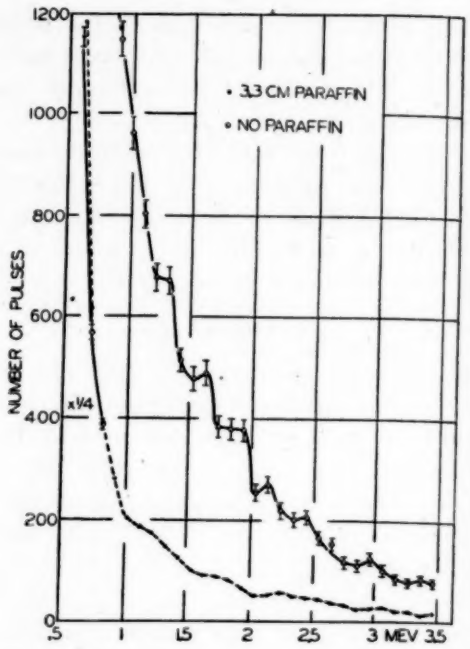

FIG. 5. Upper curve is a plot of number of pulses against $E_{\alpha+B}$ for the $_7N^{14}(n, a)_5B^{11}$ reaction. Dotted lower curve is plot of number of pulses against pulse size, with 3.3 cm of paraffin between source and detector. Nitrogen pressure is 76 cm Hg.

by battery E through potential divider R_1 and gang switch R_2, and then discharged through resistor R_3. Gang switch R_2 had 10 arms, each of which consisted of a 200 ohm resistor. The voltage across C is thus a linear function of gang switch setting R_2. In the lower circuit of Fig. 2, sinusoidal oscillations from a 1000 cycle tuning fork oscillator were fed through gang switch R_2 to the grid of the ionization chamber by means of capacity coupling. Figure 3 shows the plot of oscilloscope pulse height against gang switch setting R_2, and it is seen that the circuit response is linear in both cases.

For the purpose of determining the size of oscilloscopic pulses in terms of Mev, pulses from the monoenergetic Po alpha-particles were used, the Po being placed inside the chamber. To prevent contamination of the ionization chamber, two identical ionization chambers were built and used. One of them, the calibration chamber, contained the weak Po alpha-source, while the other did not, the latter being used as the working chamber.

That both ionization chambers were identical was shown in the following way. Both chambers were filled with hydrogen to 273 cm Hg pressure. Under identical geometry, each chamber in turn was subjected to the source, and the proton recoils counted at five minute intervals. The number of counts obtained with each chamber is shown in Table I and it is seen that the total number of counts agree to within 0.95 percent.

Microphonic response to acoustical noise or vibration was minimized by (1) coupling the ionization chamber to the grid of the first amplifying tube with lead fuse wire; (2) connecting the ionization chamber and vacuum tube housing for the first amplifying stage rigidly together; and (3) clamping this entire assemblage rigidly to supporting iron rods which rested on sponge rubber placed on a concrete floor. In addition, the first amplifying tube was wrapped in cotton and fitted snugly in the vacuum tube housing.

The microphonic response to acoustical noise was so small that it permitted use of the apparatus during the passing of classes. It was also observed that clapping one's hands close to the ionization chamber, or stamping heavily on the floor near the ionization chamber, did not cause

any increase in noise amplitude beyond the residual amplifier noise.

V. RESULTS

A. Nitrogen as Detector

Several reactions of the disintegration of the nitrogen nucleus with the emission of heavy particles are known.

The reaction (1) $_7N^{14}$ (n, a) $_5B^{11}$ yields a negative reaction energy Q of 0.25 Mev.[10] Burcham and Goldhaber,[11] have shown experimentally that this reaction cannot take place with slow neutrons.

The reaction (2) $_7N^{14}$ (n, p) $_6C^{14}$ yields a positive Q, and has been observed for fast neutrons by Kurie[12] and Bonner and Brubaker,[13] and for slow neutrons, by Bonner and Brubaker[13] and Burcham and Goldhaber.[11]

The reaction (3) $_7N^{14}$ $(n, 2a)$ $_3Li^7$ has been observed by Bonner and Brubaker[13] with very fast neutrons.

Also the reaction (4) $_7N^{14}$ (n, d) $_6C^{13}$ is energetically possible, according to Bonner and Brubaker.[13]

Tank nitrogen of purity 99.7 percent, or better, was used. With the source used, one would expect only reactions (1) and (2) to occur in any appreciable abundance.[14] The upper curve in Fig. 4 shows the result of a plot of the sum of the energies of disintegration products of nitrogen against number of associated oscillographic kicks. The curve shows several principal maxima at the energies 1.68, 2.15, 2.64, 2.98, 3.82, 4.14, and 4.48 Mev. The nitrogen pressure in the ionization chamber was 336 cm Hg.[15]

TABLE II. Comparison of maxima from $_7N^{14}$ (n, a) $_5B^{11}$ at 336 cm Hg and 76 cm Hg (Mev).

336 cm Hg	76 cm Hg	336 cm Hg. B_4C absorber
	1.33	1.25
1.68	1.64	1.68
	1.94	
2.15	2.15	2.15
2.64	2.46	2.64
2.98	2.96	2.98
3.82		
4.14		
4.48		

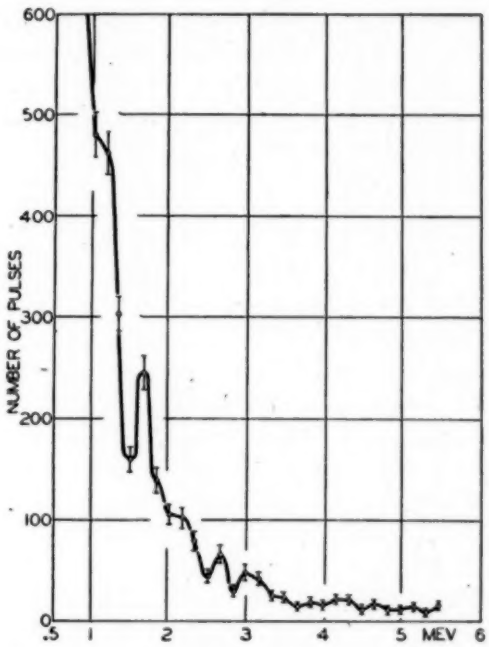

FIG. 6. B_4C absorber between source and chamber. Nitrogen pressure is 336 cm Hg.

The question then arises as to whether the observed heavy particle groups are proton groups or alpha-particle groups. To bring about a clear cut decision, the following series of experiments were performed.

First, a 3.3 cm paraffin plug was interposed between source and detector to slow down the impinging neutrons. Under these conditions, one expects proton reaction (2) to dominate. Hence if any of the groups were caused by protons, they should be enhanced, whereas the groups caused by alpha-particles should disappear. The dotted lower curve in Fig. 4 shows the result that none of the groups shows any enhancement, but, on the contrary, all the groups show a general disappearance.

If disintegrations occur in the gas of an ionization chamber, the number of disintegration particles may follow one or more courses. If the

[10] This value of Q (0.25 Mev) is calculated from the mass values of O. Hahn, S. Flügge, and J. Mattauch, Physik. Zeits. **41**, 1 (1940).

[11] Burcham and Goldhaber, Proc. Camb. Phil. Soc. **32**, 632 (1936).

[12] F. Kurie, Phys. Rev. **45**, 904 (1934); **47**, 97 (1935).

[13] T. Bonner and W. Brubaker, Phys. Rev. **49**, 223 (1936).

[14] N^{15} has a concentration of 0.3 percent and so can be neglected.

[15] The background averaged about one count per minute and showed a random distribution. It was thus neglected in the calculations.

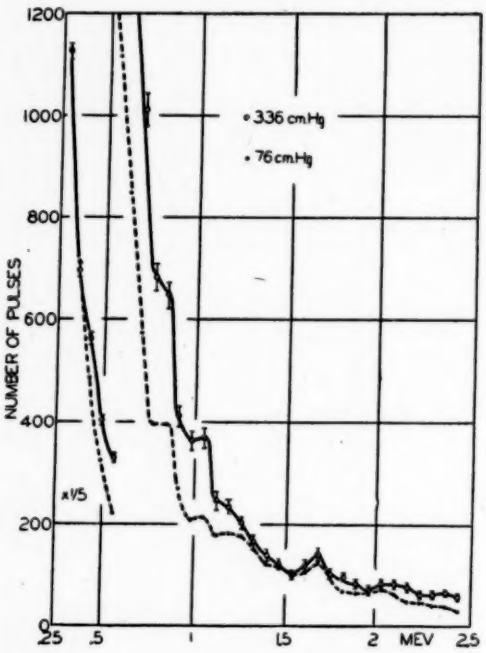

FIG. 7. The upper curve is a plot of number of pulses against pulse size. Neon pressure is 336 cm Hg. The lower dotted curve is a plot of number of pulses against pulse size with neon at a pressure of 76 cm Hg.

ranges of the disintegration particles are small compared with the dimensions of the ionization chamber, most of the particles will expend their total energy in the effective collecting volume, and, consequently, the edge effect will be small or negligible. On the other hand, if the ranges are about equal to or greater than the chamber dimensions, many will strike the walls with attendant reduction in the number of ion pairs formed. If now the pressure in the ionization chamber is lowered to the extent that the range corresponding to a definite group becomes comparable with the chamber dimensions, then this group tends to fade completely out of recognition. This is so because the specific ionization-range curve shows a maximum very nearly at the end of the range of the particles and this important portion vanishes in the case considered. At a given pressure, this fading out of groups occurs for protons rather than alpha-particles of equal energy because protons have the longer range.

The maximum depth of the ionization chamber is 4.3 cm. The stopping power of nitrogen is 0.99[16] that of air and thus the effective chamber depth with nitrogen becomes 4.2 cm. This value of range corresponds to a 1.45 Mev proton.[17] On the assumption that the highest energy group detected, the 4.48 Mev group, is an alpha-group, its range in nitrogen at 76 cm Hg is only 3 cm.[17] Thus if the pressure is lowered from 336 cm Hg to 76 cm Hg, all observed groups remain if they consist of alpha-particles, whereas all groups having an energy in excess of 1.45 Mev fade out if they consist of protons.

The result of such a study is shown in the upper curve of Fig. 5. Numerous maxima appear and the comparison of maxima at 336 cm Hg and 76 cm Hg, listed in Table II, shows good agreement. The reason more groups appear in the 0.5–3.5 Mev energy region at 76 cm Hg than in the corresponding energy region at 336 cm Hg is because of the difference in resolving power in the two cases. The resolving power at 76 cm Hg is 101,600 volts, whereas the resolving power of 336 cm Hg is 164,600 volts.

The experiment was repeated at 76 cm Hg with the 3.3 cm paraffin plug interposed between source and chamber. Under these conditions, the proton reaction should dominate. If all the groups previously detected were proton groups, only the 1.33 Mev group could be detected now, as its range alone in nitrogen (3.63 cm)[17] is less than the chamber dimensions. Thus the distribution should now show a group at 1.33 Mev, with the remainder of the curve smooth. One should also observe this same distribution if the 1.33 Mev group was caused by protons and the remaining groups caused by alpha-particles or by a mixture of alpha-groups and proton groups. If the 1.33 Mev group is caused by alpha-particles, however, the distribution should now be completely smooth.

The result is shown in the lower curve of Fig. 5 and the distribution is seen to be completely smooth.

A boron absorber (B_4C of boron thickness 0.56 g/cm²) was placed next between source and detector to permit transmission only of the fast neutrons, and the distribution measured at a pressure of 336 cm Hg. The distribution is shown in Fig. 6 and it is seen that groups appear at 1.25,

[16] J. Hoag, *Electron and Nuclear Physics* (Van Nostrand Company, Inc., New York, 1938), p. 463.

[17] M. Livingston and H. Bethe, Rev. Mod. Phys. 9, 268 (1937).

1.68, 2.15, 2.64, and 2.98 Mev. Table II shows the comparison of maxima from nitrogen both with and without the boron absorber. The 1.25 Mev group very probably corresponds to the 1.33 Mev group observed at 76 cm Hg, while the remaining groups are in exact coincidence with previously observed groups at 336 cm Hg pressure.

From the above results it appears that the groups observed are affected by fast neutrons and are alpha-particle groups arising from the reaction $_7N^{14}$ (n, a) $_5B^{11}$.

This agrees with the work of Baldinger and Huber[18] who have shown that for neutron energies of 2.8 Mev, the (n, a) reaction has a capture cross section four times that of the (n, p) reaction.

B. Neon as Detector

Neon has three stable isotopes: $_{10}Ne^{20}$, $_{10}Ne^{21}$, $_{10}Ne^{22}$, which are found in an abundance percentages of 90, 0.27 and 9.73 respectively. One can discard $_{10}Ne^{21}$ from consideration and therefore only the following neutron heavy particle reactions need be considered: (1) $_{10}Ne^{20}$ (n, a) $_8O^{17}$, (2) $_{10}Ne^{22}$ (n, a) $_8O^{19}$, (3) $_{10}Ne^{20}$ (n, p) $_9F^{20}$, and (4) $_{10}Ne^{22}$ (n, p) $_9F^{22}$.

Up to the present, the oxygen, fluorine, and neon masses reported as having been measured accurately[10] are O^{16}, O^{17}, O^{18}, Ne^{20}, Ne^{21}, Ne^{22}, F^{19}. Thus only the energy of reaction Q for Eq. (1) can be calculated, and hence one cannot predict accurately what reactions are possible with the available neutron source. In order to analyze the reactions which are detected, indirect methods must be tried. Reaction (4) is very improbable because it yields an isotope which is three mass units higher than the heaviest naturally occurring fluorine isotope, F^{19}. Reactions (1), (2), and (3) may very well occur, especially (1) as its Q calculated[10] equals—0.43 Mev.

The first observation was made at a chamber pressure of 336 cm Hg. The energy of the recoil nucleus plus the associated heavy particle was plotted against number of transformations and the plot is shown in the upper curve in Fig. 7. Maxima appear at 0.85, 1.05, and 1.68 Mev.

To try to determine whether the groups are caused by alpha-particles or protons, the pressure in the chamber was reduced to 76 cm Hg and the experiment repeated. The stopping power of neon, relative to air, in the energy range under observation is 0.57.[19] Thus the effective depth of the chamber is $4.3 \times 0.57 = 2.45$ cm of air.[20] This corresponds to a proton energy of 1.02 Mev.[17] Thus with 76 cm Hg pressure of neon in the chamber, all proton groups of energy greater than 1 Mev should fade out, whereas the 0.85 Mev group, if it consists of protons, should diminish considerably because of the edge effect.

However, if the groups are caused by alpha-particles they should still show up after the pressure in the chamber has been lowered to 76 cm Hg. To show this, assume the 1.68 Mev group, the highest neon energy group detected, to consist of alpha-particles. Its range would be 0.9 cm,[17] whereas the effective depth of the chamber is 2.45 cm, or nearly three times as long.

The results at 76 cm Hg are shown in the lower curve of Fig. 7. This curve is nearly identical with the curve at 336 cm Hg and the observed groups are alpha-particle groups. The neon data are shown in Table III.

The 1.68 alpha-group can be compared with the 1.7 Mev alpha-group found by Gailer,[8] the 1.6 Mev alpha-group from $_{10}Ne^{21}$ reported by Murrell and Smith,[21] and the 1.75 Mev alpha-group found by Pollard and Watson[22] from $_{10}Ne^{21}$.

It thus appears likely that the reaction $_{10}Ne^{20}$ (n, a) $_8O^{17}$ is responsible for the 1.68 Mev alpha group observed here. The Q calculated for this reaction equals minus 0.43 Mev and hence is a fast neutron reaction. This fits in very well with the observed data.

The cloud chamber experiment of Jaeckel[6] and

TABLE III. Results of neon experiments, groups detected.

336 cm Hg	76 cm Hg
0.85	0.85
1.05	1.05
1.68	1.68

[18] E. Baldinger and P. Huber, Helv. Phys. Acta **12**, 330 (1939).

[19] Rutherford, Chadwick, and Ellis, *Radiations from Radioactive Substances* (Cambridge University Press, London, 1930), p. 97.

[20] Maximum chamber depth = 4.3 cm.

[21] Murrell and Smith, Proc. Roy. Soc. **173**, 410 (1939).

[22] E. Pollard and W. Watson, Phys. Rev. **58**, 16 (1940).

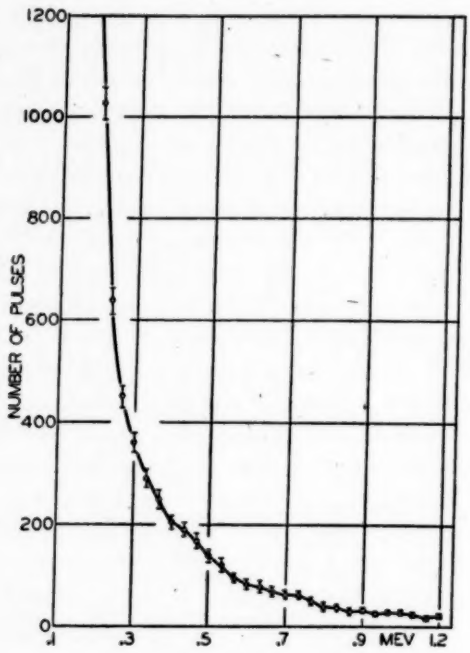

FIG. 8. Recoil proton distribution with hydrogen. Hydrogen pressure is 338 cm Hg.

Harkins, *et al.*,[7] have not led to mutually consistent values of the total energy of reaction of the transformation. This means that the end nucleus originating from the intermediate nucleus, does not always return to the same excited state or ground state, but exists in various excited states. In this case there belongs to a definite state of the intermediate nucleus several energy groups of heavy particles which differ by the energy difference of the energies of the excited state of the end nucleus.

Thus the assignment of groups with the excited states of the intermediate nucleus, $_{10}Ne^{21}$ or perhaps $_{10}Ne^{23}$, is not unique as long as it is not clear which excited states of the end nucleus can occur.

C. Hydrogen as Detector

At a test to show that the detected groups were not caused by instrumentation, the chamber was filled with hydrogen to 338 cg Hg and the distribution measured. Groups are not expected from hydrogen, and the distribution should be smooth. Figure 8 shows the result of such an investigation, and the graph is seen to be smooth without trace of maxima or minima.

VI. THEORY

The details of the processes observed here can be considered best on basis of the Bohr conception of the course of nuclear reactions. In point of time, such reactions proceed in two steps.

First, the particle is captured and its energy distributed among the number of nuclear constituents. Thus there arises an excited intermediate nucleus, the lifetime of which is finite, i.e., greater than the time required by the particle to cross the nucleus.

Secondly, these excited intermediate nuclei can go to the ground state by gamma emission, or the entire excitation energy, or an essential part thereof, can be concentrated on a particular particle so that it may acquire sufficient energy to leave the nucleus.

On account of the long lifetime of the intermediate nucleus, its excitation states are fairly sharp. Thus the reaction occurs with appreciable probability only for certain well-defined energy ranges of the incident neutrons.

The different observed resonance groups of a nucleus may correspond either to the different excitation states of the intermediate nucleus, or the different excitation states of the transformed, end nucleus. The first will be assumed, and the calculations made on the basis of the end nucleus being in the ground state. This assumption, which will be discussed later, permits the determination of the energy of reaction Q from the masses.[10]

One can deduce the energy of the incident neutron E_n by adding to the energy of the observed group E_{a+B}, the energy Q, corresponding to the change in mass in the course of the reaction.

E_t, the absolute value of the resonance level in

TABLE IV. Summary of nitrogen data for $_7N^{14}$ (n, a) $_5B^{11}$.

E_{a+B} Observed particle and recoil nucleus (Mev)	Energy of reaction Q (Mev)	Neutron energy E_n (Mev)	E_{a+B_0} Particle and recoil nucleus (Mev)	E_1 Binding energy of a particle to N^{15} (Mev)	E_t, Term of intermediate nucleus N^{15} (Mev)
1.33	−0.25	1.58	1.23	11.0	12.23
1.64		1.89	1.51		12.51
1.94		2.19	1.77		12.77
2.15		2.40	1.99		12.99
2.64		2.89	2.45		13.45
2.98		3.23	2.77		13.77
3.82		4.07	3.55		14.55
4.14		4.39	3.85		14.85
4.48		4.73	4.16		15.16

relation to the ground state of N^{15} is determined by adding the binding energy E_1, of the alpha-particle in this nucleus to E_{a+B_0}, the observed neutron energy in a system of coordinates with the center of gravity at rest.

A calculation shows that

$$E_{a+B_0}=\frac{14}{15}E_n-Q.$$

Table IV contains a summary of the nitrogen data.

A test of the question as to whether the observed resonance groups correspond either to the different excitation states of the intermediate nucleus, or the different excitation states of the end nucleus, is possible in the case of nitrogen. If the boron nucleus is in the ground state, then, and only then, is it possible for the exact inverse process to be observed when boron is bombarded with alpha particles and the alpha penetration resonance results in neutron emission according to the process $_5B^{11}$ (a, n) $_7N^{14}$. These resonance energies are expected to agree with the observed emission resonances if the motion of the center of gravity is taken into consideration. Maurer[2] carried out this investigation by measuring the energies of the inverse process $_5B^{11}$ (a, n) $_7N^{14}$.

The alpha-particle energies obtained by Maurer must be transposed so as to be comparable with the inverse process observed here. If E_{a+B} is the resonance energy of the alpha-particle plus the boron nucleus found in the (n, a) process, Q the energy of reaction of this process, E_a the alpha-resonance energy in the (a, n) process, then

$$E_{a+B}=\frac{1}{14}(11E_a+Q).$$

Table V shows the comparison of data reported here (column 1) with those of Wilhemy,[1] Comparat and Thibaud,[4] Maurer,[3] and Hansen.[5]

There is obviously good agreement among the levels in common.

The fact that the same levels of resonance of $_7N^{15}$ are found by two processes which are the inverse of each other proves that in some cases, when one of these levels is excited, the B^{11} nucleus is emitted in its ground state [(n, a) process] as previously assumed.

TABLE V. Comparison of data on resonance energy, (E_{a+B}) given in Mev.

This thesis	Wilhelmy	Comparat and Thibaud	Maurer	Hansen
		0.60		
		0.75		
		0.90		
		1.05		
		1.25		
1.33	1.42	1.40	1.40	1.31
1.64		1.60		
		1.75		1.75
1.94	2.04	2.05	2.00	1.94
2.15		2.25	2.16	2.31
		2.55		
2.64	2.59	2.75	2.70	2.58
2.98		3.05		2.93
	3.21	3.30	3.25	3.18
			3.49	
			3.74	3.7
3.82			3.86	3.82
4.14				4.12
4.48				4.37
				4.68
	4.9			4.93

But one cannot conclude that all groups found correspond to resonance levels, as certain of the observed groups may correspond to transition groups, leaving the boron nucleus excited. The statistics have shown a very large majority of impulses corresponding in low E_{a+B} energies, indicating that the energy imparted by a fast neutron to the nitrogen nucleus is only partially concentrated on the emitted alpha-particle and consequently the boron nucleus remains excited at any possible excitation level. Two such levels are known for B^{11} at 2.1 Mev and 4.4 Mev.[23] In such a case, the energy of an observed group, E_{a+B}, represents the energy of the resonance level of N^{15} minus the excitation energy of a level of B^{11}. One should observe gamma-emission in such a case. The experimental set-up employed here was inadequate for the detection of these gamma-rays because of the intense gamma-ray spectra from the Ra+Be neutron source.

The terms of the intermediate nucleus have, in the average, an interval of about 0.30 Mev, and they lie moderately close. This is understandable as the terms lie very high above the ground term and according to Bohr, the term density increases rapidly, in general, towards the higher terms.

Theoretically, from Bethe's equation[24] the

[23] M. S. Livingston and H. Bethe, Rev. Mod. Phys. 9, 341 (1937).
[24] H. Bethe, Rev. Mod. Phys. 9, 85, Eq. 304 (1937).

spacing of the energy levels in N^{15} excited to 11 Mev has a value of about 0.1 Mev. The agreement between theory and experiment is thus quite good.

Cases in which neutron transformations can be observed in the reverse direction are rare. Consequently the process described here is often the only possible one to determine experimentally the excitation states of certain intermediate nuclei. To be sure, such an assignment of groups is only possible if one has at his disposal homogeneous neutrons of any desired energy.

VII. ACKNOWLEDGMENTS

Thanks are due Professor C. W. Van der Merwe for his encouragement and interest in the work and to Professors E. O. Salant and R. D. Present for helpful discussions. We appreciate the work done by Dr. I. I. Hudes, Mr. M. G. Levy, and Mr. V. L. Parsegian in helping us take the data, and thank the Graduate School of New York University for financial aid to one of us (H. I. Z.). We also wish to express our thanks to Dr. W. W. Hansen for permission to use his results.

PHYSICAL REVIEW VOLUME 67, NUMBERS 5 AND 6 MARCH 1 AND 15, 1945

Radioactive Xenons

CHIEN-SHIUNG WU AND EMILIO SEGRÈ
Radiation Laboratory, Department of Physics University of California, Berkeley, California
(Received December 9, 1944)

The investigation of the radioactive xenons growing out from radioactive iodines following uranium or thorium fission is summarized in this paper. Two complete chains have been established and identified with their mass numbers. They are:

(1) $_{51}Sb^{133}$ 10 min.$\rightarrow$ $_{52}Te^{133}$ 60 min.$\rightarrow$ $_{53}I^{133}$ 22 hrs.$\rightarrow$ $_{54}Xe^{133}$ 5 days$\rightarrow$ $_{55}Cs^{133}$

and

(2) $_{53}I^{135}$ 6.6 hrs. $\rightarrow$ $_{54}Xe^{135*}$ 10 min. $\rightarrow$ $_{54}Xe^{135}$ 9.4 hr. $_{55}Cs^{135}$?

I. INTRODUCTION

THE investigation of radioactive xenon from iodine as a result of nuclear fission was started in 1939 and was discontinued at the end of 1941. Although parts of our results have been briefly reported in this journal[1,2] and some of the results have since been confirmed and further extended in different laboratories,[3] nevertheless, it seems desirable to give a systematic description of the whole situation as it stands now.

Our investigation concerning this problem consists mainly of three parts. First, we observed the radioactive xenons growing out of iodine and established their genetic relations with known fission chains. Second, by bombarding cesium and barium with fast neutrons, the mass numbers of these radio-xenons and consequently of the whole chains were identified. The last part was a tentative study of the nuclear isomerism in xenon.

II. EXPERIMENTAL PROCEDURE

(a) Material

The chemical form of uranium employed in this investigation was uranyl nitrate ($UO_2(NO_3)_2 \cdot 6H_2O$) or uranyl chloride (UO_2Cl_2), depending on the type of chemical manipulations required for carrying out a specific separation. The neutrons used in this investigation were

[1] E. Segrè and C. S. Wu, Phys. Rev. **57**, 552 (1940).
[2] C. S. Wu, Phys. Rev. **58**, 926 (1940).
[3] R. W. Dodson and R. O. Fowler, Phys. Rev. **57**, 966 (1940), H. Goette, Naturwiss. **28**, 449 (1940); W. Seelmann-Eggebert and H. J. Born, Naturwiss. **31**, 59 (1943); W. Seelmann-Eggebert, Naturwiss. **31**, 491 (1943).

formed by the bombardment of beryllium with 8-Mev deuterons produced by the 37″ cyclotron or by 16-Mev deuterons accelerated by the 60″ cyclotron. The samples were usually placed close to the beryllium target and imbedded in a few inches of paraffin.

(b) Apparatus

The activities were measured with ionization chambers connected to a vacuum tube electrometer system of the type modified by Dubridge.[4] Two types of chambers were used. One was made entirely of brass, lined on the inside with cardboard, and the inner cylinder was a copper net of 9-cm diameter and height. It was filled with freon (CCl_2F_2) at a pressure of about one atmosphere. The window was aluminum of 7 mg/cm² thickness. The other type, into which the active gases were directly introduced, was also made of brass and the inner cylinder had a diameter of 8 cm and a height of 10 cm. In order to facilitate taking absorption curves of the radiation, a number of small drum-shaped brass vessels of 5.5-cm radius and 4 cm in height were provided. The top of the drum which serves as a window consists either of a copper foil of 0.0025-cm thickness or a sheet of extremely thin Cellophane supported by a fine brass grating. A special scheme of connection was devised so that the ionization chamber could be easily and quickly attached to or detached from the electrometer system.

(c) Extraction of Active Gases

The extraction of active gases from iodine was performed by two different techniques. One was simply by transferring the active gases accumulated in an emanating sample into an evacuated chamber as described by Langsdorf and Segrè.[5] The other was by prolonged boiling combined with bubbling of a gas stream through the solution. The latter method was found to give more nearly quantitative results than the first one.

The radioactive iodine from which the xenon was extracted was prepared in the following way. After the uranium was irradiated, the radioactive iodine and bromine were distilled with several milligrams of iodine and bromine carriers into a dilute sodium sulphite solution. From the sulphite solution iodine alone was oxidized to a free state by adding ferric chloride and then was extracted with carbon tetrachloride. In the preparation of emanating samples, several cubic centimeters of silver nitrate-impregnated silica gel were added to this solution and shaken with it until the iodine color had disappeared. For preparing the solution used in the latter prolonged boiling method, the iodine was extracted from the carbon tetrachloride by a dilute sodium sulphite solution. From this solution xenon was collected by boiling. To prevent any possible escape of iodine during the process of boiling, the solution was also made strongly alkaline.

III. THE 9.4 HR. XENON FROM 6.6 HR. IODINE

In the first trial an emanating sample of iodine was prepared. The xenon which was extracted at 12-hr. intervals from the emanating iodine sample was not transferred directly into an ionization chamber, but into one of the small drum-shaped

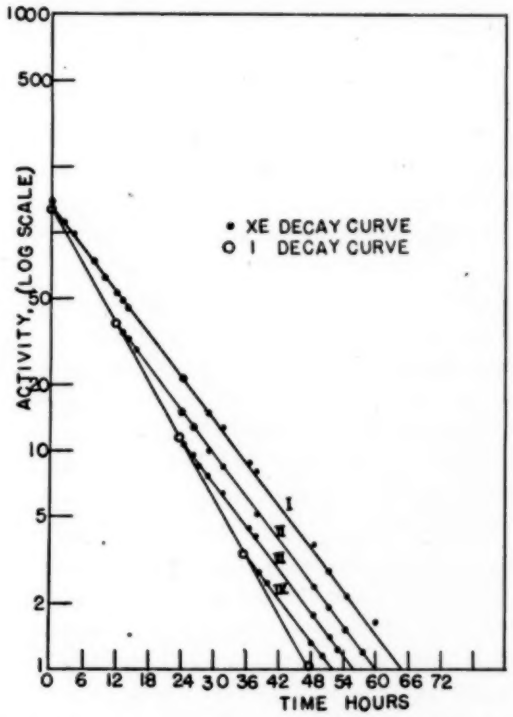

FIG. 1. Decay curves of successive xenon extracted from iodine. The dots represent the xenon activity. The curve passing through the circles represents the decay curve of the 6.6-hr. parent iodine.

[4] L. A. Dubridge and H. Brown, Rev. Sci. Inst. **4**, 532 (1933).

[5] A. Langsdorf, Jr., and E. Segrè, Phys. Rev. **57**, 105 (1940).

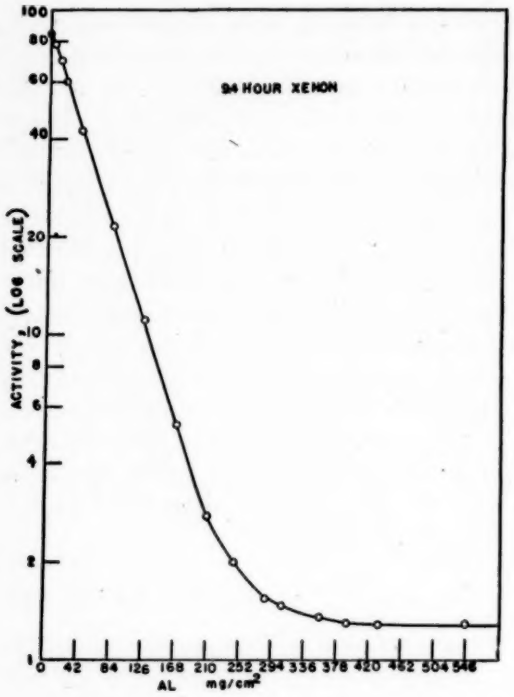

FIG. 2. Absorption in aluminum of the beta-particles from 9.4-hr. xenon.

brass vessels. The decay curves of the xenon thus obtained are shown in Fig. 1. Curves I–IV all show a half-life of 9.4 hr. The exponential line passing through the initial point of each decay curve represents the decay curve of the parent of the xenon. It is a 6.6-hr. iodine. Because of the complicated activities of iodine, it is very difficult to identify this intermediate period directly from the decay curve of iodine. Of course, it is still more difficult to find the half-life of the parent of this iodine merely by periodical extraction of iodine from tellurium. However, from the first trial it was shown that xenon extracted in this way has a simple activity. Therefore it is more advisable to determine the half-life of the grandparent of this 9.4-hr. xenon by measuring the activities of the xenon directly extracted from iodine samples successively separated from tellurium. For this purpose the uranium was prepared in uranyl chloride form. First selenium was precipitated by passing sulfur dioxide into a 12-molal hydrochloric acid solution containing appropriate carriers. Tellurium was then immediately precipitated in the same way from a hot 3-molal hydrochloric acid solution. The tellurium thus obtained was dissolved in nitric acid. Iodine was added to the solution and the solution evaporated to dryness to assure that no iodine was carried down directly. (The short-lived Te of approximate 15 min. assigned as the parent of 6.6-hr. iodine as reported in our previous letter is in error due to the omission of this step.) Then at one-half hour intervals iodine was distilled from the tellurium solution. The iodine thus collected was each time made into emanating samples and then after 12 hr. active xenon extracted. In all the extractions, there are no indications of the presence of the 9.4-hr. active xenon. If the half-life of this grandparent tellurium is shorter than five minutes, it might have escaped detection.

The absorption curve of this 9.4-hr. beta-ray activity was taken in aluminum as shown in Fig. 2. The end point 392 mg/cm² gives the upper

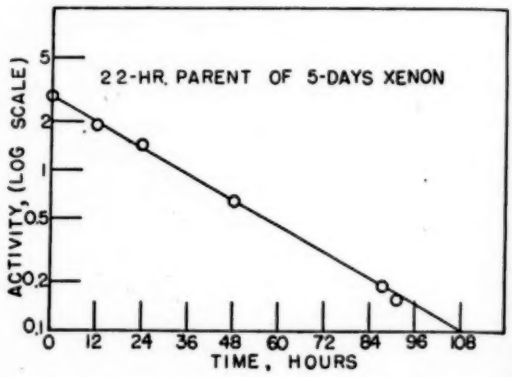

FIG. 3. Determination of half-life of the 22-hr. iodine through periodic separations of their daughter xenon activities.

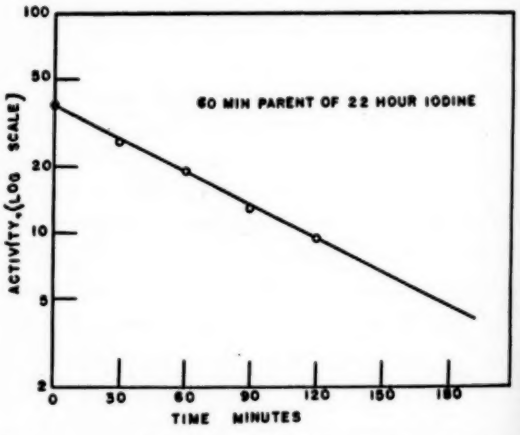

FIG. 4. Determination of half-life of the 60 minutes tellurium through periodic separations of its granddaughter 5 days xenon activities.

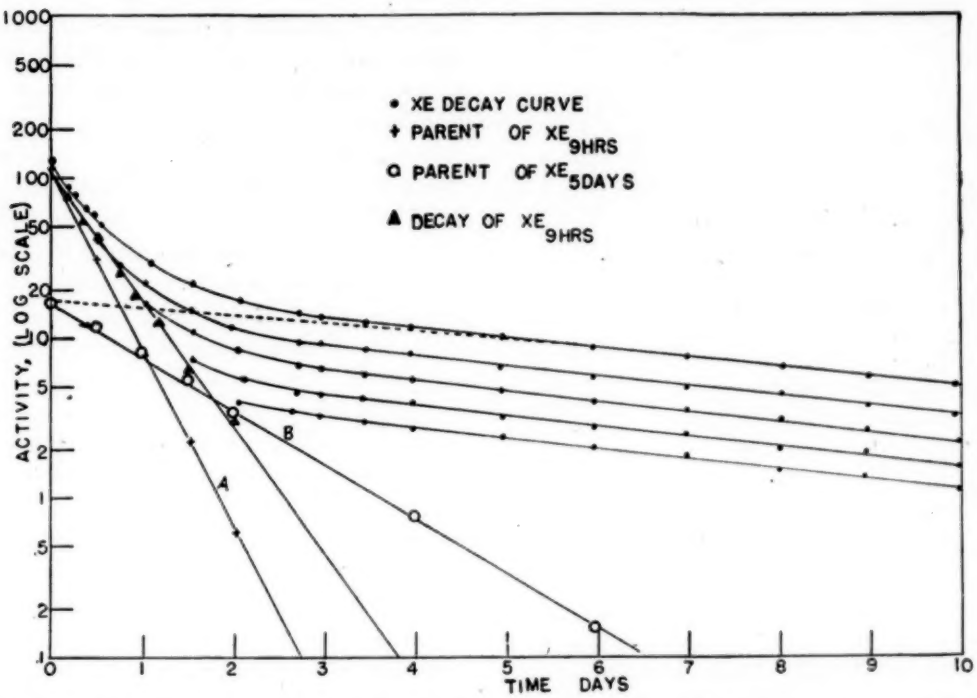

FIG. 5. Decay curves of successive xenon extracts from iodine. The curve *A* through the crosses represents the decay curve of the parent iodine 6.6-hr. The curve *B* through the circles represents the decay curve of the parent iodine 22-hr.

energy limit around 0.9 Mev which agrees with Seelmann-Eggebert's finding.[6]

It is also desirable to know whether or not this 9.4-hr. active xenon decays to an active cesium. The brass drum had stored for one day the 9.4-hr. xenon. Its interior surface was treated with dilute hydrochloric acid and the acid evaporated to dryness. No activity was found. The possibility of a very short-lived cesium daughter of 9.4 xenon was considered. An apparatus for depositing the radioactive substance from an emanating gas was designed. This apparatus consisted of a glass tube with a radius of 5 cm. The inside wall was coated with a thin layer of Aquadag in order to render the glass surface conducting and make it usable as one of the electrodes. In this arrangement one could move this piece of aluminum on which the daughter substance had been deposited to the window of the ionization chamber within a few seconds. But no active deposit was found from the 9.4-hr. xenon. However, this does not exclude the existence of a radioactive daughter cesium with a life less than one second or longer than 10 years.

[6] W. Seelmann-Eggebert, Naturwiss. **31**, 491 (1943).

These evidences, therefore, would give the chain as

$$\underset{6.6\text{ hr.}}{\text{I}} \longrightarrow \underset{9.4\text{ hr.}}{\text{Xe}} \longrightarrow \text{Cs (?)}$$

(IV) The chain

$$\underset{10\text{ min.}}{\text{Sb}} \longrightarrow \underset{60\text{ min.}}{\text{Te}} \longrightarrow \underset{22\text{ hr.}}{\text{I}} \longrightarrow \underset{5\text{ days}}{\text{Xe}} \longrightarrow \text{Cs} > 10 \text{ years}$$

After the 9.4-hr. xenon had completely decayed, the gas in the drum was then transferred directly to an ionization chamber. Here, a 5-day xenon activity was observed. This was undoubtedly the long-lived noble gas reported by Langsdorf.[7] From the curve shown in Fig. 3, we identified the parent of this long-lived xenon as the 22-hr. iodine observed by Abelson.[8] In order to confirm this identification it is necessary to determine the half-life of the grandparent of this long-lived xenon. This was done by transferring the active gas, which was prepared in an attempt to identify the grandparent of the 9.4 xenon, from the series of drums to ionization chambers. From the measurements a half-life of approximately one hour was found for this grandparent tellurium

[7] A. Langsdorf, Jr., Phys. Rev. **56**, 205 (1939).
[8] P. Abelson, Phys. Rev. **56**, 1 (1939).

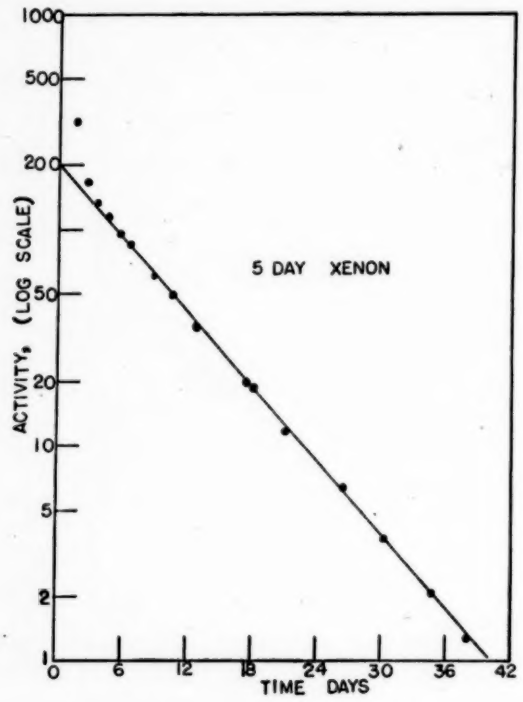

FIG. 6. Decay curve of 5-day xenon.

(Fig. 4) which is in good accord with Abelson's result.[8]

It is quite obvious that this long-life xenon must emit a very soft radiation which is easily stopped by the thin copper foil of the top of the drum and the aluminum window of the ionization chamber. An absorption curve taken through an extremely thin Cellophane window shows an end point for the beta-rays of around 70 mg/cm² of Al, which approximately corresponds to an upper energy limit of 260 kev and agrees well with Seelmann-Eggebert's[6] determination of 0.2–0.3 Mev by using a gas absorption chamber.

Furthermore, it is also very desirable to know whether there is some radioactive xenon growing out of iodine with an intermediate life or a life longer than 5 days. Therefore, the xenon accumulated in the iodine sample was directly transferred to the ionization chambers and the decay of the activity was followed for a long time. An analysis of these decay curves (Fig. 5) gives a half-life of 6.6 hr. for the parent of 9.4-hr. xenon (curve *A*) and a half-life of 22 hours for the parent of 5-day xenon (curve *B*). The 5-day xenon followed strictly an exponential decay curve as far as the intensity was measurable (Fig. 6). From this, it is safe to conclude that no active xenon is present of half-life longer than 5 days but less than 10^3 years. Also, from a careful examination of these analyzed curves, there seems little possibility of the presence of a radioactive xenon of intermediate half-life. But it must be borne in mind that this does not rule out the possibility of an active xenon of intermediate life growing out of a very short-lived iodine, for instance, a half-life of a few minutes.

To check this point it was desirable to re-examine the initial portion of the decay curve of the radioactive iodine from uranium fission for a half-life shorter than 54 minutes. The separation and purification of the iodine from activated uranium solution was accomplished within 5 minutes after the termination of irradiation. However, the initial portion of this decay curve of the mixed iodine activities as shown in Fig. 7 fails to reveal the presence of a radioactive iodine with half-life between 1 and 54 minutes.

In this case also no radioactive deposits were found.

V. IDENTIFICATION OF THESE TWO RADIOACTIVE XENONS[9]

In order to identify the mass numbers of these two radioactive xenons found in uranium fission, some samples of cesium and barium were placed immediately behind a beryllium target bombarded by 16-Mev deuterons. After the bombardment, the active cesium or barium was dissolved in water and the radioactive gas was then extracted into an ionization chamber. In the case of cesium only one radioactivity was observed which decays with a half-life of 5 days, but in the case of barium, both 9.4-hr. and 5-day periods were present. The identity of the periods and of the absorption curves of these 9.4-hr. and 5-day

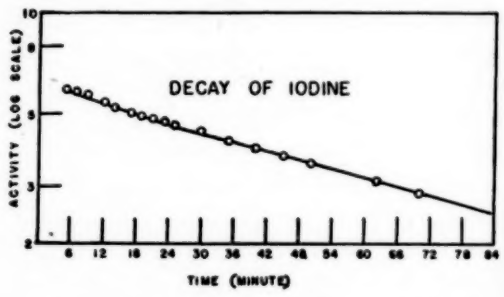

FIG. 7. Initial part of the decay curve of the iodine composite.

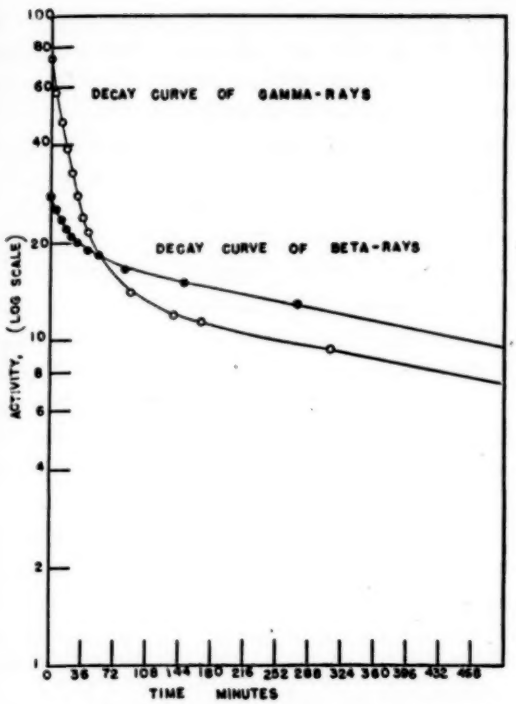

FIG. 8. (a) Composite gamma-ray decay curve of the 10-min. and 9.4-hr. xenons as measured with 67 mil of Al placed between the source and the ionization chamber. The period of accumulation in the emanating sample is 30 minutes. (b) Composite beta-ray decay curve of the same sample.

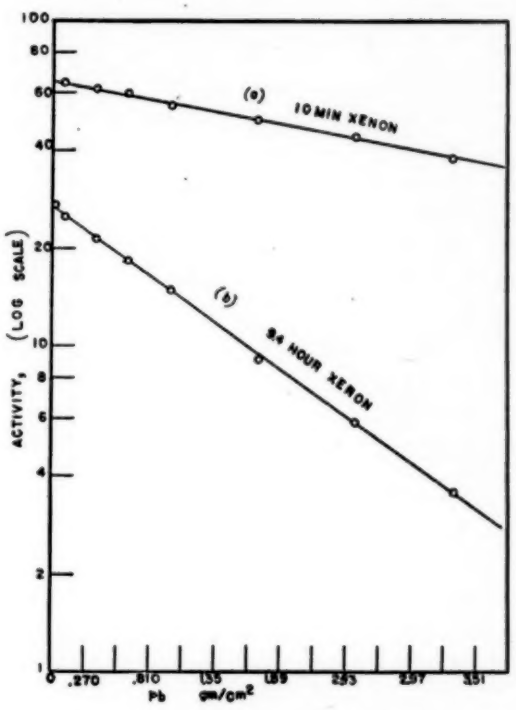

FIG. 9. γ-ray absorption curves in lead.

radioactive gases from cesium and barium with those of radioactive xenon from uranium and thorium fission proves that they are the same substances.

Cesium has only one stable isotope with a mass number of 133, and since its bombardment gives only one radioactive xenon, we assume that the 5-day xenon is produced by the following reaction,

$$_{55}Cs^{133}_{(n,p)}{}_{54}Xe^{133},$$

and assign to it the mass number 133. Subsequently, Clancy[9] has observed this 5-day xenon by bombarding xenon with deuterons and also by bombarding Te with α-particles and explained them through the reactions

$$_{54}Xe^{132}_{(d,p)}{}_{54}Xe^{133} \quad \text{and} \quad _{52}Te^{130}_{(\alpha,n)}{}_{54}Xe^{130}.$$

Although barium has seven known isotopes (130, 132, 134, 135, 136, 137, and 138), only three of them would be able to produce radioactive xenon (except for isomers of stable nuclei) by an (n, α) reaction. These are 130, 136, and 138. We have seen that Ba gives by an (n, α) reaction the 5-day xenon and we interpret this as

$$_{56}Ba^{136}_{(n,\alpha)}{}_{54}Xe^{133}.$$

Since the abundance of Ba^{130} is only 1/700 of that of Ba^{138}, it is very likely that the barium of mass number of 138 is responsible for the formation of the 9.4-hr. xenon according to the reaction

$$_{56}Ba^{138}_{(n,\alpha)}{}_{54}Xe^{135}.$$

In this case, Clancy[9] has also found this 9.4-hr. Xe by bombarding xenon with deuterons. This is probably caused by the reaction

$$_{54}Xe^{134}_{(d,p)}{}_{54}Xe^{135}.$$

Based on these results, the two chains found in uranium and thorium fission may be identified with their mass numbers

$$_{51}Sb^{133}\ 10\ \text{min.} \rightarrow {}_{52}Te^{133}\ 60\ \text{min.} \rightarrow {}_{53}I^{133}\ 22\ \text{hr.}$$
$$\rightarrow {}_{54}Xe^{133}\ 5\ \text{days} \rightarrow {}_{55}Cs^{133},$$

and

$$_{53}I^{135}\ 6.6\ \text{hr.} \rightarrow {}_{54}Xe^{135}\ 9.4\ \text{hr.} \rightarrow {}_{55}Cs^{135}?$$

[9] Edward R. Clancy, Phys. Rev. 59, 686 (1941).

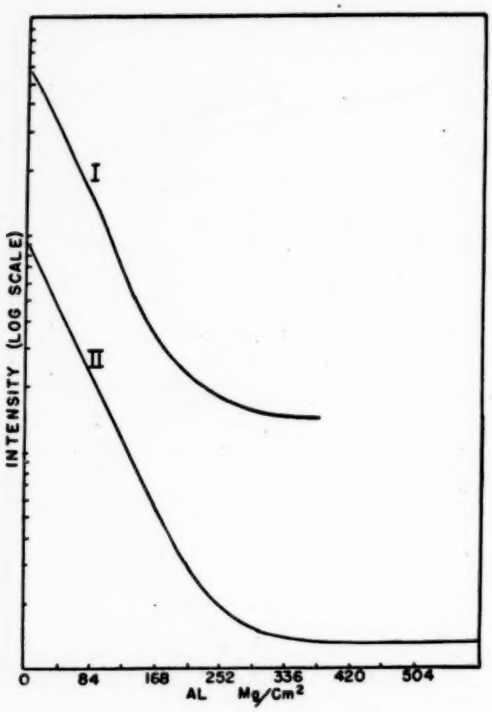

FIG. 10. β-ray absorption curves. I. β-ray absorption curve of xenon right after extraction (period of accumulation = 5 min.). (Corrected for the composite decay rate. II. Two hours after extraction (period of accumulation = more than 12 hr.).

VI. NUCLEAR ISOMERISM IN XENON

In our former letter[1] reporting some fission products from uranium fission, we mentioned that we had observed one or more xenons with shorter half-periods growing out of iodine which had not been thoroughly investigated yet. The short-lived xenon was clearly shown in the case where the time of accumulation was comparatively short. Because our interests were concentrated on the two long-lived radio-xenons, the time interval for accumulation of the radioactive gases in the emanating sample was always in the neighborhood of 12–24 hours. This long accumulation time yielded large activities of the long-lived xenons which nearly masked the existence of a short lived xenon. However, Goette[10] has confirmed and completed our observations, finding that this short-lived xenon with a half-period of 10 minutes is also growing out of 6.6-hr. iodine which was recognized by us to be the parent of 9.4-hr. xenon. In view of this fact, he concluded that the 10-minute and 9.4-hr. xenons must be isomers. Since this case appeared rather complicated and yet was accessible, we have investigated the situation in more detail.

First, the decay curves of beta-particles and gamma-rays of the xenon extracted from iodine which had been sealed for accumulation for short intervals were followed separately. The decay curve of beta-particles does not show at the beginning a prominent drop for a 10-minute half-period, but the decay curve of gamma-rays which was taken by completely absorbing electrons by 67 mils of aluminum shows a remarkable initial drop different from that of β-particles (Fig. 8). This fact indicates that the radiation of 10-minute xenon consists mostly of gamma-rays.

In our picture, then, this gamma-ray of short life must be interpreted as corresponding to the transition from the upper to the lower isomeric state which afterwards decays by β-decay with a period of 9.4 hr. to cesium. In order to check this interpretation, we have taken absorption curves for beta-particles and gamma-rays in aluminum and lead, respectively, immediately after the extraction and again on the same two hours later when the 9.4-hr. activity was the only one present. The two gamma-ray absorption curves in lead (Fig. 9) are quite different. The half-value thickness for the 10-minute gamma-rays is obtained after correction for decay and the soft gamma-ray background of 9.4-hr. xenon. It gives a value of 4.5 g/cm² and is much less than the half-value thickness 6–7 mm of Pb reported by Seelmann-Eggebert.[6] This is probably caused by our bad geometrical conditions. However, under exactly the same conditions, we found that the half-value thickness for the gamma-rays associated with the 9.4-hr. xenon is only 1.13 g/cm² of Pb.

The difference between the two beta-spectra (Fig. 10) is rather small except there is a high gamma-ray background associated with the absorption curve taken immediately after the extraction. No attempt was made to determine the upper energy limit of the β-rays from the 10-minute xenon.

The short-life beta activity observed in the initial drop of the beta-decay curve can be explained in two ways. It could be interpreted as parts of the xenon in the upper isomeric state

[10] H. Goette, Naturwiss. 28, 449 (1940).

decay to cesium by a direct beta-decay with a period of 10 minutes. But the failure to show any noticeable difference in the two beta-absorption curves and the estimate of an upper energy limit of 0.6 Mev of the beta-rays from 10-minute xenon by Seelmann-Eggebert[6] are strongly against this viewpoint. The second interpretation is that these short-period beta-particles are conversion electrons from the isomeric transition. Since the energy of the conversion electrons is so high and the conversion coefficient is rather low, it is naturally difficult to anticipate the presence of any anomaly at the beginning of the absorption curve of the beta-particles taken immediately after the extraction.

Based on the second assumption, the extent of the internal conversion of this 0.5-Mev gamma-ray transition between the two isomeric states has been estimated by comparing the β-ray intensity and the gamma-ray intensity associated with the 10-minute xenon in our calibrated ionization chamber. It is around 0.2. Dr. Alfred Nelson has kindly calculated the conversion coefficient for electric multipole radiation in two approximations, (1) non-relativistic and (2) relativistic, but neglecting binding energy of the electron (Born approximation). For elements of middle or high nuclear charge ($Z \gtrsim 40$) neither approximation is very good. However, the theoretical calculation from (1) gives a value less than our result and that of (2) is greater.

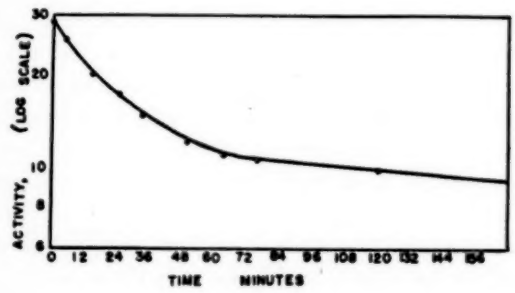

FIG. 11. Composite decay curve of xenon extracted after a period of accumulation of 5 minutes measured by β- and γ-rays.

By comparing the beta-activity of the 9.4 hr. and that of the total initial activity, it is rather obvious that the isomeric transition from the upper energy state to the lower one with a half-life of 10 minutes cannot be the only process generating the 9.4-hr. xenon. Since the 9.4-hr. half-life is approximately fifty times longer than the 10-minute one, after all the short-life xenon decays to the 9.4-hr. xenon, the activity would show only one-fiftieth as much if the detector is equally sensitive to the radiations emitted by the two substances. But since the composite decay curve of the xenon extracted from iodine even after an accumulation period of only 5 min. (Fig. 11) shows that the ratio between the total initial activity and that of the 9.4-hr. xenon is about 3:1, the major portion of the 9.4-hr. xenon must originate directly from the iodine. That is, the 6.6-hr. iodine decays with a branching disintegration into the upper and lower isomeric states of the xenon. The upper isomeric state again makes an isomeric transition by emitting a gamma-ray of around 0.5 Mev of a half-life of 10 minutes to the lower isomeric state which in turn emits a beta-particle of 9.4-hr. half-life to cesium.

The branching ratio of the iodine decay into these two states is rather difficult to determine. But estimating from the beta-activities and taking into account of the conversion coefficient of 0.2, the probability of the transition from iodine to the upper isomeric state cannot be much more than 10 percent of that to the lower isomeric state.

A disintegration scheme may be represented as:

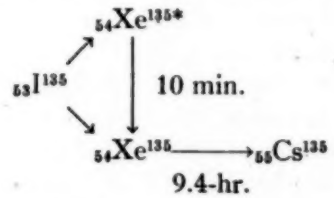

We wish to thank Professor E. O. Lawrence for his interest in this work and the Research Corporation for financial assistance.

The Adaptation of the Cauchois Spectrograph to Artificial Radioactive Sources

J. E. EDWARDS, M. L. POOL, AND F. C. BLAKE
Mendenhall Laboratory, Ohio State University, Columbus, Ohio

(Received January 8, 1945)

The transmission (Cauchois) type curved crystal spectrograph has been found to be a practical instrument for photographing characteristic x-rays associated with radioactive decay. A photograph of x-rays associated with the decay of 6.7-hour $Cd^{107,109}$ is shown. X-rays emitted during the decay of 2.7-day In^{112} and 12.8-hour Cu^{64} have also been identified.

INTRODUCTION

MANY radioactive atoms are known to emit characteristic x-rays in the process of disintegration. An accurate knowledge of the wave-length of these x-rays often helps to reveal the nature of the decay process. Such x-ray information is most useful when it is sufficiently accurate to enable one to distinguish radiations characteristic of two neighboring elements.

If x-rays are associated with the disintegration of an atom of atomic number Z, the x-rays will have wave-lengths characteristic of one or more elements having atomic numbers Z, $Z-1$, or $Z+1$. To distinguish these three possibilities the method used for studying the x-rays must be sensitive enough to distinguish wave-lengths characteristic of neighboring elements in the region Z. Absorption methods are generally successful in detecting the presence of x-rays charactersitic of the general region Z. However, absorption methods are sometimes not easily applied to distinguish x-rays characteristic of two neighboring elements, especially when radiation characteristic of both elements appears in the same chemical fraction.

Accepted x-ray methods in general have not been used to measure the wave-lengths of x-rays from radioactive materials because of the low intensity available. Even the present high intensity radioactive sources emit x-rays which are too feeble to make the ordinary slit type spectrographs of practical value. However, there are two types of curved crystal spectrographs, the reflection type and the transmission type, which may be used with present x-ray intensities. The reflection type curved crystal spectrograph has been used by Abelson[1] for wave-lengths extending from about 1.5A to 0.6A. The present work was carried out to explore the possibility of using the transmission (Cauchois) type curved crystal spectrograph for photographing the shorter wave-length x-rays emitted by radioactive sources.

THE CURVED CRYSTAL SPECTROGRAPH

The spectrograph adopted for this work is the type used successfully by Cauchois[2,3] with crystals of mica and gypsum. Quartz crystals have also been effectively adapted to this type of spectrograph by DuMond and others.[4,5,6] Although such instruments are capable of rather high resolving power, the speed factor is much more important in photographing feeble radioactive sources.

Figure 1 shows the arrangement of the spectrograph for radioactive sources which might contain high energy beta- and gamma-rays in addition to the x-rays. The strength of the magnetic field is increased until a Geiger counter between the crystal and the film shows no appreciable beta counts. Blocks of lead are placed outside the spectrograph and inside the cylinder carrying the film to shield the film from gamma-radiation at the point where a line is to be formed. Low energy beta-rays are absorbed sufficiently by the crystal to prevent the scattered electrons from fogging the film. For low energy gamma-rays the brass in the plates which hold the crystal and the iron in the spectrograph usually provide sufficient shielding.

In practice, highest efficiency is obtained by

[1] P. Abelson, Phys. Rev. **56**, 753 (1939).

[2] Mlle. Y. Cauchois, J. de Phys. **3**, 320 (1932).
[3] Mlle. Y. Cauchois, J. de Phys. **4**, 61 (1933).
[4] J. W. M. DuMond and B. B. Watson, Phys. Rev. **46**, 316 (1934).
[5] Bernard B. Watson, Rev. Sci. Inst. **8**, 480 (1937).
[6] J. W. M. DuMond and H. A. Kirkpatrick, Phys. Rev. **52**, 419 (1937).

placing the source at the most favorable angle for diffraction from an appropriate set of internal planes according to the familiar Bragg law: $n\lambda = 2d \sin \theta$. This is done with the aid of a divided circle on the back of the spectrograph having angles marked with respect to the center of the crystal. Sources such as those frequently encountered after chemical separations in radioactivity can be extended over an area of a few square centimeters to reduce self-absorption of the radiation without impairing the efficiency of the spectrograph. The position of a spectral line is to a slight extent a function of the position of the source. In the molybdenum region the maximum shift in the lines due to movement of the source is 0.004A with crystal planes having a "d" value of 2.56A. Thus an extension of the source tends to broaden the lines but the shift of a line is not important when comparing wave-lengths of two neighboring elements. The separation of the $K\alpha$ doublets of Ag and Cd is 0.024A or about 6 times the maximum displacement which could be produced in the lines by movement of the source. The displacement can be virtually eliminated by careful alignment of the source with the center of the crystal at the correct Bragg angle.

Two sizes of spectrographs were used, one having a crystal radius of 8 inches, the other a crystal radius of 15 inches. Mica and quartz crystals were employed in both spectrographs. The set of planes used in the mica has a "d" value of 2.56A and the x-ray lines are obtained in first order. This is the same set of planes employed by Cauchois[8] and reported by Favejee[7] to produce very intense reflection in powder photographs. The most suitable mica crystal thickness was found to range from about 0.15 mm to 0.5 mm. The quartz crystals were cut perpendicular to the 310 planes then ground to a thickness of .2 mm and polished. The 100, 110, and 310 planes were thus made available, all producing strong lines.[7] These planes have "d" values of 4.246A, 2.451A and 1.178A respectively.

The spectrographs were investigated with various x-ray wave-lengths to determine the optimum spectrograph size and type of crystal for greatest speed commensurate with adequate resolving power. Characteristic K lines of several elements ranging from chromium to tungsten were photographed in first order with fluorescent or direct emission radiation. In general the quartz crystals are more efficient for longer wave-lengths from 0.7A to 2.3A while the mica is more efficient at shorter wave-lengths from 0.8A to 0.2A. Highest speed was obtained with the 8 inch (crystal curved to a radius of 8 inches) quartz spectrograph in the Cu region, the 8-inch mica spectrograph in the Mo region, and the 15-inch mica instrument for shorter wave-lengths.

RESULTS

Cu^{64}

Metallic copper activated by high energy deuterons exhibits a strong 12.8-hour activity assigned to Cu^{64} by Van Voorhis.[8] Beta-rays, positrons and x-rays are associated with the decay of this activity. Abelson[1] has shown these x-rays to be characteristic of nickel by use of a reflection type spectrograph equipped with a rock salt crystal. The nickel $K\alpha$ doublet arising

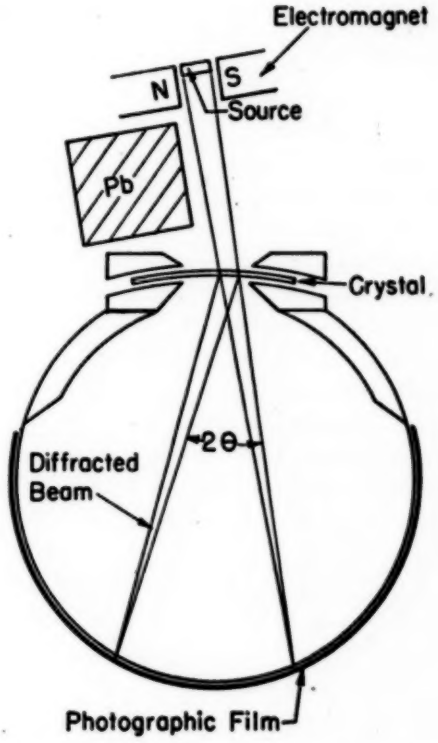

FIG. 1. Transmission type curved crystal spectrograph.

[7] T. Ch. L. Favejee, Zeits. f. Krist. **100**, 425 (1938).

[8] S. N. VanVoorhis, Phys. Rev. **50**, 895 (1936).

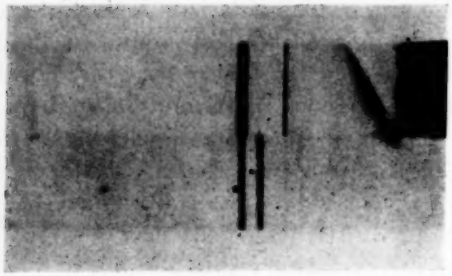

FIG. 2. Upper half—$K\alpha$, $K\beta$, and $K\gamma$ lines of Ag emitted during decay of 6.7-hour $Cd^{107,109}$. Lower half—Ag and Cd calibration lines.

from this activity was photographed in an 8-inch quartz spectrograph using the 110 planes.

Three photographs were made starting 40 minutes after bombardment. A decay curve was obtained while the exposures were in progress. The first exposure extended over 4 hours during which time the intensity of the 38.5-minute Zn^{63} dropped to 1/100 the intensity of the 12.8-hour Cu^{64}. This exposure showed no lines. The nickel lines appeared on the second photograph which was exposed for 36 hours. The third exposure of 40 hours showed no lines. Copper calibration lines were placed on half of the film by use of fluorescent radiation.

2.7-Day In^{112}

A 2.7-day activity in indium produced by deuteron bombardment of cadmium has been reported by Cork and Lawson.[9,10] The activity consists of x-rays and low energy electrons caused by two internally converted gamma-ray energies. The identification of the x-ray as characteristic of Cd by critical absorption together with the absence of positrons suggested the probability of K-capture.[10]

Photographs of Cd activated by deuterons were obtained with a 15-inch mica spectrograph. The first exposure extending over 16 hours starting immediately after bombardment showed no lines. A second exposure of 8 days gave a strong Cd $K\alpha$ line. These Cd x-rays are presumed to be caused by the 2.7-day In activity since no other isotopes have been reported which would emit strong Cd x-rays 16 hours after activation.

6.7-Hour $Cd^{107,109}$

A 6.7-hour cadmium activity has been produced by bombardment of Ag with protons[11] and by the well known Ag(d, $2n$)Cd reaction.[12] It is known to emit K and L conversion electrons,[13,14] x-rays characteristic of silver,[11,14] and a 40 second half-life has been identified in the silver fraction.[15] At one time the x-rays were thought to be characteristic of cadmium[12] but the spectrograph confirms the presence of x-rays characteristic of silver.

The photograph shown in Fig. 2 was obtained with a 15-inch mica spectrograph. The upper half of the film shows the $K\alpha$, $K\beta$, and $K\gamma$ lines of Ag resulting from the decay of $Cd^{107,109}$ produced by deuteron bombardment of Ag. The lower half shows Ag and Cd calibration lines obtained by fluorescence. The exposure to the radioactive source was carried through 4 half-lives. No cadmium lines or general radiation were detected. The Ag $K\alpha$ doublet is resolved on the original film.

The authors are grateful to Dr. DuMond for the loan of a curved crystal spectrograph which was used in preliminary experiments. It is a pleasure to acknowledge the support received from Mr. Julius F. Stone, The Ohio State University Development Fund and from The Ohio State University Research Foundation.

[9] J. M. Cork and J. L. Lawson, Phys. Rev. **56**, 291 (1939).
[10] J. L. Lawson and J. M. Cork, Phys. Rev. **57**, 982 (1940).
[11] L. A. Delsasso, L. N. Ridenour, R. Sherr, and M. G. White, Phys. Rev. **55**, 113 (1939).
[12] R. S. Krishnan and D. H. T. Gant, Nature **144**, 547 (1939).
[13] G. E. Valley and R. L. McCreary, Phys. Rev. **56**, 863 (1939).
[14] A. C. Helmholz, Phys. Rev. **60**, 415 (1941).
[15] L. W. Alvarez, A. C. Helmholz, and E. Nelson, Phys. Rev. **57**, 660 (1940).

PHYSICAL REVIEW VOLUME 67, NUMBERS 5 AND 6 MARCH 1 AND 15, 1945

Absolute *K*-Ionization Cross Section of the Nickel Atom under Electron Bombardment at 70 kv

A. EDWARD SMICK AND PAUL KIRKPATRICK
Stanford University, Stanford University, California

(Received December 10, 1944)

Nickel sheets approximately 5×10^{-6} cm in thickness were bombarded with 70 kv electrons and the intensity of the resulting $K\alpha$ radiation was measured by a special air-filled ionization chamber connected to a calibrated quadrant electrometer. Isolation of the $K\alpha$ line was effected by Ross filters of cobalt and iron, supplemented by additional filters for evaluation of a correction for the continuous background radiation. After due consideration of the effects of electron scattering in the target and all relevant x-ray absorptions, it was concluded from the observed intensities that the cross section of the nickel atom for *K* ionization by 70 kv electrons is $(3.38\pm0.2)\times10^{-22}$ cm². From this result and Williams' equation for electron energy loss it is deduced that the efficiency of production of nickel *K*-radiation by electrons of 70 kev energy is 0.35 percent.

INTRODUCTION

WHEN atoms are bombarded by electrons with energies in excess of the atomic *K*-ionization energy, there is a small but finite probability of *K* ionization. Observations[1] have told us something of the manner in which this probability varies with electron energy, but for only a few elements as targets. Theory[2] also has had something to say on this variation and, in general, has approved the observations. Concerning the *absolute magnitude* of this probability of *K* ionization through electron bombardment, we have but little precise information, either experimental or theoretical. Smith's paper contains data on helium and bombardment voltages up to 4500, but in the wide field of heavier elements and higher energies there is no experimental datum except that resulting from Clark's[3] work with silver targets at 70 kv.

The present work resembles that of Clark in that its object is to determine a *K*-ionization probability, or cross section, and its method is the measurement of the power of *K* x-ray emission. It differs in the employment of 28 Ni atoms as targets and in the abandonment of crystal reflection as the means of spectral isolation. The target material as mounted before the electron gun in our work was in the form of a sheet of nickel of surface density σ, prepared by evaporation of the metal in vacuum and condensation upon thin films of cellulose acetate which provided mechanical support without seriously contributing to the total x-ray emission. With such a target disposed for normal bombardment, the number of nickel atoms per cm² of target area is $\sigma N/A$ where N is the Avogadro number and A the atomic weight of nickel. The resulting number of *K* ionizations, being proportional to the atomic density and to the number n of bombarding electrons, may be written,

$$N_K=\Phi_K n\sigma N/A. \qquad (1)$$

The evaluation of Φ_K was the object of this investigation.

The definition of Φ_K by Eq. (1) is not unique unless attended by a limitation on the types of paths permitted to the bombarding electrons within the target, for a long path naturally means numerous ions. We impose the requirement that the electrons of Eq. (1) shall pass through the target by the shortest possible path, i.e., along a straight line normal to the target faces. Thus defined, Φ_K, which has the dimensions of an area, may be thought of as the area per nickel atom (not per *K* electron) which must be hit to insure *K* ionization. Since real electrons do not and will not follow the required minimum path, we shall have to deduce the actual path, observe the number of ionizations and compute from these

[1] Webster, Clark, and Hansen, Phys. Rev. **37**, 115 (1931); P. T. Smith, Phys. Rev. **36**, 1293 (1930). Webster, Hansen, and Duveneck, Phys. Rev. **43**, 839 (1933).
[2] H. S. W. Massey, Proc. Roy. Soc. **A129**, 616 (1930); H. S. W. Massey and C. B. O. Mohr, *ibid.* **135**, 258; **136**, 289 (1932); **139**, 187 (1933). C. Møller, Zeits. f. Physik **70**, 786 (1931); C. Møller, Ann. d. Physik **14**, 531 (1932); H. Bethe, Ann. d. Physik **5**, 325 (1930).
[3] J. C. Clark, Phys. Rev. **48**, 30 (1935).

data the number N_K of ionizations which *would have occurred* had the ideal path been followed.

The method of this investigation was to determine σ by weighing and to infer N_K by a measurement of the ionization produced in a standard ionization chamber by the Ni $K\alpha$ radiation emerging from the target in consequence of the K ionizations. For purposes of measurement, the $K\alpha$ characteristic radiation was separated from other radiations, both characteristic and continuous, by five critically balanced filters of the kind first described by Ross.[4]

This battery of filters sufficed to isolate three spectral bands, of which one included the Ni $K\alpha$ wave-length and two furnished data on the continuous spectrum power at either side. An interpolation based upon the side-band powers yielded a value for the continuous spectrum power measured with the alpha-lines and made it possible to obtain the line power alone by subtraction of this background.

The ionizations included in N_K are supposed to have been produced exclusively by the direct action of the n electrons; in a real experiment a few ionizations from other causes must be expected. We have considered the production of K ionization by electrons rediffused into the nickel target by the backing film, and by absorption in the nickel of continuous x-radiation originating in the nickel itself, in the backing film and in the aluminum cup where the bombarding electrons finally came to rest. It was found possible to show that none of these processes would, under the conditions of our experiment, produce so many as 0.001 N_K K ionizations. Because of the smallness of this error, no attempt at a correction will be made in what follows.

X-RAY SOURCE

The fragile target was supported by a springy structure of 2 mil copper wire so designed as to yield to any strains which changes of temperature or pressure might impose upon the plastic film. This structure was housed in a field-free cylinder of brass, since experience had shown how short is the life of a thin target exposed to the principal accelerating field of an x-ray tube or to the violence of the discharges which are prone to occur when high potential is first applied to a newly evacuated tube. The accelerated electrons entered the shielded space through a hole $\frac{1}{16}$ inch in diameter located on the axis of the brass cylinder and were received after passing through the target in an aluminum cup 6 inches deep from which few of them could rediffuse to the target and none could escape without flowing through the attached microammeter. No sketch is furnished here since none of the x-ray tube dimensions was critical and the whole arrangement closely resembled the tube shown in a drawing by Harworth and Kirkpatrick.[5]

Though the total area of the target was about 30 cm², the focal spot itself covered less than a tenth of this area. By a well-controlled process of evaporation the thickness of metal was held to about 500A. The surface density σ, a quantity more important than the thickness, was determined with some precision by methods to be discussed below. The Cellophane window which permitted x-rays to pass from the target to the external measuring apparatus was located so as to transmit radiation emerging from the target face at a grazing angle between two and three degrees. No measurable radiation could be picked up at the ion chamber when the tube was operated with the target removed.

FILTERS

For determining the background at the short wave side of the Ni $K\alpha$ line a balanced Cu-Ni pair was used. A sheet of nickel was brought to a thickness of 0.0035 inch by jeweler's rolls and a copper sheet was adjusted to it by electroplating copper on and off until the filters transmitted equally to about 0.25 percent at 0.200, 0.600, 0.710, 0.800, and 1.538A and also for the fluorescent radiations from strontium and nickel with their predominating constituents at 0.875 and 1.656A respectively. None of these radiations lies within the Cu-Ni pass band; transmissions in this band were investigated by the use of Zn $K\alpha$ fluorescence radiation isolated by a Bragg spectrometer from the output of a strongly irradiated piece of zinc. Of the Zn $K\alpha$ radiation, which lies right in the middle of the Cu-Ni pass band, the copper filter transmitted 50.2 percent, while the

[4] P. A. Ross, J. Opt. Soc. Am. and Rev. Sci. Inst. **16**, 433 (1928).

[5] K. Harworth and P. Kirkpatrick, Phys. Rev. **62**, 334 (1942).

TABLE I. Filter characteristics.

Filter	Type	K-limit wave-length	Pass band trans-mission coef.	To isolate	Trans-mission coef. of pair
25 Mn	Evaporated	1.8916A	0.035	Long wave background	$0.520 = T_1$
26 Fe	Electroplated	1.7394	0.555		
26 Fe	Electroplated	1.7394	0.068	Ni $K\alpha$	$0.571 = T_2$
27 Co	Electroplated	1.6040	0.639		
28 Ni	Metal sheet	1.4839	0.003	Short wave background	$0.499 = T_3$
29 Cu	Metal sheet	1.3774	0.502		

corresponding transmission coefficient of the nickel filter was 0.3 percent. These filters, perhaps because of some impurity in the nickel, came into nice balance without the addition of any third material for K-jump correction.[6]

The background at the long wave side of the Ni $K\alpha$ line was determined by using a Fe-Mn pair. The iron member was prepared by electroplating on aluminum foil from an aqueous solution of ferrous ammonium sulfate, and its mate was formed by evaporation of manganese in vacuum upon aluminum foil. Like the Cu-Ni pair, the Fe-Mn filters were balanced at several wave-lengths, a special x-ray tube with targets of copper, nickel, iron, and chromium being used, in conjunction with a spectrometer, to provide the necessary monochromatic radiations. At 1.816A, within the pass band of this pair, the transmission coefficients of the iron and manganese filters were, respectively, 55.5 and 3.5 percent.

To isolate the Ni $K\alpha$ line and its neighboring continuous radiation from the thin target, a Co-Fe filter pair was required. This pair was procured by matching the iron filter described above with a cobalt filter produced by electroplating on aluminum foil from a cobaltous ammonium sulfate bath. Each of the successful electroplated filters was the end product of a series of only partially successful attempts[7] to obtain uniform, adherent coats of filter metal upon backing sheets of aluminum of proper thickness to compensate for the dissimilarity of the K jumps of the filters to be balanced. As finally adjusted, the cobalt filter passed 63.9 percent in the pass band (at 1.656A) and its iron companion passed 6.8 percent.

[6] P. Kirkpatrick, Rev. Sci. Inst. **10**, 186 (1939).

[7] Production of these and other filters was discussed in earlier papers. See P. Kirkpatrick, Rev. Sci. Inst. **15**, 223 (1944).

By the transmission coefficient, T, of a *pair* of filters is meant the difference between the transmission coefficients of the individual members of the pair for radiation whose wave-length is the mean wave-length of the pass band. The concept has a definite significance: The difference between the powers transmitted by the two filters from an incident spectrum *of any composition* needs only to be divided by the transmission coefficient of the pair to give the power which would be recorded by the same measuring equipment if it were possible to irradiate it solely with the full-strength pass-band component of the incident beam.

Table I summarizes the properties of the five filters.

RADIATION POWER MEASUREMENT

Emerging from the Cellophane window of the x-ray tube, the thin-target radiation passed through vertical and horizontal lead-jawed slits whose carefully measured widths and positions were such as to transmit to the ion chamber a diverging beam including a solid angle Ω of 2.638×10^{-4} steradian. The chamber itself, specially designed for absolute measurements, had the internal structure shown in Fig. 1. In this view, the axis of the chamber (and of the entering x-ray beam) is seen in a vertical position, though in use this axis was horizontal. The several electrodes of the chamber consisted, as shown, of grids of fine aluminum wire. This open structure harbors little radioactive contamination and renders unnecessary any calculation of a contribution to the observed ionization from secondary x-rays or electrons originating in the electrodes. The large diameter (9.5 inches) of the envelope of the chamber (not shown in Fig. 1) allowed a clearance around the collecting volume adequate to dispose of wall effects from the envelope.

The grid wires in the space between A and B of Fig. 1 constituted the collecting electrode. Grounded guard grids of identical construction extended the plane of the collector and helped to preserve the uniformity of the collecting field. This uniformity was further promoted by a set of Taylor[8] grid loops (C) in the form of six parallel and equally spaced rectangles of wire thrown

[8] L. S. Taylor, Bur. Stand. J. Research **5**, 507 (1930).

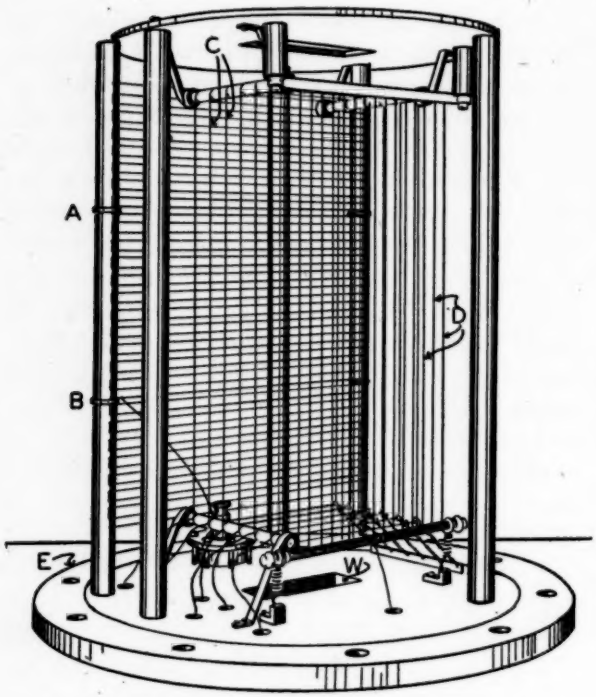

FIG. 1. Internal structure of ion chamber for absolute beam power measurement. Cylindrical brass envelope (not shown) surrounds electrode structure and is held against end plate E by bolts passed through holes shown.

about the collecting field and maintained at equally spaced potentials appropriate to their positions. The effectiveness of these grids in keeping the lines of force straight at the front and rear boundaries of the collecting region was a matter of importance, since it is necessary in absolute radiation power measurement to know the effective length of the collecting region with accuracy. Since the field was highly uniform at both ends of the collecting region it was possible to take as the effective length of the beam segment producing collected ions simply the distance separating the centers of the gaps between the collecting electrode and its adjacent front and rear guards. This distance was 10.075 cm.

In Fig. 1 may be seen the S-shaped glass hooks and spiral springs which kept the Taylor grids taut, the high voltage grid D maintained in tension by its two springs, the brass end plate E which carried the entire structure and admitted the ionizing radiation through its central cellophane window at W. The collecting electrode was fully insulated from adjacent grounded elements by amber. The chamber was filled with dry air at atmospheric pressure after some preliminary measurements with argon had shown that the heavier gas yielded the fewer collectible ions under Ni K radiation. This ineffectiveness of argon resulted from its strong absorption in the space between the entrance window of the chamber and the forward end of the collecting region.

Collected charges were measured by a Compton electrometer. Ion current saturation offers no problem with air in the chamber. The whole measuring system as calibrated by comparison with a standard condenser showed a sensitivity of approximately 10^{13} mm/coulomb. This sensitivity was not exactly constant over the entire range afforded by the electrometer scale so individual deflections were always interpreted and translated into coulombs by reference to a calibration curve.

DETERMINATION OF σ

Eight different nickel targets were used in the course of this investigation, but not all of them yielded useful data. Some were discarded because of wrinkling or fine visible perforations and some were lost through accident. The conclusions to follow were based upon three good targets here designated A, B, and C. The thickness or surface density of a metal deposit produced by evaporation may be roughly determined from the loss of weight of the filament or other source and certain geometrical considerations. In our experience, this method is dependable to about 10 percent, but no better; several other schemes for the determination of σ were considered and abandoned in favor of direct weighing.[9]

After a target had served its purpose in the x-ray tube, it was carefully removed to a punching device which cut out a neat disk 1.616 inches in diameter and concentric with the focal spot. This target specimen, of known area, was transferred to a weighed microcrucible and heated to incipient redness in the presence of oxygen in an electric furnace. This treatment presumably drove off anything that may have been left of the

[9] We are greatly indebted to Dr. J. H. C. Smith of the Carnegie Institution of Washington and Stanford University for suggesting the microbalance techniques, for making the necessary facilities available and for performing all of the weighings and associated operations.

cellulose backing and oxidized the nickel to Ni O. The oxide and crucible were then weighed on a microbalance and the weight of nickel was calculated. The Ni O was then reduced to metallic nickel by heating in the presence of hydrogen. Another weighing at this point furnished a second determination of the weight of nickel. A third value was obtained by weighing again after converting to nickel sulfate by heating with a few drops of nitric and sulfuric acids, fuming off the acid and bringing the sulfate to constant weight by heating almost to redness.

It is most unlikely that any cellulose survived this treatment, and the good agreement among the three determinations tends to justify the view that it departed completely during the initial heating.

The processes just described yielded the mean surface density of each nickel disk, but not that of the focal spot at its center. In the evaporation process the plane, horizontal cellulose film was supported above a concentrated filament of hot nickel. This arrangement deposits a metal film whose thickness is proportional to the fourth power of the cosine of the angle θ between the metal beam and the vertical; the thickest part is thus directly above the source and this is the portion of the target which subsequently receives the electron bombardment. The mean surface density directly determined by the weighing operations is evidently smaller than the required σ at the focal spot. It may be shown from the $\cos^4\theta$ law that the ratio of these surface densities is the inverse ratio of the squares of the cosines of the angles θ for the peripheries of the concentric circular areas to be compared. For all of our targets this argument indicates that the mean surface densities resulting from the weighings should be multiplied by a correction factor 1.023 to give σ.

Table II summarizes these results.

TABLE II. Focal spot surface densities. Tabulated masses are in milligrams.

Target designation	*A*	*B*	*C*
Mass of Ni O	0.926	0.635	0.790
Mass of Ni calculated from Ni O	0.728	0.499	0.621
Mass of Ni after reduction	0.733	0.507	0.630
Mass of Ni SO_4	1.938	1.303	1.644
Mass of Ni calculated from Ni SO_4	0.735	0.494	0.624
Mean mass of Ni	0.732	0.500	0.625
Mean surface density over test disk (gm/cm²)	5.54×10^{-4}	3.78×10^{-4}	4.73×10^{-4}
Mean surface density σ over focal spot (gm/cm²)	5.67×10^{-4}	3.87×10^{-4}	4.84×10^{-4}

DETERMINATION OF N_K

The relation between N_K and the charge collected and measured in the ion chamber involves a number of auxiliary constants. We consider first the ratio of N_K to the real number of K ionizations produced. For a target so thin that it absorbs only a small fraction of the energy of the average bombarding electron, the number of K ionizations may be regarded as proportional to the path length in the metal. For those electrons deviated only by multiple scattering, the ratio of the mean path length to the thickness of a thin target is adequately given[10] by $a=1+(1/2)\lambda^2$ where λ is Bothe's[11] most probable emergence deflection from the direction of incidence. For the present case, which is that of metallic nickel in sheets of surface density σ subjected to normal bombardment at 70 kv, the equation above becomes $a=1+247\sigma$. Values of a for the various targets, computed from the values of σ of Table II, are listed in Table III.

TABLE III. Single and multiple scattering correction factors at 70.0 kv.

Target	*a*	*b*	*ab*
A	1.013	1.011	1.024
B	1.009	1.008	1.017
C	1.012	1.009	1.021

The multiple scattering corrections developed above take care of electron-nucleus collisions where the impact parameter exceeds 0.8×10^{-10} cm, a limit set by Bothe's theory. It remains to consider the effect of the large-angle single scattering which befalls those electrons (about 1 percent of the total in our targets) which experience closer approaches. Correction factors for such collisions were computed by assuming Rutherford scattering and summing the effects of all the paths extended by this cause. The details of this calculation will be explained in another

[10] D. L. Webster, H. Clark and W. W. Hansen, Phys. Rev. **37**, 127 (1931).

[11] W. Bothe, *Handbuch der Physik* (1927), Vol. XXIV, Chap. 1, Sec. 9. A. H. Compton and S. K. Allison, *X-Rays in Theory and Experiment* (D. Van Nostrand Company, Inc., New York, 1935), p. 76.

connection.[12] Table III presents the results in the form of a constant b defined as a ratio in which the numerator is the mean nickel path length of all electrons under the assumption that those not subject to single scattering pass through by the shortest or normal route, and the denominator is the thickness of the target.

The actual number of K ionizations in a given target, after its determination by radiation measurements, must be divided by the appropriate ab from Table III to obtain N_K. This carries out the general plan explained in the introduction.

Other constants involved in the determination of N_K are the transmission coefficients of the various absorbers through which the x-radiation must pass, the mean x-ray energy expended per ion pair produced in air, the K fluorescence yield, w_K, of nickel, and the ratio c of the number of emitted nickel $K\alpha$ quanta to the total number of emitted quanta in all lines of the K series. This latter constant is easily obtained from measurements[13] of relative intensities of spectral lines. Williams found the intensity ratio of nickel $K\beta_1$ to $K\alpha_1$ to be 0.187 at a thick target face, and calculated this figure to be one percent higher than would have been the case had no x-ray absorption taken place in the target. For the ratio of α_2 to α_1 the figure was 0.495, with or without target correction. Meyer measured the ratio of the intensities of nickel β_2 to α_1, obtaining 0.0020, a result too small and inexact to merit target correction. No other K lines of comparable strength exist. Using the fact that the ratio of the intensities of two lines is the product of the ratio of their frequencies by the ratio of the numbers of quanta emitted, we find $c=0.898$.

TABLE IV. Corrections for absorption of $K\alpha$ radiation by targets.

Target	θ (radians)	σ	k_1
A	0.0486	5.67×10^{-5}	0.967
B	0.0358	3.87×10^{-5}	0.970
C	0.0332	4.84×10^{-5}	0.956

The K fluorescence yield, w_K, is defined as the ratio of the number of fluorescence K quanta emitted by an assemblage of similar atoms in any time interval to the number of atoms ionized in the K shell in the same time. From the six available determinations[14] for nickel, ranging from 0.364 to 0.436, we adopt Stephenson's value of 0.385 as being the most recent and also close to the unweighted mean of the group.

To determine the x-ray energy absorbed in the ionization chamber, it is necessary to apply to the ionization charge measurements the factor ϵ, defined as the mean energy (in ergs) absorbed in the air per ion pair produced. Binks'[15] survey of all work up to 1936 on this often-measured quantity shows that those determinations which seem the most reliable vary by 10 percent among themselves. In adopting the value 5.13×10^{-11} ergs (32 ev) we are introducing at this point the largest single source of uncertainty afflicting the final results of the present paper.

Between emission in the target and arrival in the collecting volume of the ion chamber the nickel radiation was subject to absorption in the target, in the Cellophane windows of tube and chamber, in the filters, and in air both within and without the chamber. The absorption by the filters has already been discussed. The air absorption was determined by investigation of an air sample contained within a brass tube 69.6 cm long between its aluminum windows. This tube was connected to a vacuum pump and placed between an ion chamber and a sheet of metallic nickel, excited to strong fluorescence by a neighboring Coolidge tube. Operation of the pump connections served to admit or remove the absorbing air, and the balanced Co-Fe filters described above separated the nickel α and β fluorescence radiations and excluded the latter. On taking due account of temperature and pressure (though not of humidity), a mass absorption coefficient[16] of 12.0 $cm^2\ g^{-1}$ for air at λ1.656A was

[12] L. Pockman, D. L. Webster, K. Harworth and P. Kirkpatrick. A paper on the variation of the Ni K-ionization cross section with electron bombardment energy will be submitted to the Physical Review.

[13] J. H. Williams, Phys. Rev. **44**, 146 (1933). H. T. Meyer, Veroff. wiss. Siemens-Konzern **7**, 108 (1929). A. H. Compton and S. K. Allison, *X-Rays in Theory and Experiment* (D. Van Nostrand Company, Inc., New York, 1935), p. 640.

[14] M. Balderston, Phys. Rev. **27**, 696 (1926); R. J. Stephenson, Phys. Rev. **51**, 637 (1937). This paper cites all previous work except that of Balderston.

[15] W. Binks, *Reports on Progress in Physics* (London Physical Society, 1936), Vol. 3, p. 347.

[16] W. Stockmeyer, Ann. d. Physik **5**, 12, 71 (1931), gives a formula for the mass absorption coefficients of air which likewise indicates a value of 12.0 $cm^2\ g^{-1}$ at the wave-length of our observations. We also obtained the value 7.78 $cm^2\ g^{-1}$ at the wave-length of Zn $K\alpha$ as against Stockmeyer's 7.77.

computed. Under the conditions of thin-target measurements an air path of 52.7 cm intervened between the tube window and the collecting region, transmitting a fraction 0.467 of the incident Ni $K\alpha$ emerging from the tube. This fraction we denote by k_a.

By methods similar to those used to determine air absorption, the two Cellophane windows were found to transmit 0.764 of the Ni $K\alpha$ power and this fraction is designated k_w.

It was assumed that the radiation emerging from the thin target had to traverse a mean path length $x/(2 \sin \theta)$ within the target, where x is the normal target thickness and θ is the grazing angle of emergence of those rays destined for the ion chamber. This is merely assuming that radiation is produced uniformly throughout the target thickness and that the target surfaces are plane. The emerging fractions, designated k_t in Table IV, will then be given by $\exp(-(\mu/\rho)\sigma/(2 \sin \theta))$.

The length of the region of the ion chamber within which x-rays could be absorbed with full collection of the resulting ions was stated above to be 10.075 cm. Such a length of air absorbs 0.134 of the Ni $K\alpha$ radiation, a fraction later to be designated as k_c.

The problem of separating line radiation from continuous background may be considered in relation to Fig. 2 which illustrates in a purely schematic manner both constituents of the thin nickel spectrum as incident upon the filters. Vertical lines have been drawn at the K limits of the filters to show the boundaries of the pass bands. It will be noted that the region of the β lines has been avoided. The figure is far from correct in its portrayal of the relative powers of line and continuous, since in reality the continuous radiation in the panel numbered 2 should be of the order of one percent of the $K\alpha$ line power, a fact of which we were unaware when this work began.

The function of the filters isolating panels 1 and 3 was to determine this almost negligible background. The ionization charge collected in some selected time of observation t with the nickel filter in the beam is subtracted from that collected with copper. The difference divided by the transmission coefficient of the pair gives the entire band power represented by the shaded area 1. Further division by the wave-length

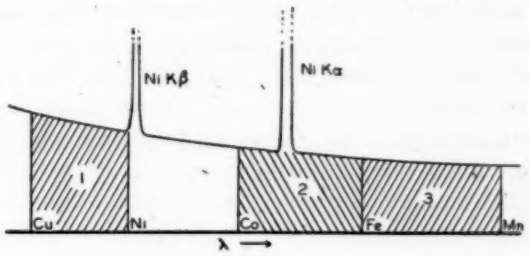

FIG. 2. Schematic plot of a portion of the continuous and line spectra from a nickel target, with spectrum power or intensity plotted against wave-length λ. Vertical lines beside atomic symbols show wave-length positions of the respective K absorption limits and divide the spectra into pass-band panels of which 1, 2, and 3 were measured.

breadth of the pass band gives a result proportional to the mean ordinate of panel 1. Panel 3 is then treated in the same way and an interpolation is effected which yields the continuous spectrum ordinate of panel 2. Multiplying this ordinate by the breadth of panel 2 gives the ionization charge which would have been collected had it been possible to irradiate the chamber with all the *continuous* radiation of panel 2 without the line. This small indirectly ascertained charge must be deducted from the *total* content of panel 2 to give Q_a, the charge (in coulombs) produced by the Ni $K\alpha$ line alone in the adopted time t of observation.

During this time n electrons have struck the thin target, producing $N_K ab$ ionized nickel atoms. From what has gone before we may now set up the relation between the defined magnitudes in the form

$$N_K = 4\pi Q_a \epsilon / abc\Omega w_K h \nu_a e k_a k_w k_t k_c T_2. \quad (2)$$

In this equation h is the Planck constant, ν_a is the frequency of the nickel $K\alpha$ line and e is the electronic charge in coulombs.

DETERMINATION OF Φ_K

With a current i (in amperes) impinging upon the target for time t the total number n of bombarding electrons is it/e. Substituting this expression and Eq. (2) into Eq. (1), we find,

$$\Phi_K = 4\pi Q_a \epsilon A / abc\Omega w_K h \nu_a k_a k_w k_t k_c T_2 N \sigma i t. \quad (3)$$

The quantities (Q_a/it), a, b, σ, k_t have different values for the differing targets used. The current i also varied from time to time and its mean value during each ionization observation was recorded.

Using Q as a general symbol for a measured ionization charge, with a subscript to indicate the filter in use during the measurement, we may form the dimensionless ratio $(Q/it)_x$ for each set of observations and summarize the results with one of the targets (B) in the manner of Table V. Insertion of this last result in Eq. (3) gives

$$\Phi_K = 3.36\times10^{-22}\ \text{cm}^2.$$

Each datum in Table V is a mean of ten observations. It is evident that the background measurements are quite undependable and the background deduction may well be wrong by 100 percent. Its effect upon Q_α is slight however, and causes no trouble.

Targets A and C gave, respectively, 3.39 and 3.38×10^{-22} cm² for Φ_K. The ionization measurements are reliable to better than one percent, so the error of the final result is practically the error of (ϵ/w_K), which at present is of the order of ±5 percent. It is concluded therefore, on the basis of this investigation, that $\Phi_K=(3.38\pm0.2)\times10^{-22}$ cm². Future improvement of our knowledge of (ϵ/w_K) may be able to cut the stated error in half.

Theoretical studies in print do not carry the problem far enough to supply an entirely satisfactory check on the experimental result. The classical quantum theory of Thomas,[17] though quite out of date, has the merit that its conclusions may be evaluated without ambiguity. The addition of a refinement due to Webster, Hansen, and Duveneck[18] puts the prediction of this theory relative to K-ionization cross section into the form

$$\Phi_e=\frac{2\pi e^2}{V_K^2}\cdot\frac{1-U^{-1}+(2T/3)(1-U^{-2})}{U}, \qquad (4)$$

where U is the ratio of bombardment energy to K-ionization energy, T is the ratio of orbital kinetic energy to ionization energy, V_K is the K-ionizing potential and e the electronic charge, both in electrostatic units. For our case $U=8.38$, $T=1.19$, and $\Phi_e=3.70\times10^{-22}$, a result ten percent higher than the experimental value. This finding resembles that of Clark[3] whose observed cross section for silver was somewhat below the prediction of Eq. (4).

[17] L. H. Thomas, Proc. Camb. Phil. Soc. **23**, 829 (1927).
[18] Webster, Hansen, and Duveneck, Phys. Rev. **43**, 839 (1933).

TABLE V. Ratios of collected ion charges to bombardment charges for target B.

$(Q/it)_{Co}$	8.32×10^{-9}
$(Q/it)_{Fe}$	2.15×10^{-9}
$(Q/it)_{Co}-(Q/it)_{Fe}$	6.17×10^{-9}
$(Q/it)_{Cu}$	5.30×10^{-9}
$(Q/it)_{Ni}$	5.27×10^{-9}
$(Q/it)_{Cu}-(Q/it)_{Ni}$	0.03×10^{-9}
$(Q/it)_{Mn}$	2.06×10^{-9}
$(Q/it)_{Fe}-(Q/it)_{Mn}$	0.09×10^{-9}
Background deduction	0.06×10^{-9}
(Q_α/it)	6.11×10^{-9}

Turning to wave-mechanical treatments of the problem, we find that the theory of Bethe[19] may almost be applied. His K-ionization cross section may be written as

$$\Phi_B=(2\pi e^2 b/V_K^2 U)\ln(4U/B). \qquad (5)$$

The quantities b and B are constant for any given element and electron shell. Bethe gives the value $b=0.35$ for K electrons of 29 Cu and since the variation of b with Z is apparently slow and regular, we use the copper value for 28 Ni. Unfortunately B is not defined explicitly; it is said to be of the order of unity, though Webster, Hansen and Duveneck[18] found the value 6 to fit their *relative* measurements of silver K-ionization probabilities best. It is some advantage that this speculative constant occurs under the logarithm. Without an exact theoretical value we cannot do more than remark that Eq. (5) would predict the result we observed *if* B possessed the value 4.5.

These agreements between theory and experiment are neither good enough to be highly gratifying nor bad enough to be alarming. The degree of agreement suggests that no major blunders afflict either the theoretical or the experimental work; the remaining disagreement indicates the need for more work, particularly on the theoretical side.

ENERGY AND PRODUCTION EFFICIENCY OF NICKEL K RADIATION

The number n_α of $K\alpha$ quanta emitted within the target is $\Phi_K N\sigma w_K c/A$ per bombarding electron. This expression, which includes all directions of emission, has for nickel targets under 70

[19] H. Bethe, Ann. d. Physik **5**, 325 (1930).

kv bombardment the value 1.19σ if the values we have determined or adopted for Φ_K, w_K and c are correct. The total energy of nickel K series lines, as may be deduced from relative measurements[18] of line intensities, is $1.351\times10^{-8}n_a$. Substituting $n_a=1.19\sigma$ in this result, we have as the total energy of K radiation emitted by nickel subjected to electron bombardment at 70 kv the value $1.61\times10^{-8}\sigma$ ergs per bombarding electron. Again it is noted that σ must be small enough so that all depths of the target are subjected to substantially the incidence bombarding energy and so that the electrons experience, on the average, only small deviations within the target.

It is not difficult to compute the efficiency of x-ray production under these conditions. The energy loss suffered by an electron having the relative speed β in passing through a layer of surface density σ may, by a slight modification of the formula of Williams,[20] be stated in the form $-E=3.38\times10^{-6}Z\beta^{-1.4}\sigma/A$. Upon evaluating this loss for a 70-kv electron in nickel and dividing the result into the K radiation output of the preceding paragraph, we arrive at an efficiency of 0.0035 or 0.35 percent. This is not the efficiency of production of nickel K radiation from a *thick* target under 70 kv bombardment; in such a case the electron remains productive while its energy declines from the initial 70 kev to K-ionization energy at 8.35 kev. Evaluation of the radiant output and efficiency then requires knowledge of the variation of Φ_K with electron energy, a subject beyond the scope of this paper.

[20] E. J. Williams, Proc. Roy. Soc. **A130**, 310 (1932). A factor $2Z/A$ has been applied to Williams' expression, following the recommendation of D. L. Webster.

PHYSICAL REVIEW VOLUME 67, NUMBERS 5 AND 6 MARCH 1 AND 15, 1945

Forbidden Lines λ2967.5 and λ2269.8 of Mercury HgI

S. MROZOWSKI
Department of Physics, University of Chicago, Chicago, Illinois

(Received December 18, 1944)

The structure of the forbidden lines λ2967.5 ($6^1D_2\rightarrow6^3P^\circ_0$) and λ2269.8 ($6^3P^\circ_2\rightarrow6^1S_0$) of neutral mercury was studied with a high resolving power in order to get evidence for their perturbational nature. It was predicted some time ago by several authors that these lines should be emitted only by the odd isotopes of mercury. The emission would be of the electric dipole type, the selection rule $\Delta J=0, \pm1$ being partially invalidated by the weak interaction of the outer electrons with the nuclear magnetic moment. Only one line, namely λ2655.8 ($6^3P^\circ_0\rightarrow6^1S_0$) of mercury was analyzed in the past and definitely shown to belong to this category. The structure of the line λ2967.5 was fully resolved in the third order of a 30-foot Chicago grating. The structure of the line λ2269.8 was obtained by means of an aluminized Fabry-Perot etalon and a medium size quartz spectrograph. All components predicted for both cases were observed, except a very weak one for the line λ2269.8. The distances and intensities are in a very good agreement with theoretical predictions, hence establishing beyond doubt the nuclear perturbational nature of the forbidden transitions in the spectra of unperturbed atoms of zinc, cadmium, and mercury.

THERE is a certain ambiguity in the definition of a forbidden line. The definition that only the lines emitted by an unperturbed atom and obeying the selection rules for the electric dipole radiation should be called allowed, all the others—forbidden, is a very impractical one, since most of the quantum designations are approximate, the degree of approximation depending from the coupling conditions. It seems most convenient to call forbidden for the atom not perturbed by external forces all the lines not emitted at all or emitted with a transition probability not greater than about 10^{-4} of the highest transition probability found for the given atom in the optical region. Some forbidden lines appear only and acquire a considerable intensity in

external fields—the so-called enforced dipole lines; they can be easily recognized by their considerable broadening if a spectrograph with a high resolving power is used. A large number of forbidden lines are caused by an electric dipole radiation enforced by internal interactions occurring between different electrons in atomic shells. These interactions are making approximate all quantum number designations, with the exception of the total angular momentum J and the even-odd symmetry relation. The remaining forbidden lines—likewise emitted spontaneously by an unperturbed atom—are violating one or both of the selection rules for the electric dipole radiation: (1) Laporte's odd⇄even rule, and (2) angular momentum rule $\Delta J=0, \pm 1$ with $0\rightarrow 0$ excluded. The lines violating the first and some of them also at the same time the second rule are the electric quadrupole, and the lines violating only the first one are the magnetic dipole lines. All these lines were thoroughly investigated in the past, and it was shown that their type can be easily determined by study of their Zeeman effect or their hyperfine structure.[1]

There is, however, a whole group of forbidden lines known especially well in the spectra of HgI, CdI and ZnI, which are violating only the second rule, and therefore the corresponding radiation can be only (a) electric dipole or, (b) electric octopole (magnetic quadrupole). The second possibility (b) is very improbable. It has been therefore suspected for quite a long time, that the emission of these lines, among them of the two famous mercury lines, λ2655.8 and λ2269.8, is caused by coupling of the electronic shell with the nuclear magnetic moment I. The process of emission would be essentially similar to the electric dipole emission enforced by the interelectronic interactions. In the given case, the total angular momentum J of all electrons becomes only an approximate quantum number, the total angular momentum of the system being given by the quantum number F. Therefore, the rule $\Delta J=0, \pm 1$ is no more strictly valid and a violation can occur with a probability depending of the strength of interaction between J and I.

A direct evidence for the assumption was obtained in case of the mercury line λ2655.8 ($6^3P^\circ_0\rightarrow 6^1S_0$) by a direct observation of its hyperfine structure.[2] Two components are found with a separation indicating that they correspond to two mercury isotopes with masses differing by two units. There are two odd mercury isotopes 199 and 201 with nuclear spins of $\frac{1}{2}$ and $\frac{3}{2}$. The even isotopes 198, 200, 202 and 204 have no nuclear spin and no emission can take place in view of the rigorous application of the selection rule number 2. Opechowski[3] calculated the theoretical transition probabilities for those two isotopes and showed that the intensities of the two components should be in a ratio slightly different from the ratio of the concentration of isotopes. This seems to be in agreement with the observations. However, no measurements of intensities were performed at that time. Further it is not quite certain if the relative concentrations of metastable atoms are equal to the relative concentrations of isotopes in the mixture, since several processes of different kinds lead to the destruction and formation of metastable atoms, among others the refilling of the $6^3P^\circ_{10}$ state by collisions with metastable atoms of the even isotopes (infinite lifetimes). Finally the distance of the two components was calculated indirectly as the distance of centers of gravity of multiplets from the hyperfine structure pattern of the line λ2537. It seemed therefore worthwhile to secure a still better check for the theoretical relations by studying the structure of the other forbidden line of mercury λ2269.8 ($^3P^\circ_2\rightarrow {}^1S_0$) and observe the positions and relative intensities of different components belonging not to two different, but to the same isotope.

Goudsmit and Bacher[4] discussed the source of the perturbation in the positions of the hyperfine levels of the 6^3D_1 and 6^1D_2 states for the odd isotopes of mercury and suggested that the very faint line λ2967.5 observed next to the allowed line λ2967.3 ($6^3D_1\rightarrow 6^3P^\circ_0$) is caused by the interaction of the nuclear moment with the

[1] See the reviews on forbidden lines: W. Rubinowicz and J. Blaton, Ergeb. d. Exakt. Naturwiss. XI, 176 (1932); I. S. Bowen, Rev. Mod. Phys. **8**, 55 (1936); H. Niewodniczanski, Acta Phys. Polonica **5**, 111 (1936); S. Mrozowski, Bull. Polish Inst. Arts and Sci. Am. **2**, 200 (1943), or S. Mrozowski, Rev. Mod. Phys. in preparation.

[2] S. Mrozowski, Zeits. f. Physik **108**, 204 (1938).

[3] W. Opechowski, Zeits. f. Physik **109**, 485 (1938).

[4] S. Goudsmit and R. F. Bacher, Phys. Rev. **43**, 894 (1933).

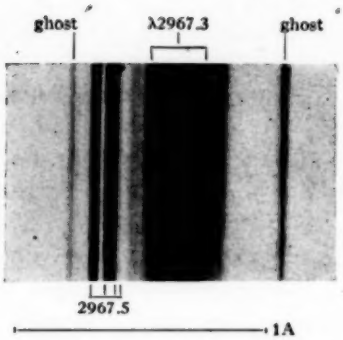

FIG. 1. Photograph of the forbidden line λ2967.5 obtained in the third order of a 30-foot grating (dispersion 0.2A/mm).

outer electrons. This line would be then in principle analogous to the line λ2269.8. Since the forbidden line λ2967.5 was only partially resolved by Wendt[5] (two components, one of them unsharp) it was decided first to study the structure of this line and after that to proceed with the much more difficult task of investigating the line λ2269.8. Only a big grating with a high dispersion can be used as a spectrograph for this purpose. The weak line λ2967.5 is so close to the strong line λ2967.3 that only for a very high dispersion the line is not disappearing in the halo surrounding the line λ2967.3. For the same reason a ghost free grating has to be used. The resolving power of the grating is not of such great importance, since the distances of the components are not very small (a resolving power of 160,000 is just sufficient). Wendt[5] used the fourth order of an excellent 21-foot Rowland grating and failed to split the short wave triplet because his source probably emitted too broad lines. Maybe also the temperature fluctuations in the grating room prevented him from obtaining the highest resolution in long exposures. In the experiments described in this paper the third order of a 30-foot, 30,000 lines per inch grating number 1 was used. This grating is giving a less intense spectrum and is possessing less resolving power than the grating number 3 used for most of other spectroscopic work in this laboratory, but is showing considerably weaker ghosts. Exposure times were relatively short (1–3 hours), so no special precautions had to be taken into consideration.

As a strong source of the forbidden line an all quartz high vacuum water-cooled mercury arc of a special design[6] in an end-on arrangement was used. The current was adjusted to a quite high level (10–12 amp), so as to weaken the line λ2967.3 by reabsorption, keeping at the same time the width of the components at a reasonably low value. It was found before[6] that this mercury arc provides very sharp lines even at such high density of current. A photograph of the line λ2967.5 obtained with this source is reproduced in Fig. 1. Between the line λ2967.3 (wide over-exposed dark band) and its long wave-length ghost a group of four components can be recognized with the relative positions: 0 (10), +0.553 (5), +0.828 (4) and 1.048 cm^{-1} (<1), the intensities given in parenthesis are, values estimated roughly on a scale of ten.

In Fig. 2 the level scheme for the two odd isotopes of mercury is presented after Goudsmit and Bacher.[4] On the outside are drawn the unperturbed hyperfine structure levels for the states 6^3D_1 and 6^1D_2, and towards the center the same levels are inserted after a correction for the mutual repulsion of the levels with the same quantum number F was introduced. Only perturbed levels of the 6^1D_2 state are combining with the $6^3P^\circ_{10}$ state, since they have an admixture of the eigenfunctions of the 6^3D_1 state, and are producing the structure of the forbidden line represented in the lower part of Fig. 2. The structure obtained experimentally is in excellent agreement with the predictions of Goudsmit and Bacher. Even the weakest component is well visible on Fig. 1. The calculated splittings of the levels deviate considerably from the distances obtained experimentally by Schüler and Jones.[7] This deviation induced Casimir[8] to express a pessimistic view about the ability of the perturbation theory to give an explanation for the observed interaction. According to the opinion of Goudsmit and Bacher,[4] however, Casimir[8] was overestimating the accuracy of the measurements of Schüler and Jones.[7] The results here reported show a very good agreement with the values of Goudsmit and Bacher and confirm their suspicions regarding the work of Schüler and Jones.

[5] G. Wendt, Ann. d. Physik **37**, 545 (1912).

[6] S. Mrozowski, Zeits. f. Physik **95**, 524 (1935).

[7] H. Schüler and E. G. Jones, Zeits. f. Physik **77**, 801 (1932).

[8] H. Casimir, Zeits. f. Physik **77**, 811 (1932).

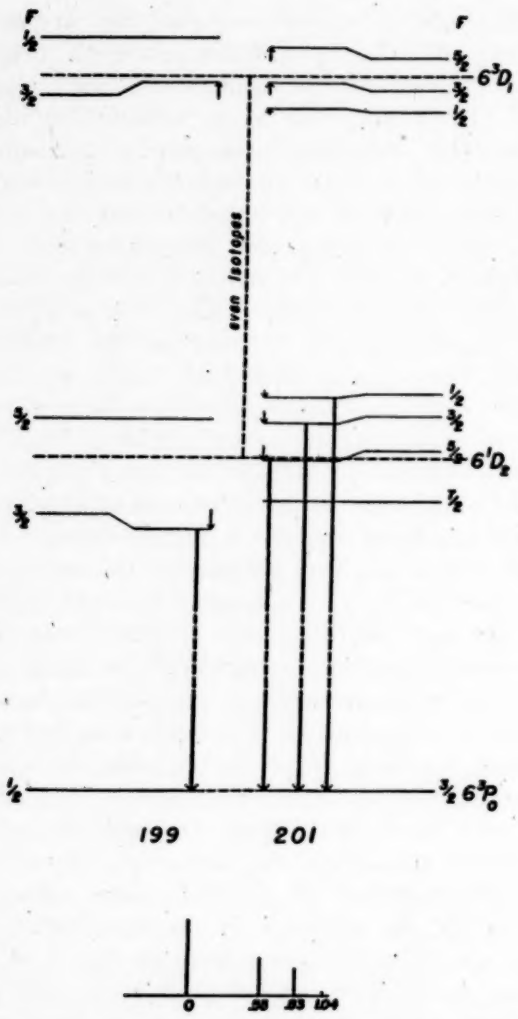

FIG. 2. The level scheme for the isotopes 199 and 201 of mercury. Unperturbed levels outside, levels after introduction of the mutual perturbational repulsion—closer to the center. Below the predicted structure of the forbidden line λ2967.5 according to Goudsmit and Bacher (reference 4) (corrected for isotope shift).

Schüler and Jones investigated the lines corresponding to allowed transitions from the states 6^3D_1 and 6^1D_2 to $6^3P^\circ_{2,1,0}$ and from their structures derived the level scheme. A careful inspection of the structures of these lines reveals however that most of the components corresponding to low values of the quantum number F are either very weak or are at least partly overlapped by other stronger components. Therefore any analysis must be in consequence of a relatively lower accuracy for the levels having low F-quantum numbers.

The forbidden line λ2269.8 has been obtained in a condensed discharge by Hansen, Takamine, and Werner[9] and later with a much higher intensity in a branched arc by Takamine and Fukuda.[10] Foote, Takamine, and Chenault[11] studied the optimum conditions for the excitation of this line and showed that a current of 0.25 amp/cm² gives the highest relative intensity of the line. Pure mercury vapor at a comparatively low density was used. As it became clear later, this condition was necessary in order to keep the number of collisional transfers to lower states $6^3P^\circ_{1,0}$ as low as possible. On the other hand, the current has to be kept low as to decrease the probability of destruction of metastable atoms by excitation to higher states. End-on observation of the above mentioned mercury arc showed that the line in question can be obtained with a considerable intensity if the current is kept low and the arc is well cooled. Although the intensity relative to other lines decreases above 0.25 amp per cm², however, the absolute intensity increases steadily to about 0.9 amp per cm². In order to have an intensity as high as possible without increasing too excessively the intensity of other lines and of the continuous background in the neighborhood of the line, a current of about 0.6 amp per cm² was maintained. At first an attempt was made to obtain a picture with the second order of the 30-foot aluminized grating number 3, however without success (48 hr. exposure did not reveal even the slightest traces of the line). Subsequently a quite heavily aluminized Fabry-Perot etalon in conjunction with a medium quartz spectrograph (Hilger E3) was tried. The greatest difficulty was encountered in the presence of a continuous background, which can be only partly avoided by a corresponding decrease of slit width. Photographs of the line were obtained with this arrangement in 2–3 hours. Longer exposures could not be made in view of the interference of the background. Three components were found with decreasing intensities: 0(5), 0.300(2) and 0.620 cm^{-1}(1), the distances being very uncertain in view of the haziness of the components. The photograph

[9] H. Hansen, T. Takamine, and S. Werner, Kgl. Danske Vid. Sels. Math.-Fys. Medd. V, 3 (1923).
[10] T. Takamine and M. Fukuda, Phys. Rev. 25, 23 (1925).
[11] P. D. Foote, T. Takamine, and R. L. Chenault, Phys. Rev. 26, 165 (1925).

cannot be reproduced here, since the pattern is very weak and of a low contrast (low reflection coefficient of aluminum for such a short wavelength).

If the assumption about the origin of the line λ2269.8 is correct and the emission of the line is caused by the interaction of the nuclear magnetic moment with the electrons, the case would be exactly analogous to the case of the line λ2967.5 with the slight difference, that the perturbing levels are below the perturbed levels and that the perturbation is much weaker in view of the great distance of perturbing levels (4630 cm^{-1} instead of 3 cm^{-1}, ratio of 1543 times). Four components are therefore expected with positions 0, 0.325, 0.613 and 0.793 cm^{-1}, the first belonging to the isotope 199 and the other three to the isotope 201. The relative intensities, as predicted by Einaudi[12] are 63.6, 23.0, 11.6 and 1.8 percent. The calculations are simplified in this case by the fact that the distance of all perturbing levels is practically the same (separation of $6^3P^\circ_2$ and $6^3P^\circ_1$ states). In Fig. 3 the predicted and observed patterns are represented. They are in a quite good agreement. The failure to observe the fourth component is easily explainable by its weakness.

The results obtained in this work are furnishing an additional evidence for the perturbational nature of the forbidden lines in the spectra of ZnI, CdI and HgI and are showing that the lines are emitted only by the odd isotopes of those elements. It is important to keep in mind that the relative intensities of components are not proportional to the concentrations of isotopes and for a given isotope not proportional to the statistical weights of the levels. Obviously in these spectra all the other forbidden lines, which violate the Laporte's rule and whose intensities increase proportional to the square of the current[13] are caused by the perturbing effect of the electric fields in the discharge. For one of these lines at least the evidence of its character was given by observation of its width and its Zeeman effect by Segrè and Bakker.[14]

In connection with these experiments it may be worth while to mention that the two other forbidden lines λ2536.04 and λ2379.45 mentioned by Goudsmit and Bacher[4] and presumably also of a nuclear perturbational type were carefully looked for and found not present in the spectrum of the mercury arc. The high intensity with which the line λ2967.5 can be obtained suggests that an investigation of the Zeeman

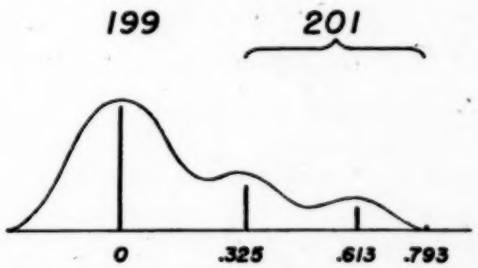

FIG. 3. Predicted and observed structures of the forbidden line λ2269.8.

effect in such a perturbational line, especially of the Paschen-Back transformation, can be of a considerable interest.

The author is very much indebted to Professor G. S. Monk for a loan of a Fabry-Perot etalon and for the kind permission to use his apparatus for aluminizing the plates.

[12] R. Einaudi, Rend. R. Acc. dei Lincei **17**, 552 (1933).

[13] M. Fukuda, Jap. J. of Phys. **3**, 139 (1924).

[14] E. Segrè and J. C. Bakker, Nature **128**, 1076 (1931).

PHYSICAL REVIEW VOLUME 67, NUMBERS 5 AND 6 MARCH 1 AND 15, 1945

An Investigation of Short-Time Thermionic Emission from Oxide-Coated Cathodes

ROBERT L. SPROULL*
Cornell University, Ithaca, New York
(Received July 12, 1943)

Vacuum-tube circuits were developed to measure thermionic current as a function of time for times ranging from 0.2 to 300 μsec. The decay with time of the temperature-saturated electron emission from oxide-coated cathodes was observed with this apparatus. Simultaneously with the application of anode voltage to an experimental diode the thermionic current density rose to an initial value and subsequently decayed to a steady value 1/5 to 1/15 of the initial value. The rate of decay was proportional to the current density, the decay requiring about 20 μsec. at 1200°K and about 500 μsec. at 900°K. The initial current exhibited a somewhat greater anode-voltage effect than did the steady-state current. The range of decay was independent of the thickness of cathode coating over the region 1 to 30 mg of oxide per cm². An electrolytic conduction hypothesis of the decay process is proposed. The form of the observed current as a function of time agreed with the form predicted by this theory. The observed rate of decay, as interpreted on the basis of the electrolytic conduction hypothesis, indicated that within a single crystal of barium or strontium oxide between 0.05 and 0.5 of the total conduction current is ionic. The possible connection of this decay and the "flicker effect" is noted.

I. INTRODUCTION

ALTHOUGH the first oxide-coated cathode was prepared forty years ago, knowledge of the process of thermionic emission from such cathodes is still in a very unsatisfactory state. Recently, experimenters have applied to these emitters periodic fields such that current was drawn during a pulse of a few μsec. duration and no current was drawn for the rest of a period. It was discovered that the average temperature-saturated current during each pulse was considerably greater than the current which could be emitted continuously by the same cathode under the same conditions of temperature and electric field. The present work was directed toward finding the decay characteristics of oxide cathodes, and the dependence of the decay time and the maximum current on temperature and on the chemical properties of the cathode coatings. There was a threefold purpose for this investigation: First, knowledge of the decay characteristics would enable one more confidently and efficiently to design cathodes for delivering current intermittently. Second, any increase in our knowledge of the emission process from oxides which might result from such an investigation would be very welcome. Third, it might happen as a result of this work that, by suitable changes in cathode material, thickness, or core metal, the initial (maximum) current could be drawn for a longer time or, perhaps, continuously.

II. APPARATUS

The experimental tubes used in this investigation were "sealed-off," high vacuum diodes. Anodes were nickel blocks drilled to provide a 0.32-cm diameter hole for the anode surface; a small peep-hole was provided in the anode, so that an optical pyrometer could be focused on the emitting surface of the cathode. Cathode sleeves were 0.127-cm diameter tubes of nickel containing 0.2 percent silicon. The sleeves were hydrogen-fired and then sprayed with alkaline-earth carbonate mixtures suspended in amyl acetate. Each cathode was trimmed to the required emitting area (about 0.05 cm²) by scraping away the undesired part of the coating and polishing the underlying nickel. Tests on cathodes of widely different trimmed areas showed that the nickel from which carbonates had been removed exhibited the thermionic electron emission characteristic of pure nickel.

A cathode and anode were assembled into a tube and aligned concentrically with mica spacers. A rigorous heat treatment was employed during the exhaust of each tube in order to outgas all parts. Cathodes were activated by glowing at

* Now at RCA Laboratories, Princeton, New Jersey.

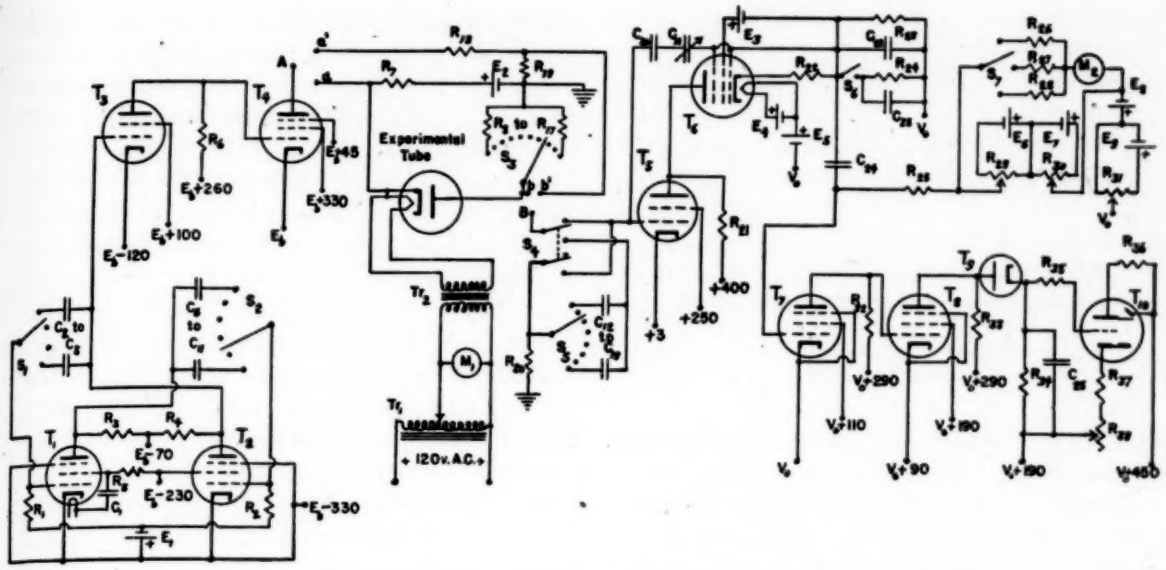

FIG. 1. Square wave generator, experimental tube, and pulse measuring circuits.

$T_1, T_2, T_7 \rightarrow 6C6$.
$T_3 \rightarrow 6L6$.
$T_4 \rightarrow 804$.
$T_5 \rightarrow 6L6G$.
$T_6 \rightarrow 6J7$.
$T_8 \rightarrow 6D6$.
$T_9 \rightarrow 6H6GT$ (one diode).
$T_{10} \rightarrow 6E5$.

$C_1 \rightarrow 16\ \mu f$ elect.
$C_3, C_7 \rightarrow .0005\ \mu f$.
$C_5, C_8, C_{24} \rightarrow .001\ \mu f$.
$C_4 \rightarrow 0.003\ \mu f$.
$C_6, C_9, C_{22} \rightarrow .005\ \mu f$.
$C_8 \rightarrow 0.0002\ \mu f$.
$C_{10} \rightarrow 0.01\ \mu f$.
$C_{11} \rightarrow 0.02\ \mu f$.
$C_{12} \rightarrow 58\ \mu\mu f$.
$C_{13} \rightarrow 100\ \mu\mu f$.
$C_{14} \rightarrow 245\ \mu\mu f$.
$C_{15} \rightarrow 555\ \mu\mu f$.
$C_{16} \rightarrow 890\ \mu\mu f$.
$C_{17} \rightarrow 0.00211\ \mu f$.
$C_{18} \rightarrow 0.00527\ \mu f$.
$C_{19} \rightarrow 0.0112\ \mu f$.
$C_{20} \rightarrow 40\ \mu\mu f$.
$C_{21} \rightarrow 20$–$80\ \mu\mu f$.
$C_{23} \rightarrow 0.03\ \mu f$ mica.
$C_{25} \rightarrow 0.05\ \mu f$.

$Tr_1 \rightarrow 2$ Kva. Variac.
$Tr_2 \rightarrow$ Filament transformer, rewound.

$M_1 \rightarrow 0$–150 volt a.c.
$M_2 \rightarrow 0$–$200\ \mu$amp.
$S_1, S_2, S_3, S_5 \rightarrow$ tap switches.
$S_4 \rightarrow DPDT$, low capacity.
$S_6 \rightarrow SPST$, time sensitivity selector.
$S_7 \rightarrow SP3T$, range selector for M_2 used as voltmeter.

$E_1, E_7, E_9 \rightarrow 1.5$ v.
$E_2, E_4 \rightarrow 6$ v.
$E_3 \rightarrow 45$ v.
$E_5 \rightarrow 23$ v.
$E_6, E_8 \rightarrow 4.5$ v.
$E_b, V_0 \rightarrow$ see text.

$R_1 \rightarrow 300K$.
$R_2, R_{34} \rightarrow 2M$.
$R_3 \rightarrow 25K$.
$R_4 \rightarrow 15K$.
$R_5, R_{37} \rightarrow 1K$.
$R_6 \rightarrow 3.5K$, 50 watt.
$R_7 \rightarrow 175K$.
$R_8 \rightarrow 38.7$.
$R_9 \rightarrow 49.4$.
$R_{10} \rightarrow 75.7$.
$R_{11} \rightarrow 100.3$.
$R_{12} \rightarrow 153.1$.
$R_{13} \rightarrow 193$.
$R_{14} \rightarrow 304$.
$R_{15} \rightarrow 507$.
$R_{16} \rightarrow 1.24K$.
$R_{17} \rightarrow 1.83K$.
$R_{18} \rightarrow 2.5K$, 4 watt.
$R_{19} \rightarrow 75$.
$R_{20} \rightarrow 4.92K$.
$R_{21} \rightarrow 2.5K$, *MPO* 50 watt non-inductive.
$R_{22} \rightarrow 2K$.
$R_{23} \rightarrow 500K$.
$R_{24} \rightarrow 75K$.
$R_{25} \rightarrow 20M$.
$R_{26} \rightarrow 1.5K$.
$R_{27} \rightarrow 6K$.
$R_{28} \rightarrow 30K$.
$R_{29} \rightarrow 25K$ pot.
$R_{30} \rightarrow 5K$ pot.
$R_{31} \rightarrow 1K$ pot.
$R_{32} \rightarrow 250K$.
$R_{33} \rightarrow 50K$.
$R_{35} \rightarrow 150K$.
$R_{36} \rightarrow 750K$.
$R_{38} \rightarrow 1K$ pot.

Condensers above 0.01 μf are paper, 0.01 μf and below are mica, unless otherwise noted; $K = 10000\Omega$; $M = 1{,}000{,}000\Omega$; Resistors are 1 watt unless otherwise noted.

1300°K and slowly applying a potential difference between anode and cathode. A nickel-clad barium getter was flashed in each tube, and the tube sealed from the pumping system at a station pressure of less than 10^{-6} mm of mercury.

The requirements for an instrument with which to investigate the time effect under consideration were: (1) An electric field must be applied to the cathode surface in such a manner that the thermionic current increases from zero to a temperature-limited value in a time short compared to one μsec.; (2) after a short interval, this field must be removed, in order to allow time for the cathode to recover; (3) the current *vs.* time characteristic of a cathode must be faithfully reproduced, even when the current peaks are of only a few μsec. duration; (4) current pulses differing by a factor of fifty or more in amplitude and in decay time must be accessible, in order to ascertain the temperature dependence of the effect. Further requirements were imposed by the impossibility of procuring at the present time certain tubes, notably thyratrons, transmitting tubes, and high transconductance amplifying tubes.

The vacuum tube circuits developed to meet these requirements are outlined in Fig. 1. Tubes T_1, T_2, T_3, and their adjacent circuits constitute a square wave generator which delivers positive pulses to T_4. The width of these pulses can be selected by S_1 (about 100, 300, 600, or 2000 μsec.) and the pulse repetition frequency can be selected by S_2 (about 20, 30, 60, 120, 600, or 1500 pulses per second). Condenser C_1 synchronizes

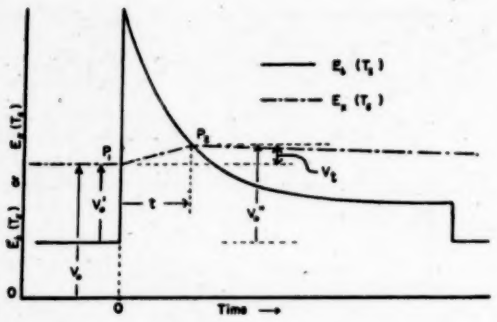

FIG. 2. Method of measuring current *vs.* time characteristics.

the pulses with the 60-cycle power line in order to minimize the effects of ripple and pick-up in the subsequent circuits. The control grid of T_4, which is about 70 volts negative with respect to T_4 cathode during most of a cycle, is driven positive for the duration of the pulse. The potential E_b (less the small drop across T_4) is applied suddenly to the experimental tube, if "A" is connected to "a:" The value of E_b ranges from -100 to -1000 volts, depending on the plate voltage desired at the experimental tube. The function of E_2 and R_7 is to apply a small negative potential to the plate of the experimental tube during the (major) fraction of the cycle in which T_4 conducts only a few microamperes. The transformer Tr_2 is specially constructed to minimize the capacitance between secondary and ground. The entire capacitance which must be charged through T_4 is less than 30 $\mu\mu$f, which permits applying a potential difference of 500 volts to the experimental tube in about 0.05 μsec.

The remainder of the circuits serve to measure the size and shape of the current pulse in the experimental tube. Switch S_3 selects an appropriate resistance so that the potential drop between ground and the point "B" will be about 15 or 20 volts at the maximum of the current pulse. With "B" connected to "b" and S_4 in the upper position, a negative pulse is applied to the grid of T_5. This pulse is mirrored in the plate circuit of T_5 and subsequently measured. With "A" connected to "a'," and "B" to "b'," a negative square wave is applied to "B." If S_4 is in the lower position, the resistance-capacitance combination of R_{20} and one of the condensers C_{12} to C_{19} serves to apply an exponential (negative) pulse to the T_5 control grid. The values of R_{20} and of these condensers can be determined by bridge measurements, and hence a calibrating pulse of known shape and time constant can be applied to the measuring circuit. (The resistors used had negligible skin effect at frequencies less than 2 Mc).

The performance of T_6 approximates a diode in which the current passed is zero whenever the plate is negative with respect to the cathode and is a fixed value for any positive plate potential. Figure 2 shows the principle of measurement by use of such an ideal circuit element. The solid line shows the plate potential E_b of T_5 as a function of time; E_b rises abruptly from its quiescent value when the pulse arrives, then decreases. When E_b rises above the value of V_0 (approximate quiescent cathode potential of T_6), T_6 begins to conduct, charging C_{22}. The cathode potential of T_6 (dashed line in Fig. 2) rises slowly until E_b falls to P_2, at which point T_6 ceases to conduct. The T_6 cathode potential then slowly decreases (time constant of R_{23} and C_{22} is 0.0025 sec.) to V_0 again in preparation for the arrival of another pulse. The amplitude V_t of the cathode potential's excursion from V_0 is a measure of the time t elapsed between P_1 and P_2. By setting V_0 at successively different values and measuring the time t corresponding to each, a plot of V_0'' *vs.* t reconstructs the shape and size of the experimental tube current pulse. Closing S_6 introduces a larger condenser to be charged (but about the same time constant) and hence decreases the time sensitivity of the instrument.

Of course, T_6 is not such an ideal circuit element as assumed above, but because of its low screen potential and the cathode bias resistor R_{22}, T_6 forms a fairly good approximation to the ideal diode. Figure 3 shows the static characteristic of this tube in the circuit in which it is used. The deviation of this characteristic from ideal is im-

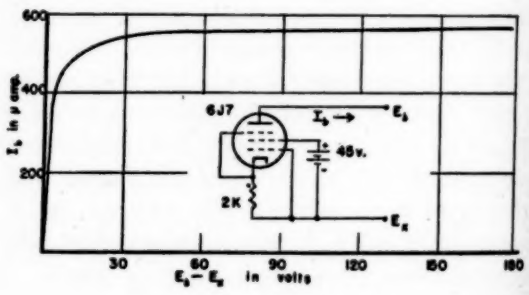

FIG. 3. Static characteristic.

portant only when examining a current pulse in a region where curvature of the current *vs.* time relation is large.

As E_b rises abruptly, a displacement current flows through T_6. In order to neutralize this, a simultaneous current pulse of opposite sign is applied by condensers C_{20} and C_{21}; C_{21} is adjusted to produce a minimum net effect of displacement currents.

The circuit beyond T_6 is merely a very sensitive vacuum tube voltmeter of the peak, slideback type; its function is to measure the amplitude V_t of the pulse generated by T_6 and its associated circuit. T_7 and T_8 are direct-coupled amplifiers; T_9 operates to increase the time constant of the pulse being measured from 0.0025 sec. to 0.1 sec. T_{10}, an eye type indicator tube, gives a visual indication when the balance point of the voltmeter has been reached. The network connecting R_{25} to V_0 is, of course, the control grid bias of T_7. When no pulses are applied to T_7, R_{31} is adjusted so that T_{10} shows the existence of a balance. When pulses are applied, the potential increment V_t which must appear across R_{29} and R_{30} to restore T_{10} to balance is a measure of the height V_t of the pulse and hence of the time during which T_6 was conducting. Switch S_7 selects the sensitivity of meter M_2, which measures V_t; the maximum sensitivity is 0.3 volt full scale, which allows measurement to 0.001 volt. Pulse amplitudes less than 0.2 volt can be measured to within 0.002 volt with this circuit; E_6 and E_7 total 6 volts, thus permitting measurement of pulses up to 6 volts in amplitude. An oscilloscope, connected from plate to cathode of T_7, serves as a monitor of the circuit operation.

Power supplies, various coarse and fine controls, and filter and by-pass condensers are not shown in Fig. 1. Voltage regulation is obviously important in the supplies for the direct-coupled amplifier, for the adjustable voltage V_0, and for the plate voltage of T_5. Since constant alternating current voltage was also needed for the heater of the experimental tube, the alternating current supply for all power supplies was taken from a motor-generator set with electronically regulated output voltage. In addition, all power supplies were electronically regulated.

Only the linear region of T_5 was used. The voltage gain of this circuit was measured in the usual manner, with precautions to insure that the screen grid potential during the measurements was the same as it was in actual operation. A meter circuit was devised which measured V_0' directly, the zero of this meter being set at the quiescent plate potential of T_5 (this circuit is not shown in Fig. 1).

The method for calibrating this instrument has already been outlined. If the circuit operates properly, V_t will be proportional to the time t

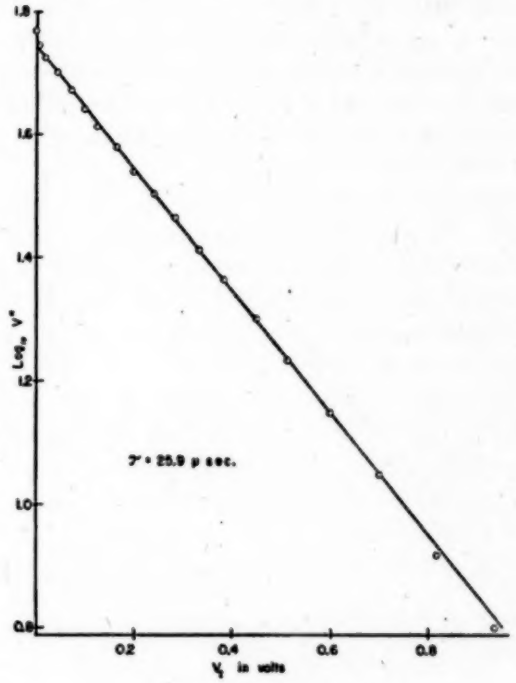

FIG. 4. Calibrating pulse.

elapsed from the beginning of the calibrating pulse, and we may write $t=CV_t$. Since the calibrating pulse is exponential with the time constant τ, we know that

$$V_0''=(\text{constant})\exp(-t/\tau). \quad (1)$$

A plot of $\log_{10} V_0''$ *vs.* V_t should then yield a straight line of slope m, where

$$m=(\Delta \log_{10} V_0'')/(\Delta V_t)=-C/(2.303\tau). \quad (2)$$

Figure 4 shows such a plot for $\tau=25.9$ μsec., with S_6 closed (that is, low sensitivity to time); the points lie on a line, except for two points toward the "tail" of the pulse. The slope is evidently $m=-0.995$ per volt, and hence

$$C=-2.303\tau m=59.5 \text{ μsec./volt}. \quad (3)$$

Calibrations were made for several pulses differing widely in time constant, and a calibration was taken each time the instrument was used. All calibrations were within 2 percent of $t=60V_t$ μsec. for the low sensitivity (S_6 closed) and within 4 percent of $t=9.5V_t$ μsec. for the high sensitivity (S_6 open).

The fidelity with which the instrument reproduces pulses of small time constant (of the order of several μsec.) and the rapidity with which the square wave rises must also be determined. In order to accomplish this, exponential pulses of time constants ranging from 2.5 to 50 μsec.were applied to the grid of T_5. The amplitudes of these pulses were equal at the grid, but unequal at the plate of T_5; the amplitudes at the plate were compared by using the voltmeter circuits as usual. Analysis of the circuit associated with T_5 enables one to determine the time constant of the T_5 plate circuit from these data. By this method the time constant of the T_5 plate circuit was found to be about 0.07 μsec.

The time constant of the rise of the square wave generated by T_4 could not be measured directly in this way. It can be inferred, however, that this time constant was less than 0.05 μsec. by two considerations: First, a comparison of the known resistances and estimated capacitances of the T_4 and T_5 circuits indicated that the T_4 circuit should have a smaller time constant than the T_5. Second, the analysis of the T_5 circuit assumed a perfectly sharp square wave; if the time constant of the rise of the square wave were greater than 0.05 μsec., then the above measurements would indicate that the time constant of the T_5 plate circuit was less than 0.05 μsec., which would be inconsistent with the known load resistance of T_5 and estimates of the minimum capacitance at the T_5 plate. Of course, this estimate of the time of rise of the square wave is for the case in which the square wave generator supplies calibrating pulses to the T_5 circuit. When the generator is connected to the experimental tube, the capacitance added and the flow of thermionic current in the experimental tube reduce the time constant of the rise of the square wave to about 0.2 μsec. From this analysis we conclude that thermionic current pulses of 0.1 μsec. time constant can be detected with this circuit, and pulses of time constant greater than about 3 μsec. can be accurately measured.

In using this circuit to measure the current *vs.* time characteristics of experimental tubes, we must assume that the thermionic current rises to its maximum value immediately that anode voltage is applied to the experimental tube. That this assumption is justified, if "immediately" is interpreted as "in less than 0.2 μsec.," can be inferred from the following experiment: Suppose that instead of using resistors R_{18} and R_{19} (Fig. 1) to generate a square wave for a calibrating pulse as outlined above, the experimental tube is connected to the resistance-capacitance pulsing circuit (R_{20} and one of the condensers C_{12} to R_{19}) by throwing switch S_4 into the lower position. This will be as effective in producing pulses of time constant 2 to 10 μsec. as the R_{18}, R_{19} circuit, provided the thermionic current rises to its maximum value in a time short compared to 0.2 μsec. This experiment was performed, and the result indicated that the thermionic current increased to its maximum value in less than 0.2 μsec.

Temperatures of the experimental tube cathodes were observed with an optical pyrometer. The brightness temperature of the actual emitting surface, rather than of the nickel core, was observed in order to avoid errors caused by temperature gradients in the coatings and to afford observation of any change in temperature with changes in thermionic current density. The spectral emissivity e_λ for optical pyrometry ($\lambda=0.65\mu$) of barium and strontium oxides is a matter of some disagreement; e_λ apparently varies with thickness of oxide layer,[1] state of aggregation of the oxide particles, and choice of core metal.[2] In the present work, e_λ was assumed to be 0.45 for all coatings; absorption in the glass envelope of the tube reduced the effective e_λ to about 0.40.

It is well known[3] that the temperature-limited current from an oxide-coated cathode is subject to wide variations. Two cathodes installed in different tubes, but constructed as nearly as possible identically, frequently yield widely different work functions. The emission from a single

[1] P. Clausing and J. B. Ludwig, Physica **13**, 193 (1933).
[2] G. E. Moore and H. W. Allison, J. App. Phys. **12**, 431 (1941).
[3] J. P. Blewett, J. App. Phys. **10**, 688 and 831 (1939).

cathode will frequently change with time in an unpredictable manner. The temperature-limited emission depends markedly on the treatment of the cathode for the time just preceeding measurement. Glowing at a different temperature, drawing current at the same or different temperatures, application of strong fields, or allowing the cathode to operate space-charge limited—all affect the saturation current by unpredictable amounts. In addition, there are several time effects of a few minutes or a few seconds duration: Joule heating, poisoning of cathode by gas liberated from the anode, and a decay effect investigated by Blewett.[4]

It was only natural, then, that the attempts to measure short-time currents at first yielded data which were thoroughly scattered and quite unreproducible. The usual vagaries of oxide emitters here caused more than the usual error in measuring thermionic constants, since ten or fifteen minutes were required to obtain the decay characteristic at a single temperature (as contrasted with the few seconds required to read an ammeter if only steady current were being measured).

After considerable experimenting, the following technique of measurement was developed: (1) The cathode was glowed at $T+100°$ for about 55 sec. (glowing at $T°$ yielded the same results, but 5 to 10 min. were required instead of 55 sec.); (2) heater power was then reduced to an amount sufficient to maintain the temperature $T°$, and hence the cathode cooled to this temperature (one min. was allowed for cooling); (3) the square wave pulses were applied and measurement begun, the actual balance of the circuit being obtained 3 sec. after pulsing began. A reliable reading could not be taken in less than 3 sec., and measurement showed that the decay in this time was always less than 3 percent (3 sec. of pulsing entails less than 0.1 sec. of actually drawing current). This procedure was followed for each point on the current *vs.* time characteristic. At the end of a series of readings at a single temperature, an attempt was made to repeat the first of the series; if this could not be done within 2 or 3 percent, the entire series was discarded. A similar check was employed at the end of a group of characteristics for different temperatures. After six or eight characteristics were taken (in order to find the temperature dependence of the short-time decay effect), an attempt would be made to repeat several points on the first characteristic. If this could not be accomplished within 8 or 10 percent, all the characteristics were discarded and the cathode was aged by applying pulses to it for an hour before subsequent measurements. This procedure resulted in data much more reproducible and regular than are usually associated with oxide-coated cathodes.

When anode voltage was suddenly applied to the experimental tube, the charging of the anode-cathode capacitance necessitated a flow of displacement current through the resistance selected by S_3 (Fig. 1). This current was of the same order of magnitude as the smallest thermionic currents measured. By observing the displacement current with the cathode at room temperature and analyzing the circuit (including distributed capacitance) adjacent to the experimental tube, this displacement current could be determined and subtracted from the total observed current, yielding true thermionic cathode current.

It is not necessary to make a similar correction for the current resulting from abruptly collecting electrons from the "space-charge cloud" surrounding the cathode, since calculations based on the theory of Langmuir[5] show that this current is several orders of magnitude lower than the thermionic currents observed.

Current and time measurements with this apparatus were accurate to ± 4 percent at any values of current and time considered, and to ± 2 percent for all times greater than 10 μsec. Lack of knowledge of the spectral emissivity of oxide cathodes limited the accuracy of measurement of temperature to about ± 2 percent.

III. A THEORY OF THE THERMIONIC CURRENT DECAY

Before discussing experimental results, we shall digress to propose a theory of the decay of thermionic emission during the short time interval (about a millisecond) after drawing of current is initiated. This theory is based on the assumption that the enhanced emission of oxide cathodes is

[4] J. P. Blewett, Phys. Rev. **55**, 713 (1939).

[5] I. Langmuir, Phys. Rev. **21**, 419 (1923).

caused by a layer of barium atoms on the emitting surface. (We shall write "barium" for "barium, strontium, or calcium" except when referring to the work of other investigators.)

Langmuir[6] demonstrated that the electron emission from a metallic surface could be increased a million-fold if a layer of thorium atoms were adsorbed on the surface. This increase comes about because each "adatom" exists during a fraction (of the order of 0.1) of the time as a positive ion, having lost an electron to the metallic surface; Gurney[7] has showed that the average charge of an adatom depends on its distance from the metal. Becker[8] investigated films of barium on tungsten and on barium oxide.[9] His work with barium oxide confirmed the hypothesis proposed by Koller[10] and Rothe[11] that the enhanced emission from oxide-coated cathodes was caused by a surface layer of barium. The small A factor in the thermionic emission equation and the activation effects observed (Blewett[3]) with these coatings substantiated this hypothesis.

Becker[9] showed that unless barium was deposited on the cathode from an external source, the barium layer residing on the cathode surface was always thinner than that required for maximum emission. Thus any process which removes barium from the emitting surface should increase the thermionic work function. Such a process is evidently the drawing of thermionic current, since the electric field at the cathode surface necessary to sustain current flow forces barium ions away from the surface and into the interior of the cathode coating. The net flow of barium ions inward would cease when the rate of diffusion outward and subsequent ionizing of barium atoms equals the rate of removal of ions under the influence of the electric field. The electrolytic current density of barium ions is proportional to the electric field which is in turn proportional to the thermionic current density i. The diffusion current density is proportional to the concentration gradient of barium atoms, which is in turn proportional to the net number of atoms which have left unit area of the surface. Hence we obtain:

$$\frac{dN}{dt}=-\frac{\alpha i}{e}+\beta(N_0-N), \tag{4}$$

where N is the number of adsorbed atoms per cm² of surface at the time t, i is the thermionic current density (amp/cm²), e is the absolute magnitude of the electronic charge (coulombs), α is a constant proportional to the ionic mobility, and β is a constant proportional to the atomic diffusion coefficient and inversely proportional to the thickness of the layer in which the concentration gradient is set up. The subscript 0 refers here and hereafter to conditions at the instant drawing of thermionic current is begun, that is, at $t=0$.

Langmuir's[6] equation for the thermionic current from an emitter possessing a layer of adatoms is:

$$\log (i/i_{N=0})=\theta \log (i_{N_c}/i_{N=0}), \tag{5}$$

where i_{N_c} is the current when $N=N_c$, $i_{N=0}$ is the current when $N=0$, $\theta=N/N_c$, and N_c is the number of barium atoms per cm² in a complete monatomic layer. From Becker's[9] data for barium films on tungsten or barium oxide we learn that Eq. (5) is not strictly correct. We can say, however, that

$$\log (i/i_{N_c})=\theta L, \tag{6}$$

where L is a slowly varying function of θ; over the range of θ's producing a range of a factor of 10 in thermionic current, L is approximately constant. For θ near 0, $L\geqq 2\log (i_{N_c}/i_{N=0})$; for $\theta\geqq 0.7$, $L\geqq 0.6\log (i_{N_c}/i_{N=0})$.

If we write an equation like Eq. (6), but with i_0 and θ_0 in place of i and θ, and subtract it from (6), we obtain:

$$\log (i/i_0)=L(\theta-\theta_0). \tag{7}$$

Differentiating (7) with respect to time and combining with (4) yields:

$$\frac{1}{i}\frac{di}{dt}=L\frac{d\theta}{dt}=\frac{L}{N_c}\frac{dN}{dt}=-L\beta(\theta-\theta_0)-\left(\frac{\alpha L}{eN_c}\right)i. \tag{8}$$

We can eliminate θ by using (7) again and obtain:

$$\frac{1}{i}\frac{di}{dt}=\beta\log\left(\frac{i_0}{i}\right)-\left(\frac{\alpha L}{eN_c}\right)i. \tag{9}$$

[6] I. Langmuir, Phys. Rev. **22**, 357 (1923).
[7] R. W. Gurney, Phys. Rev. **47**, 479 (1935).
[8] J. A. Becker, Trans. Am. Electrochem. Soc. **55**, 153 (1929).
[9] J. A. Becker, Phys. Rev. **34**, 1323 (1929).
[10] L. R. Koller, Phys. Rev. **25**, 671 (1925).
[11] H. Rothe, Zeits. f. Physik **36**, 737 (1926).

Equation (9) represents approximately the dependence of thermionic current upon time.

Physical processes other than the one postulated might lead to Eq. (9). For instance, the density of barium adatoms might remain constant with time, but the average charge of each might decrease as current was drawn. If an adatom moves inward under the influence of an electric field, its average charge must eventually decrease, since it becomes indistinguishable from an interstitial barium atom and conductivity data[12] show that only a very small fraction of such atoms are ionized at 1200°K. Thus, the decay of the emitting power would be caused by a slight displacement toward the oxide, and consequent decrease in average charge, of the barium layer. However, it is probable that this process produces a steady state in a time of the order of 1 μsec., which is much shorter than the decay times observed in this investigation.

Let us define i_1 by:

$$\beta=\left(\frac{\alpha L i_1}{eN_c}\right)\left(\frac{1}{\log(i_0/i_1)}\right), \tag{10}$$

and write

$$\eta=i/i_1;\quad \eta_0=i_0/i_1;\quad \xi=(i_1\alpha L/eN_c)t. \tag{11}$$

We have as yet ascribed no meaning to i_1. Using (10) and (11), we find Eq. (9) becomes:

$$\frac{1}{\eta}\frac{d\eta}{d\xi}=\left(1-\frac{\log\eta}{\log\eta_0}\right)-\eta. \tag{12}$$

Consider the behavior of (12) as ξ increases from 0. When $\xi=0$, $t=0$, $\eta=\eta_0$. Initially, $(1-\log\eta/\log\eta_0)=0$, so the initial slope is $(d\eta/d\xi)=-\eta^2$; thus η decreases rapidly at first as ξ increases. The term $(1-\log\eta/\log\eta_0)$ slowly increases as η decreases. The asymptotic behavior of (12) for large ξ can be seen by separating the variables and integrating:

$$\xi=\int_{\eta_0}^{\eta}\frac{d\eta'}{\eta'(1-\log\eta'/\log\eta_0-\eta')}. \tag{13}$$

Evidently as the upper limit of the integral approaches 1, the integrand becomes approximately proportional to $d\eta'/(1-\eta')$; hence as $\eta\to1$, $\xi\to\infty$. We thus identify the case $\eta=1$, $i=i_1$, with the steady state condition ($t=\infty$).

Returning to (12) we note that, although the variables are separable, this equation cannot be integrated easily as it stands. Furthermore, one cannot perform a single numerical integration and solve the problem completely, because of the presence of the parameter η_0. To obtain an approximation to $\eta(\xi)$ we shall write

$$1-\log\eta/\log\eta_0\cong1/\eta. \tag{14}$$

This is not so severe an approximation as it may seem. The term represented by Eq. (14) is small relative to η except in the region near $\eta=1$; at $\eta=1$, Eq. (14) is exact. After obtaining $\eta(\xi)$ upon the basis of the approximation contained in (14) we shall compare our result with a numerical integration of (12).

Using Eq. (14), we find Eq. (12) becomes

$$d\eta/(\eta^2-1)=-d\xi. \tag{15}$$

Upon integrating, we obtain

$$\xi=\tfrac{1}{2}\log\left[\frac{(\eta+1)(\eta_0-1)}{(\eta-1)(\eta_0+1)}\right], \tag{16}$$

or, solving (16) for η,

$$\eta=1+\frac{2}{\left(\frac{\eta_0+1}{\eta_0-1}\right)\epsilon^{2\xi}-1}. \tag{17}$$

Figure 5 shows $\eta(\xi)$ from Eq. (17) for three different values of η_0. The dots in Fig. 5 are the results of a numerical integration of Eq. (12) for the case $\eta_0=11$. Evidently $\eta(\xi)$ as given by (16) provides a solution of Eq. (12) that is sufficiently accurate for the purpose of comparison with the experimental data presented below.

IV. EXPERIMENTAL RESULTS

In this section we shall report successively five features of the experimental results, and compare each with predictions based on the hypothesis proposed above. We shall use results from five tubes for each of these features, and in connection with the dependence of the decay on coating thickness we shall use the results of two additional tubes (No. 3 and No. 4, to which the

[12] W. Meyer and A. Schmidt, Zeits. f. tech. Physik **13**, 137 (1932).

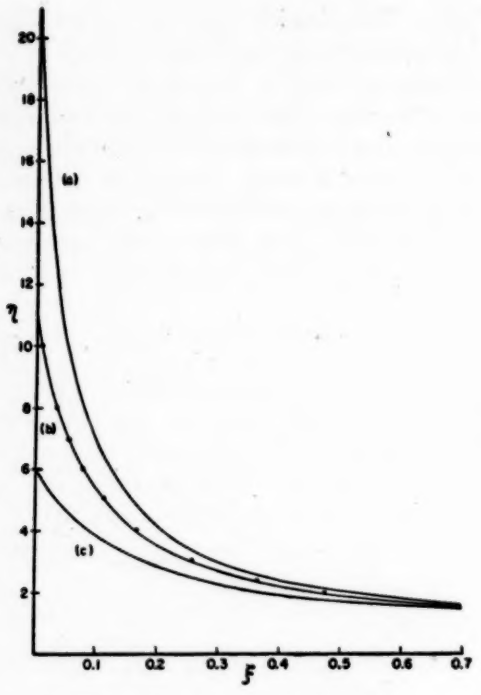

FIG. 5. $\eta(\xi)$ for three values of η_0.

measurement cycle of glowing and pulsing described in the first section was not applied).

All of the data exhibited in Figs. 6–8 and in Table III were taken under the following conditions: (1) Anode voltage was applied to the tubes in pulses of about 300-μsec. duration; (2) these pulses were repeated at the rate of 30 per sec.; (3) between pulses, a small retarding field was applied to the cathode; (4) the amplitude of the anode voltage pulse was 450 volts.

1. Current as a Function of Time

Figure 6 shows the decay of thermionic current at a fixed cathode temperature. The solid line is a plot of Eq. (16) with the scale factors (ξ/t) and (η/i) and the parameter $\eta_0(=i_0/i_1)$ chosen to give the optimum fit; the dashed line is a fit of the exponential function, $i=A+B\exp(-t/\tau)$, to the same data. Equation (16) evidently represents the experimental data much more closely than does the simple exponential function.

Figure 7 shows decay characteristics of tube No. 11 at 3 different cathode temperatures. The scales for the 3 temperatures are different, and the solid lines were obtained from Eq. (17). Equation (17), with the three adjustable constants properly chosen, represents the data of Fig. 7, and all of the 25 decay characteristics obtained, with error of about the same magnitude as the scattering of the experimental points.

By fitting Eq. (17) to data on 5 tubes, the values of i_0 (initial current) and i_1 (final current) portrayed in Fig. 8 were obtained; all the points above the dashed line represent i_0, all those below are values of i_1.

2. Dependence of Decay on Cathode Thickness

Table I shows the compositions and thicknesses of the cathode coatings studied. Since the points in Fig. 8 from tubes No. 8 and No. 11 practically coincide, we conclude that the "range" i_0/i_1 of the decay phenomenon does not depend on cathode coating thickness, at least when this thickness is of the order of a few mg/cm.^{2} Furthermore, tubes No. 3 and No. 4 produced nearly identical results for range and rate of decay. Comparison of Table I and Fig. 8 indicates that the two different compositions of coating material produced about the same decay range.

Tube No. 14 exhibited less range of decay than the others. The cathode of this tube was removed and examined. About one-half of the cathode area looked as if most of the oxides had been removed during activation and use, leaving a layer of oxide more or less combined with the nickel core. The tube No. 12 currents show a more marked dependence on temperature than exhibited by other tubes, which suggests that the cathode in this tube may have been incompletely activated.

Consequently, these data indicate that over a wide range of thickness of oxide coatings the initial and final currents at a particular tempera-

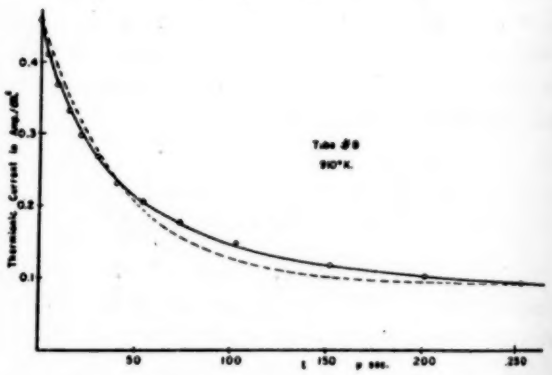

FIG. 6. Decay characteristics.

ture are substantially constant. On the other hand, Eqs. (4) and (10) require that the final current be inversely proportional to the thickness of the layer in which the electrolytic conduction and diffusion take place. Thus this layer cannot be identified with the thickness of the cathode coating, but must be a layer of the same thickness in all coatings. Such a layer could arise because of the granular nature of the oxide cathode. Within any single oxide particle, electrolytic conduction may be a substantial fraction of the total current. The conduction between two adjacent oxide particles should be largely electronic, since the wave-length of a barium ion is much greater than that of an electron, and hence an electron can more easily cross the gap between particles. The diffusion-conduction layer would thus be the layer of oxide particles lying at the emitting surface. In the cathodes used in this investigation, this layer would be about 2 microns in thickness.

According to this barium conduction hypothesis, the steady-state current i_1 should increase as the size of oxide particles decreases. This is because there is no reason to believe that i_0 should depend sensitively on particle size, but the logarithm of the decay ratio i_0/i_1 should be proportional to the thickness of the particles composing the cathode surface. Benjamin, Huck, and Jenkins[13] investigated the dependence of thermionic current upon size of oxide particles and found an increase in steady-state current with decreasing particle size.

Measurement of the ratio of thermionic current decay i_0/i_1 on a cathode composed of a single, fairly thick crystal of barium oxide should indicate whether or not this electrolytic conduction hypothesis can be correct. If it is correct, the thermionic emission from such crystals should be extremely small when current is drawn continuously.

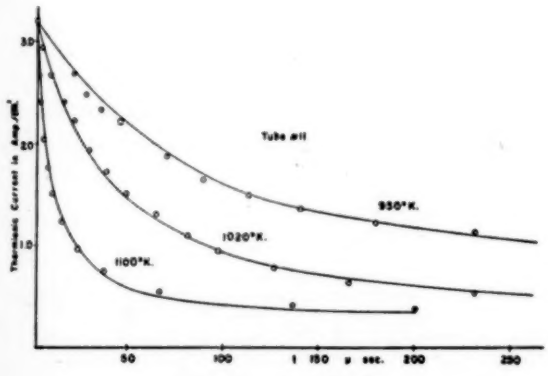

FIG. 7. Decay characteristics.

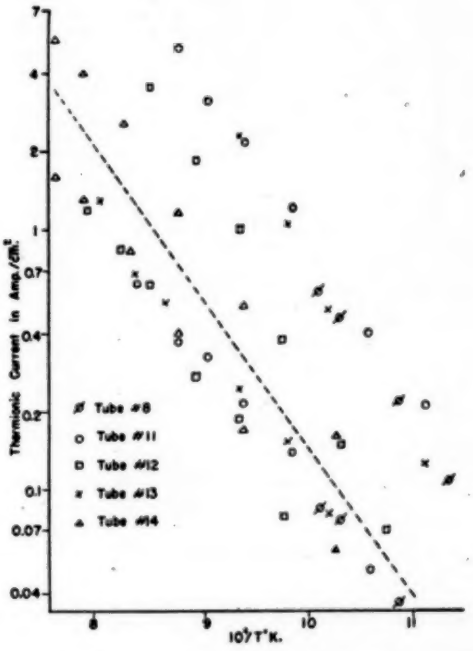

FIG. 8. Initial and final currents.

If the emitting surface decays by electrolytic conduction, increasing the electronic conductivity of the cathode coating should decrease the ratio of decay. This suggests that in order to obtain larger values of i_1, which for most purposes is the only useful current, we might try to maintain layers of barium on materials with greater electronic conductivity than barium oxide but with the same or smaller work function. It might, for example, be possible to maintain barium films on silicon, which apparently meets the above requirements.

3. Anode Voltage Effect and Recovery Time

All the data reported so far were taken with an anode-cathode potential difference of 450 volts. This potential difference is about 3 times as large as necessary to prevent space-charge limitation of cathode current at the highest observed current densities. Such a potential produces, of course, an

[13] M. Benjamin, R. J. Huck, and R. O. Jenkins, Proc. Phys. Soc. 50, 345 (1938).

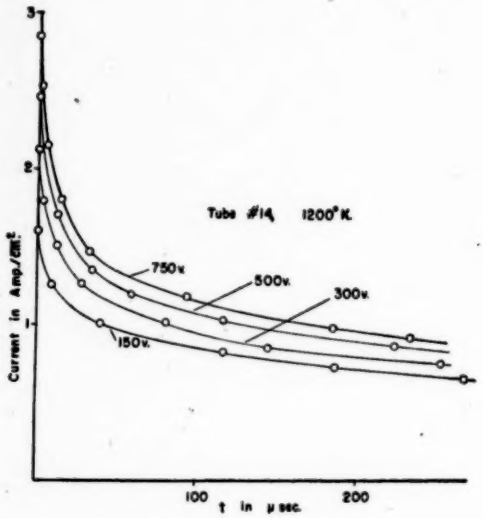

FIG. 9. Anode voltage effect.

appreciable Schottky effect in the thermionic emission.

The effect on the decay phenomenon of changing the electric field applied at the cathode was naturally of interest. Accordingly, the data plotted on Fig. 9 were taken; this plot shows decay characteristics of tube No. 14 at a cathode temperature of 1200°K, with four different values of anode potential differing in magnitude by a factor of 5.

Figure 10 shows plots of log i_0 *vs.* (anode voltage)$^{\frac{1}{2}}$ and log i_1 *vs.* (anode voltage)$^{\frac{1}{2}}$. The slope of the i_0 line in Fig. 10 corresponds to an anode voltage effect about $2\frac{1}{2}$ times the effect calculated from the tube geometry and the assumption that the emitter acted as a pure metallic surface. The slope of the i_1 line is about twice the value calculated on these assumptions. Such deviations are to be expected with oxide-coated cathodes or other composite surfaces, where some "patches" of the emitting surface have lower work functions than others.[14]

The difference in slopes between the i_0 and i_1 lines in Fig. 10 is easily explained on the basis of the theory we have proposed. Since the amount of surface positive charge which disappears when current is drawn is proportional to the emission current density, the patches which have the lowest work function will deteriorate most when current is drawn. The passage of current thus increases the work function of the patches of lowest work function more than it increases the work function of other patches. The variation of work function over the surface is therefore more extreme in the i_0 case, before appreciable current has been drawn, than in the i_1 case, and hence i_0 is a more sensitive function of anode voltage than is i_1.

Since all data assembled in Fig. 8 were taken at the same anode potential, these measurements have not been corrected for the anode voltage effect.

An investigation was also made to determine whether the decay depended sensitively on the duration of the current pulse or the rate at which pulses were repeated. At a fixed repetition frequency of 30 cycles per sec., changing the duration of drawing current (the width of the current pulse) from 100 to 300 μsec. produced no change in the decay ratio or decay rate. Similarly, at a fixed pulse width of 300 μsec., changing the repetition frequency from 20 to 120 cycles per sec. produced no change in the phenomenon. At 600 cycles, the ratio i_0/i_1 was decreased by about 20 percent from its value when relatively longer periods were allowed for the cathode to recover; this datum was taken on tube No. 8 at a cathode temperature of 920°K. This result is not very reliable, and the recovery time could not be further decreased, because of the design of the square wave generator and time measuring circuits. When the pulse width was an appreciable fraction of a cycle the power dissipating ability of some of the circuit elements was exceeded and certain potentials could not be kept fixed.

4. Work Functions

Using Fig. 8 we can compute values of ϕ' in the equation for thermionic emission from an elec-

TABLE I. Composition and thickness of cathode coatings.

Tube	Composition (by weight)	Thickness (mg/cm²)
No. 3	60% BaO, 30% SrO, 10% CaO	0.7
No. 4	60% BaO, 30% SrO, 10% CaO	16
No. 13	60% BaO, 30% SrO, 10% CaO	32
No. 8	50% BaO, 50% SrO	1.2
No. 11	50% BaO, 50% SrO	5.2
No. 12	50% BaO, 50% SrO	9
No. 14	50% BaO, 50% SrO	0.8

[14] A. Rose, Phys. Rev. 49, 838 (1936).

tronic semi-conductor:[15]

$$i = AT^{5/4} \exp(-\phi' e/kT), \qquad (18)$$

or we can compute values of ϕ in the ordinary equation for thermionic emission from a pure metallic surface;

$$i = AT^{2} \exp(-\phi e/kT). \qquad (19)$$

With the help of Fig. 10, we can correct the values of ϕ' and ϕ for the anode voltage effect. When this is done, we obtain the values shown in Table II, representing approximately the behavior of tubes No. 8, No. 11, and No. 13.

These results appear anomalous in that the steady-state current i_1, though smaller than i_0, corresponds to a lower work function than the initial current i_0. However, we must not regard these values of ϕ' as literally work functions. Equation (18) is valid only if the surface potential barrier is absolutely fixed in magnitude, independent of temperature. A small change with T of the barrier height would, of course, make a significant change in the measured value of ϕ'. If, as we supposed in the last section, the copious thermionic emission arises from the existence of a surface layer of barium, the fraction of the surface covered with active metal can easily change with T. According to Becker,[9] a change in θ from 0.2 to 0.3 produces a change of at least a factor of 10 in the thermionic emission. Thus only a small change with temperature of θ_0 or θ_1 or both would be required to produce this divergence of the i_0 and i_1 lines.

5. Rate of Decay

Our experimental data yield values of $t/\xi = eN_e/i_1 \alpha L$, which measures the time of decay. Before we can obtain values of α from these results we must know L and N_e.

From the information presented in conjunction with Eq. (6), we see that L decreases from about

TABLE II. Work functions.

	ϕ'	ϕ
i_0	1.17 v	1.12 v
i_1	0.98 v	0.91 v

[15] R. H. Fowler, *Statistical Mechanics* (Cambridge University Press, London, 1936), second edition, p. 401.

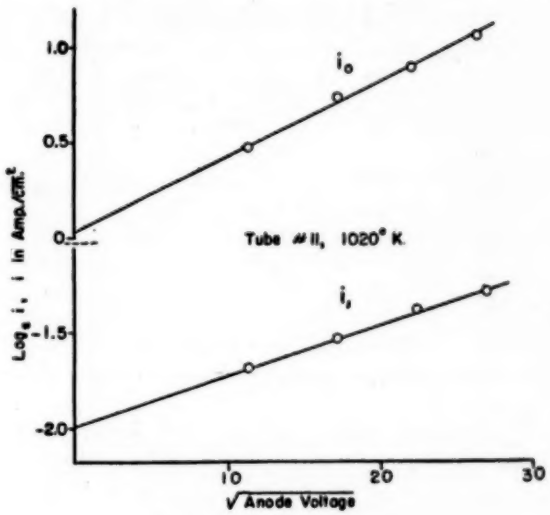

FIG. 10. Schottky lines.

2 log $(i_{N_e}/i_{N=0})$ to about 0.6 log $(i_{N_e}/i_{N=0})$ as θ, the fraction of the surface covered with barium atoms, increases from 0 to 0.7. To get an estimate of log $(i_{N_e}/i_{N=0})$, we use the measurement by Becker.[9] He observed currents differing by a factor of 10^5 as barium atoms were brought to the emitting surface electrolytically by sending a stream of electrons into an oxide coating from the vacuum. He believed that his surface may have had some barium adsorbed on it at the beginning of the experiment, so the actual ratio $i_{N_e}/i_{N=0}$ may have been 10^6 or 10^7. Of course, his cathode coating may have differed considerably from ours, but we shall probably not err greatly if we assume log $(i_{N_e}/i_{N=0}) \cong 15$. Then L should decrease from about 30 for dilute films to about 10 for $\theta \cong 0.7$.

The value of N_e is also subject to a certain amount of doubt. Both BaO and SrO form face-centered cubic crystal lattices, with the fundamental cubes about 2.77A and 2.58A, respectively, along an edge. If the (100) plane of the lattice lies in the surface, there should be about 2.8×10^{15} atoms per cm² lying at the surface, for either BaO or SrO. Metallic strontium forms a face-centered cubic lattice, 6.06A on a side. If we assume that the distance of closest approach of strontium atoms in a surface layer is the same as the distance of closest approach in solid strontium, there should be about 6.3×10^{14} atoms per cm² on the surface. Barium has an edge length of the fundamental cube equal to 5.01A, but it is a

TABLE III. Values of αL.

Temp., °K	Tube No. 8	Tube No. 11	Tube No. 12	Tube No. 13
920	5.1			
950		3.9		
970	5.2			
980				3.9
990	5.4			
1020		2.1	1.6	3.7
1070		3.1	1.7	5.0
1100		3.1		
1120			1.3	
1150		3.2		
1180			1.3	

body-centered cubic lattice, and hence yields about the same density of surface layer as strontium. Thus, we might expect in a complete monolayer about one adsorbed atom to every 4 atoms of the crystal surface. We shall assume that N_c equals 6×10^{14} atoms per cm².

Table III shows the values of αL computed from the decay characteristics of 4 tubes at several different temperatures. In this table are fifteen determinations of this quantity, corresponding to the fifteen point pairs (i_1 and i_0 at a particular temperature) in Fig. 8. (Actually, Fig. 8 contains 53 points, but 11 of these are values of i_0 for temperatures at which i_1 could not be measured, or vice versa; another 12 points represent data from tube No. 14, which are not included here because of the considerations presented in the preceding section.) It appears that αL is sensibly constant for any one tube over a wide range of temperatures and currents.

It will be recalled that $\alpha i/e$ is the net number of ions leaving the surface per sec. per cm² when the current i flows. If the entire current in the region near the surface were borne by singly-charged barium ions, then $\alpha=1$. If only part of the current in this region were electrolytic, α might equal any number less than 1.

The data in Table III, with the interpretation of these data based on Eq. (4), indicate that a large fraction of the current in a single small crystal of BaO is carried by barium ions. Using the limits we have placed on L and values from this table, we see that this fraction is at least 5 percent and at most 50 percent. Measurements of the electrolytic conductivity of BaO have been made by Becker;[9] he estimated that about 1/200 of the current in BaO at 800°K is carried by barium ions, and a smaller fraction at higher temperatures. But his measurements were of the conductivity of cathode coatings, rather than of single crystals of BaO. By the argument put forward in connection with the dependence of the decay on thickness, we should expect that the fraction of conduction current borne by barium atoms should be much greater for a single crystal than for an aggregation of small crystals. Thus, Becker's measurements are not in conflict with the interpretation placed on values in Table III, provided that the distinction between the conductivity of a cathode coating and of a single BaO crystal is valid. We must use the fact that the conductivity of small BaO crystals packed together is largely electronic to explain the lack of dependence of the ratio i_0/i_1 on the thickness of the cathode coating.

This short-time decay effect is quite possibly related to the "flicker effect" originally observed by Johnson[16] and discussed by Schottky.[17] The latter effect is the great increase in shot noise in diodes with oxide-coated cathodes when the frequency of the pass-band of the amplifier with which the noise is measured is decreased below about 5000 cycles per sec. Schottky estimated that a surface process of some kind (re-orientation of surface atoms or change in work function of the surface at a localized spot) which has a characteristic time of the order of 10^{-3} sec. must be postulated in order to account for Johnson's data. Unfortunately, the temperature at which these data were taken was not reported, but if this temperature were about 900°–1000°K, the decay we have investigated would occur in about the proper time interval to be the process Schottky requires.

Part of the work presented in this paper was carried out while the writer held a Charles A. Coffin Fellowship. The author is particularly indebted to Professor Lloyd P. Smith for suggesting this study and for frequent suggestions and assistance in the course of the work.

[16] J. B. Johnson, Phys. Rev. **26**, 71 (1925).
[17] W. Schottky, Phys. Rev. **28**, 74 (1926).

PHYSICAL REVIEW VOLUME 67, NUMBERS 5 AND 6 MARCH 1 AND 15, 1945

On a Supplement to the Field Equations with an Application to Cosmology

CHRISTOPHER GREGORY*
Department of Physics, University of Hawaii, Honolulu, T. H.
(Received June 8, 1943)

The addition of a set of plausible equations (the supplemental equations) to the field equations of general relativity makes possible the construction of a cosmological model possessing the postulated features of the Weyl-Robertson kind together with the consequence of a "stationary" universe. The red shift phenomenon is still explainable as caused by velocity shifts via the deduction of a pseudo-variable function entailed by the consistency conditions between the two sets of equations. Under the assumptions of the smallness of the cosmological constant and the curvature, the proper constant density of energy T_4^4 is found to be connected with the recession factor k by the formula $8\pi T_4^4 = 3k^2$.

INTRODUCTION

IN cosmological applications of the field equations of general relativity and other related problems, investigators have not been able to come to conclusions regarding the properties of the universe en masse without making specific assumptions regarding the distribution of the stress-energy-momentum tensor therein. Theoretically, if the equation of state of the material comprising the universe were known, a solution of the problem can be effected. Certain plausible assumptions have been made by workers in this field.[1] It is the object of this work to introduce a supplement to the field equations and to apply it in particular to the Robertson-Weyl cosmological model.[2]

The invocation of the principle of Mach that the metrical field is determined by the distribution of matter and energy together with the requirement of covariance made possible the development of an analogue to Poisson's equation.[3] The principal requirement in regards to the stress-energy-momentum tensor which occurs in these field equations is that its tensor divergence be nil, and indeed the equation is so constructed that this becomes an identity. Now suppose we introduce the hypothesis that the distribution of matter and energy is determined by the metrical field by means of another set of equations: the supplement to the field equations. To acquire an explicit form for these supplemental equations, appeal is made to the quantum mechanics in order to obtain *qualitatively* the nature of these equations. In Schroedinger's equation, if one undertakes to eliminate the potential energy which occurs therein, an equation of the fourth degree results in the wave function ψ which can be roughly interpreted as the square root of the density if $\psi = \psi^*$. In this example the field equations have for their counterpart the second order equation involving the potential, and the supplemental equations are to have for their counterpart the Schroedinger equation (in a qualitative sense). The principal conclusion we come to is that the result of eliminating from the field equation the stress-energy-momentum tensor is to yield equations of the fourth degree which are not necessarily linear—of course, these equations are to be covariant in character.

THE SUPPLEMENTAL EQUATION

If we denote $\mathcal{G}_{\mu\nu}$ the components of the stress-energy-momentum tensor and $g_{\mu\nu}$ the components of the metrical tensor, then the field equations can be written as

$$-8\pi\mathcal{G}_{\mu\nu} = R_{\mu\nu} - \tfrac{1}{2}Rg_{\mu\nu} + \Lambda g_{\mu\nu}, \qquad (1)$$

where $R_{\mu\nu}$ is the contracted Riemann-Christofel curvature tensor, R the scalar formed from $g^{\mu\nu}$

* On leave at National Bureau of Standards, Washington, D. C.

[1] A. Einstein, Ber. d. Berl. Akad., p. 142 (1917); W. de Sitter, Proc. Akad. Wetensch. Amst. **19**, 1217 (1917); G. Lemaitre, Ann. Soc. Sci. Bruxelles **A47**, 49 (1927); W. de Sitter, Bull. Astronom. Inst. Netherlands **5**, 211 (1930); O. Heckmann, Göttingen Nachrichten, p. 97 (1932). A very instructive discussion is given in R. C. Tolman, *Relativity, Thermodynamics and Cosmology* (Clarendon Press, Oxford, 1934), Chap. X.

[2] H. P. Robertson, Proc. Nat. Acad. **15**, 822 (1929); H. P. Robertson, Rev. Mod. Phys. **5**, 62 (1933); R. C. Tolman, Proc. Nat. Acad. **16**, 320 (1930).

[3] A. Einstein, Ann. d. Physik **55**, 241 (1918).

and $R_{\mu\nu}$ by tensor multiplication and Λ the so-called cosmological constant. We take as the supplemental equations

$$-8\pi k g_{\mu\nu}=\bar{R}_{\mu\nu}-\tfrac{1}{2}\bar{R}\bar{g}_{\mu\nu}+\Lambda_1\bar{g}_{\mu\nu}, \tag{2}$$

where $\bar{R}_{\mu\nu}$ and $\bar{R}$ are formed from the $\bar{g}_{\mu\nu}$ in the same way that $R_{\mu\nu}$ and R were formed from the $g_{\mu\nu}$, k and Λ_1, are constants introduced by considerations of dimensionality. From (1) and (2) we see that the elimination of either $g_{\mu\nu}$ or $\bar{g}_{\mu\nu}$ leads to an equation involving either $g_{\mu\nu}$ or $\bar{g}_{\mu\nu}$ and their partial derivatives up to the fourth degree in compliance with our findings regarding the appeal to a quantum mechanical example cited in the introduction. The form of (2) can be said to have been dictated by the imputation of symmetry in regards to the roles played by $g_{\mu\nu}$ and $\bar{g}_{\mu\nu}$ in the equations.

As a consequence of the structure of the Eqs. (1) and (2), we have

$$(T^{\mu\nu})_{,}=0, \quad (\bar{T}^{\mu\nu})_{\bar{;}}=0$$

or

$$(T_{\mu}{}^{\nu})_{,}=0, \quad (\bar{T}_{\mu}{}^{\nu})_{\bar{;}}=0 \tag{3}$$

where

$$\begin{aligned} T^{\mu\nu}&\equiv g^{\mu\alpha}g^{\nu\beta}\bar{g}_{\alpha\beta},\\ T_{\mu}{}^{\nu}&\equiv g^{\nu\alpha}\bar{g}_{\mu\alpha},\\ \bar{T}^{\mu\nu}&\equiv \bar{g}^{\mu\alpha}\bar{g}^{\nu\beta}g_{\alpha\beta},\\ \bar{T}_{\mu}{}^{\nu}&\equiv \bar{g}^{\nu\alpha}g_{\mu\alpha}, \end{aligned} \tag{4}$$

and $(\ )_{,}$ denotes covariant differentiation with respect to the $g_{\mu\nu}$ space and $(\ )_{\bar{;}}$ the same with regard to the $\bar{g}_{\mu\nu}$ space, (3) following from the fact that the tensor divergence of the left-hand sides of (1) and (2) with respect to $g_{\mu\nu}$ and $\bar{g}_{\mu\nu}$ [4] are respectively and identically zero.

Further, in conjunction with the field equation and its supplement, it will be supposed that the condition for "empty" space

$$\bar{g}_{\mu\nu}=\lambda g_{\mu\nu} \tag{5}$$

is valid where λ is another constant expressible in terms of Λ, Λ_1, and k. The introduction of (5) in (1) and (2) entails for consistency the relationship

$$\lambda=\frac{8\pi k-\Lambda}{8\pi-\Lambda_1}. \tag{6}$$

[4] Meaning that the Christoffel symbols of the second kind which occur in covariant differentiation are constructed from the $\bar{g}_{\mu\nu}$.

This condition is introduced because of the difficulty encountered if the usual condition for empty space $\bar{g}_{\mu\nu}=0$ is used in the computation of the derived elements $\bar{R}_{\mu\nu}$ and $\bar{R}$. Flat space in the theory could have been realized previously if $\bar{g}_{\mu\nu}=-(\Lambda/8\pi)g_{\mu\nu}$ which if the coordinates are Cartesian would imply a tension and negative density of energy of constant value throughout space if $(\Lambda>0)$ unless the cosmological constant were equal to zero. Thus flat space is not necessarily empty space unless it can be established that $\Lambda=0$.

Also it is to be noted that the structure of $\bar{g}_{\mu\nu}$ in regards to the source of the stress-energy-momentum components does not occur. This may prove to be advantageous from a philosophical point of view in that the phenomenon of electricity and magnetism can be attributed to symmetry properties of the region under consideration involving the stresses. On the other hand, this may prove to be a serious disadvantage.

Another interesting feature flows from the structure of the equations. Just as we have the line element

$$ds^2=g_{\mu\nu}dx^{\mu}dx^{\nu} \tag{7}$$

constructed via the $g_{\mu\nu}$ we can define the differential quadratic form involving the $\bar{g}_{\mu\nu}$

$$d\bar{s}^2=\bar{g}_{\mu\nu}dx^{\mu}dx^{\nu} \tag{8}$$

and apply a result of differential geometry[5] which states that a real transformation of coordinates exists such that (7) and (8) in the *neighborhood* of a point can be put into the forms

$$\begin{aligned} ds^2&=-dx^2-dy^2-dz^2+dt^2,\\ d\bar{s}^2&=-\rho_1dx^2-\rho_2dy^2-\rho_3dz^2+\rho_4dt^2, \end{aligned} \tag{9}$$

where the ρ's are invariants and roots of the determinant equation

$$|\bar{g}_{\mu\nu}-\rho g_{\mu\nu}|=0. \tag{10}$$

Of course (7) and (8) can be transformed into

$$\begin{aligned} ds^2&=-\frac{1}{\rho_1}dx^2-\frac{1}{\rho_2}dy^2-\frac{1}{\rho_3}dz^2+\frac{1}{\rho_4}dt^2,\\ d\bar{s}^2&=-dx^2-dy^2-dz^2+dt^2. \end{aligned} \tag{11}$$

[5] L. P. Eisenhart, *Riemannian Geometry* (Princeton University Press, 1926), p. 108.

Equation (9) admits the possibility of abolishing the gravitational field in the neighborhood of a point *together* with the off-diagonal elements of the tensor $\bar{g}_{\mu\nu}$ which would correspond physically to the "abolishment" of a flow of energy and momentum at the point of interest. Equation (11) yields results of a similar nature corresponding to the indication that in the region of a point the off-diagonal elements of the metric are not present. Both (9) and (11) yield $T_1^1=\rho_1$, $T_2^2=\rho_2$, $T_3^3=\rho_3$, and $T_4^4=\rho_4$.

APPLICATION TO THE ROBERTSON-WEYL COSMOLOGICAL MODEL

On the basis of the assumptions of spatial homogeneity and isotropy together with the introduction of a cosmic time orthogonal to the spatial part of the line element, Robertson's line element

$$ds^2=-e^{f(r)+g(t)}(dr^2+r^2d\theta^2+r^2\sin^2\theta d\varphi^2)+dt^2 \quad (12)$$

yields when one imposes the condition $(T_\mu^\nu)_{,\nu}=0$,

$$\frac{dT_4^4}{dt}+\tfrac{3}{2}\dot{g}(T_4^4-T_1^1)=0, \quad (13)$$

where the T's are at most functions of t and $T_1^1=T_2^2=T_3^3$. Using (4) we can then write

$$\begin{aligned}\bar{g}_{11}&=-e^{f+g}T_1^1,\\ \bar{g}_{22}&=-r^2e^{f+g}T_1^1,\\ \bar{g}_{33}&=-r^2\sin^2\theta e^{f+g}T_1^1,\\ \bar{g}_{44}&=T_4^4.\end{aligned} \quad (14)$$

In (14) if one puts $e^{g_1}=e^gT_1^1$ and changes the scale of t in a suitable fashion, (14) is rendered similar to the metrics in (12) with g replaced by g_1. Consequently, one has analogously to (13) after transforming back to the old t

$$\frac{d\bar{T}_4^4}{dt}+\tfrac{3}{2}\dot{g}_1(\bar{T}_4^4-\bar{T}_1^1)=0, \quad (15)$$

remembering that

$$e^{g_1}=e^gT_1^1. \quad (16)$$

From (4), (12), and (14) one readily verifies that

$$(T_1^1)(\bar{T}_1^1)=(T_4^4)(\bar{T}_4^4)=1. \quad (17)$$

Putting (17) and (16) in (15) and (13) it can be shown that

$$(T_1^1-T_4^4)\left(\frac{dT_4^4}{dT_1^1}-\frac{3}{2}\frac{T_4^4}{T_1^1}\right)=0. \quad (18)$$

Consequently $(T_\mu^\nu)_{,\nu}=0$ and $(\bar{T}_\mu^\nu)_{;\nu}=0$ simultaneously if either

$$T_1^1=T_4^4$$

or

$$T_4^4=a(T_1^1)^{\frac{1}{4}}, \quad (19)$$

where a is a constant of integration. The first equation of (19) implies from (13) that $T_1^1=T_4^4=$const. or equivalently $\bar{g}_{\mu\nu}=\lambda g_{\mu\nu}$ as demanded for consistency [see (5) and (6)]. The above recalls our definition of "empty" space. Thus we have as a possibility

$$\bar{g}_{\mu\nu}=\lambda g_{\mu\nu}, \quad (20)$$

where the g's are for those in the Robertson-Element. (This is also a possibility for the general case.) It must be pointed out that the constancy of the T's does not necessarily require the constancy of g. From (13) we see that if $T_1^1=T_4^4=$const., g is not necessarily constant.

To investigate the case $T_1^1\neq T_4^4$ one notes from (13) and (19) that

$$g=-2\log b\left((T_1^1)^{\frac{1}{4}}-\frac{1}{a}\right). \quad (21)$$

The field equations for the Robertson element, however, are summarized as[6]

$$\begin{aligned}8\pi T_1^1&=\frac{e^{-g}}{R_0^2}+\ddot{g}+\tfrac{3}{4}\dot{g}^2-\Lambda,\\ 8\pi T_4^4&=\frac{3e^{-g}}{R_0^2}+\tfrac{3}{4}\dot{g}^2-\Lambda,\\ 0&=\frac{dT_4^4}{dt}+\tfrac{3}{2}\dot{g}(T_4^4-T_1^1),\\ T_4^4&=a(T_1^1)^{\frac{1}{4}}.\end{aligned} \quad (22)$$

Only three of the Eqs. (22) are independent, the first two being connected by the third. $f(r)$ is

[6] R. C. Tolman, reference 1, pp. 377, 380.

given by

$$e^{\prime}=\frac{1}{\left(1+\frac{r^2}{4R_0^2}\right)^2}. \tag{23}$$

Defining

$$\omega^2=\frac{8\pi}{3a^2},\quad b_1=\frac{\Lambda}{8\pi},\quad b_0=\frac{3b^2}{8\pi R_0^2},\quad x=a(T_1^{\,1})^{\frac{1}{2}}, \tag{24}$$

and using the second and last equation of (22) with (21) an equation for x is obtained:

$$\left(\frac{dx}{dt}\right)^2=\omega^2(x-1)^2\{x^3-b_0(x-1)^2+b_1\}. \tag{25}$$

Equation (25) can be integrated in terms of known functions.[7] Considering the supplemental equations: The $\bar{g}_{\mu\nu}$ in (14) can be put in the same form as the metrics in (12) by defining $e^{\bar{g}_1}=T_1^{\,1}e^{g}$ and changing the scale of t according to $dt_1=dt(T_4^{\,4})^{\frac{1}{2}}$, and if one defines

$$\bar{\omega}^2=\frac{8\pi ka^2}{3},\quad \bar{b}_1=\frac{\Lambda_1}{8\pi k},\quad \bar{b}_0=\frac{3\bar{b}^2}{8\pi kR_0^2},$$
$$\bar{x}=\frac{1}{a}(T_1^{\,1})^{\frac{1}{2}} \tag{26}$$

the analog of (25) follows:

$$\left(\frac{d\bar{x}}{dt_1}\right)^2=\bar{\omega}^2(\bar{x}-1)^2\{\bar{x}^3-\bar{b}_0(\bar{x}-1)^2+\bar{b}_1\}. \tag{27}$$

Recalling that $T_1^{\,1}\bar{T}_1^{\,1}=1$ and changing back to the old t, we find Eq. (27) becomes

$$\left(\frac{dx}{dt}\right)^2=\frac{\bar{\omega}^2}{a^2}x^2(x-1)^2\{x^3-\bar{b}_0(x-1)^2+b_1\}. \tag{28}$$

For consistency, in this case, the result of integrating (25) should be the same as (28). In the first place, the result obtained by elimination of dx/dt from (25) and (28) will be a quintic equation for x, $(x\neq 1)$, which will have for its solution five numbers

$$x_1, x_2, x_3, x_4, x_5=\text{const.} \tag{29}$$

If one denotes the integrals of (25) and (28) by I_1 and I_2, respectively, then

$$x=I_1(t)-I_1(0)+x_0,$$
$$x=I_2(t)-I_2(0)+x_0. \tag{30}$$

But for consistency

$$I_1(t)-I_2(t)=I_1(0)-I_2(0). \tag{31}$$

Equation (31) in principle can be solved for t to obtain a series of values t in general. Hence, in case $T_4^{\,4}=a(T_1^{\,1})^{\frac{1}{2}}$ the solution of the problem consists of five discrete sets of number pairs:

$$\begin{array}{ccccc} x_1 & x_2 & x_3 & x_4 & x_5 \\ t_1 & t_1 & t_1 & t_1 & t_1 \\ t_2 & t_2 & t_2 & t_2 & t_2 \\ \cdot & \cdot & \cdot & \cdot & \cdot \\ \cdot & \cdot & \cdot & \cdot & \cdot \\ \cdot & \cdot & \cdot & \cdot & \cdot \end{array} \tag{32}$$

where the t's are solutions of (31) and the x's the roots of the quintic obtained by the elimination of dx/dt from (25) and (28). The nature of the solution is such as to suggest that knowledge of x in the intervals $t_i<t<t_{i+1}$ is not ascertainable, a result the physical significance of which is not readily understandable. The number set (32) is determined so as to be consistent with (25) and (28) with regards to x and dx/dt. The set will at least consist of one point in general. In our case, since the equation is a quintic, at least one real root x exists. It is possible to choose the initial condition so that when $t=0$, $x=x_1=x_0$, since a root of (31) is obviously $t=0$. Hence, the consistency condition leads to the result that at least one number pair $(x, 0)$ exists for which the field equation is consistent with its supplement for the case $T_1^{\,1}\neq T_4^{\,4}$. Furthermore, at this point x and dx/dt are determined. The physical interpretation of this result for the case now under consideration is that knowledge of x and consequently $T_1^{\,1}$, $T_4^{\,4}$, and g at the present time $t=0$ is not sufficient to enable the evaluation of the above quantities at later times. The values when $t=t_1$ are those obtained when measurements are made when $t=t_1$, a somewhat puerile result under the circumstances. Nevertheless, the result of measurement at a future time $t=t_1$ will still lead to $x=x_0$ and with $dx/dt\neq 0$ but will have that value determined by substituting

[7] As elliptic functions of the third kind.

$x=x_0$ in either (25) or (28). Thus, one is led to a function "constant" in time but with $dx/dt\neq 0$, a paradoxical result indeed.[8]

At this point one may apply the foregoing results to the red-shift problems. Suppose we assume that when $t=0$, $g=1$. Then from (21) one obtains

$$g=-2\log\frac{x-1}{x_0-1},\quad \frac{dg}{dt}=-\frac{2}{x-1}\frac{dx}{dt}. \tag{33}$$

Also for purposes of computation, it is believed permissible to define the pseudo-variable functions as

$$x=x_0+\dot{x}_0 t,\quad g=0+\dot{g}_0 t, \tag{34}$$

which is tantamount to assuming that the higher derivatives of x are nil. From (31) one sees that $\dot{g}_0$ is given by

$$\dot{g}_0=\frac{2}{1-x_0}\dot{x}_0, \tag{35}$$

and comparing this with Tolman[9] one comes to the conclusion that

$$\begin{aligned} k&=\frac{1}{1-x_0}x_0,\\ l&=0,\\ m&=0\\ &\cdot\\ &\cdot\\ &\cdot \end{aligned} \tag{36}$$

and consequently that

$$\frac{\delta\lambda}{\lambda}=k\bar{r}+0+\frac{k}{6R_0^2}\bar{r}^3+\cdots. \tag{37}$$

From (25) one obtains

$$\dot{x}_0=\pm\omega(1-x_0)(x_0^3-b_0(x_0-1)^2+b_1)^{\frac{1}{2}}, \tag{38}$$

so that choosing the positive sign

$$k=\omega(x_0^3-b_0(x_0-1)^2+b_1)^{\frac{1}{2}}. \tag{39}$$

Under the assumption $T_4{}^4\gg 1/R_0^2-\Lambda/3a^2$ (24) and (39) yield

$$k^2=\frac{8\pi}{3a^2}x_0^3=\frac{8\pi}{3}T_4{}^4. \tag{40}$$

Consequently

$$8\pi T_4{}^4=3k^2. \tag{41}$$

Equation (41) shows that the proper density of energy is equal to the square of the recession factor aside from the factor $3/8\pi$.

It is not too difficult to show that for the case $T_1{}^1=T_4{}^4$ or equivalently $\bar{g}_{\mu\nu}=\lambda g_{\mu\nu}$

$$e^{f+g}=\begin{cases}\dfrac{3\cosh^2\left(\frac{\lambda_1}{3}\right)^{\frac{1}{2}}(t+\delta)}{|R_0^2|\lambda_1\left(1-\frac{r^2}{4|R_0^2|}\right)^2}, & \lambda_1>0,\ R_0^2<0\\[2ex] \dfrac{3\cos^2\left(\frac{|\lambda_1|}{3}\right)^{\frac{1}{2}}(t+\delta)}{R_0^2|\lambda_1|\left(1+\frac{r^2}{4R_0^2}\right)^2}, & \lambda_1<0,\ R_0^2>0\end{cases} \tag{42}$$

where $\lambda_1=\Lambda+8\pi\lambda$. δ is an arbitrary constant which can be chosen so that when $t=0$, $r=0$, $e^{f+g}=1$. Doing so, one obtains from the two equations (42), respectively,

$$\begin{aligned}\cosh^2\left(\frac{\lambda_1}{3}\right)^{\frac{1}{2}}\delta&=\frac{|R_0^2|\lambda_1}{3},\\ \cos^2\left(\frac{|\lambda_1|}{3}\right)^{\frac{1}{2}}\delta&=\frac{R_0^2|\lambda_1|}{3}.\end{aligned} \tag{43}$$

Comparing with Tolman[9] again, one obtains for the coefficients k and l in the expansion of $\delta\lambda/\lambda$

$$\begin{aligned} k&=\left(\frac{\lambda_1}{3}-\frac{1}{|R_0|^2}\right)^{\frac{1}{2}}, & k&=-\left(\frac{R}{R_0^2}-\frac{|\lambda_1|}{3}\right)^{\frac{1}{2}},\\ l&=-\frac{1}{2|R_0^2|}, & l&=-\frac{1}{2R_0^2},\\ \lambda_1&>0, & \lambda_1&<0. \end{aligned} \tag{44}$$

Observationally, however, $k>0$ so that the case $\lambda_1<0$ can be ruled out on this ground alone. Making the assumption that $|R_0|^2=\infty$, and

[8] The pseudo-variable function $x(t)$ is defined to have the properties $dx/dt\neq 0$, $x=$const. Since $dx/dt=$const. also, it is necessary to specify that $d^{2n}x/dt^{2n}=0$, $n\geq 1$. The integral properties of the pseudo-variable function can be obtained from its differentiation properties. Thus $\int_0^t x(t)dt=0+x(0)t+\frac{1}{2}\dot{x}(0)t^2$ as obtained by expanding the integral about $t=0$. These definitions suffice to maintain consistency.

[9] Reference 1, pp. 470–472.

$\Lambda=0$, we find Eq. (44) yields

$$8\pi\lambda=3k^2, \tag{45}$$

so that

$$8\pi T_4{}^4=8\pi T_1{}^1=3k^2, \tag{46}$$

whence the proper density of energy *and* negative pressure are connected in the same way as the proper density of energy in the case $T_1{}^1\neq T_4{}^4$.

The algebraic consequences of the theory could be carried out further.

CONCLUSION

On the basis of the field equation and the proposed supplement, it was found possible to construct a universal model having a pseudo-stationary property capable of explaining the red-shift as caused by velocity shifts. It is not maintained, however, that the supplemental equations are universal in scope although the possibility for this may exist. Nevertheless, in regards to the large scale behavior of matter, the equations may be the correct ones to use inasmuch as most of the facts of observational cosmology are consistent with the deductions, such as those which flow from the structure of the Robertson element itself, together with the rather attractive feature of a constant proper-density of energy and the aforementioned stationary character of the universe. Reality, however, is not always very attractive.

PHYSICAL REVIEW VOLUME 67, NUMBERS 5 AND 6 MARCH 1 AND 15, 1945

Auxiliary Conditions and Electrostatic Interaction in Generalized Quantum Electrodynamics

BORIS PODOLSKY, *Department of Physics, University of Cincinnati, Cincinnati, Ohio*

AND

CHIHIRO KIKUCHI, *Department of Physics, Haverford College, Haverford, Pennsylvania**

(Received October 9, 1944)

Paralleling a work of Fock we are able to eliminate the auxiliary conditions in our generalized quantum electrodynamics. As in the work of Fock this leads to a determination of both the electrostatic self-energy and electrostatic particle-particle interaction. Both turn out to be finite and in agreement with results obtained classically.

1. INTRODUCTION

IN an earlier paper[1] we have developed the quantum-mechanical formalism of a generalized electrodynamics. Here we shall derive further consequences, particularly those of the auxiliary conditions derived earlier.

Consider the wave equation

$$\left(\bar{H}_f+H_a-i\hbar\frac{\partial}{\partial T}\right)\Psi=0, \tag{1.1}$$

where $\bar{H}_f$ is the Hamiltonian of the radiation field, H_a the sum of the relativistic Hamiltonian of charged particles and their field-particle interactions, and T is the common time

$$H_a\equiv\sum_{s=1}^{n}(H_s+V_s)=\sum_{s=1}^{n}\{c\boldsymbol{\alpha}_s\cdot\mathbf{p}_s+c^2m_s\alpha_s{}^4+\epsilon_s[\phi(\mathbf{r}_s,T)-\boldsymbol{\alpha}_s\cdot\mathbf{A}(\mathbf{r}_s,T)]\}.$$

---

* Now at Michigan State College, East Lansing, Michigan.

[1] The two previous papers, B. Bodolsky, Phys. Rev. **62**, 68 (1942) and B. Podolsky and C. Kikuchi, **65**, 228 (1944) will be referred to as GE I and II, respectively.

Rosenfeld[2] has shown that, if the dynamical variables are transformed according to

$$F'=\exp(i\bar{H}_f T/\hbar)F\exp(-i\bar{H}_f T/\hbar),$$

Eq. (1.1) can be written as

$$\left[\sum_{s=1}^{n}(H_s+V_s')-ih\partial/\partial T\right]\Psi'=0, \tag{1.2}$$

where

$$\Psi'=\Psi'(\mathbf{r}_1, \mathbf{r}_2, \cdots \mathbf{r}_n; J; T)=\exp(i\bar{H}_f T/\hbar)\Psi.$$

Now Dirac[3] has shown that the conditions under which this equation can be replaced by the set

$$(R_s-ih\partial/\partial t_s)\Psi'(\mathbf{r}_1, \mathbf{r}_2, \cdots \mathbf{r}_n; t, t_1, t_2, \cdots t_n; J)=0, \tag{1.3}$$

where

$$\Psi'(\mathbf{r}_1, \mathbf{r}_2, \cdots \mathbf{r}_n; J; T)\equiv[\Psi'(\mathbf{r}_1, \cdots \mathbf{r}_n; t, t_1, \cdots t_n; J)]_{t=t_1=\cdots=t_n=T}$$

and

$$R_s=c\boldsymbol{\alpha}_s\cdot\mathbf{p}_s+c^2m_s\alpha_s^4+\epsilon_s[\phi(\mathbf{r}_s, t_s)-\boldsymbol{\alpha}_s\cdot\mathbf{A}(\mathbf{r}_s, t_s)], \tag{1.4}$$

are

(A)
$$\frac{\partial\Psi'}{\partial T}=\left[\left(\frac{\partial}{\partial t}+\sum_{s=1}^{n}\frac{\partial}{\partial t_s}\right)\Psi'\right]_{t=t_1=\cdots=t_n=T} \tag{1.5}$$

and

(B)
$$[R_i, R_j]=0, \tag{1.6}$$

for every pair i, j.

2. ELIMINATION OF AUXILIARY CONDITIONS

The quantity J includes, if the field variables are expressed in the Fourier components, the argument functions[4]

$$\phi(\mathbf{k}), A_1^*(\mathbf{k}), A_2^*(\mathbf{k}), A_3^*(\mathbf{k}), \quad \text{and} \quad \tilde{\phi}(\mathbf{k}), \tilde{A}_1^*(\mathbf{k}), \tilde{A}_2^*(\mathbf{k}), \tilde{A}_3^*(\mathbf{k}). \tag{2.1}$$

Fock has shown that, in Maxwellian electrodynamics, the scalar and the longitudinal component of the vector potential can be eliminated from the wave functional. It does not seem possible to carry through the same elimination from the set (2.1), because the longitudinal component of the extraordinary field does not vanish even in the absence of charged particles. Our problem, therefore, becomes that of finding "how much" of the longitudinal component can be eliminated.

We have found that if the operators

$$Q(\mathbf{k})=\frac{\mathbf{k}\cdot\mathbf{A}(\mathbf{k})}{k}, \quad \tilde{Q}(\mathbf{k})=\frac{a\mathbf{k}\cdot\tilde{\mathbf{A}}(\mathbf{k})-\tilde{B}_0(\mathbf{k})}{a\tilde{k}} \tag{2.2}$$

are introduced, the calculation can be carried through in a manner very similar to Fock's. As in GE I and GE II, $k=|\mathbf{k}|$ and $\tilde{k}=(1+a^2k^2)^{\frac{1}{2}}/a$. The operator $\tilde{B}_0(\mathbf{k})$ is related to $\tilde{B}(\mathbf{k})$, defined in GE II, Eq. (5.2), through the following equation:

$$\tilde{B}_0(\mathbf{k})=i\tilde{B}(\mathbf{k}).$$

It is to be noted that although $Q(\mathbf{k})$ is the total longitudinal component of the ordinary vector potential, the quantity $\mathbf{k}\cdot\tilde{\mathbf{A}}(\mathbf{k})/\tilde{k}$ is not the total longitudinal part of $\tilde{\mathbf{A}}(\mathbf{k})$. Using the commutation rules for $A_i(\mathbf{k})$, $\tilde{A}_i(\mathbf{k})$, and $\tilde{B}_0(\mathbf{k})$, it is easy to show that

$$[Q(\mathbf{k}), Q^*(\mathbf{k}')]=\frac{ch}{2k}\delta(\mathbf{k}-\mathbf{k}'), \quad [\tilde{Q}(\mathbf{k}), \tilde{Q}^*(\mathbf{k}')]=-\frac{ch}{2\tilde{k}}\delta(\mathbf{k}-\mathbf{k}'). \tag{2.3}$$

---

[2] L. Rosenfeld, Zeits. f. Physik **76**, 729 (1932).

[3] P. A. M. Dirac, *Quantum Mechanics* (Oxford University Press, 1935), p. 286.

[4] This section closely parallels the work of V. Fock, Physik. Zeits. Sowjetunion **6**, 449–460 (1934). Actually we ought to distinguish the operators $A_1^*(\mathbf{k})$, $\tilde{A}_2^*(\mathbf{k})$, etc. from their argument functions $\tilde{A}_1(\mathbf{k})$, $\bar{\tilde{A}}(\mathbf{k})$, etc., as was done by Fock, but we prefer not to do this because the notation would become very cumbersome. The context will make it clear whether we mean the operator or the corresponding argument function.

Fock has further shown, for Maxwellian electrodynamics, how the field potential operators can be represented by functional derivatives. For the appropriate representation of the extraordinary field potentials, we note that, if Ω is a functional of some functions, say $\tilde{b}(\mathbf{k})$, the following general relation will be satisfied:

$$\frac{\delta}{\delta\tilde{b}(\mathbf{k}')}\tilde{b}(\mathbf{k})\Omega-\tilde{b}(\mathbf{k})\frac{\delta\Omega}{\delta\tilde{b}(\mathbf{k}')}=\delta(\mathbf{k}-\mathbf{k}')\Omega.$$

Comparing this with the commutation rules developed earlier, we see that it is possible to make the following associations:[5]

$$\begin{aligned}
&\phi^*(\mathbf{k})\rightarrow\frac{ch}{2k}\frac{\delta}{\delta\phi(\mathbf{k})}, \quad \tilde{\phi}^*(\mathbf{k})\rightarrow-\frac{ch}{2\tilde{k}}\frac{\delta}{\delta\tilde{\phi}(\mathbf{k})},\\
&A_l(\mathbf{k})\rightarrow\frac{ch}{2k}\frac{\delta}{\delta A_l^*(\mathbf{k})}, \quad \tilde{A}_l(\mathbf{k})\rightarrow-\frac{ch}{2\tilde{k}}\frac{\delta}{\delta\tilde{A}_e^*(\mathbf{k})},\\
&Q(\mathbf{k})\rightarrow\frac{ch}{2k}\frac{\delta}{\delta Q^*(\mathbf{k})}, \quad \tilde{Q}(\mathbf{k})\rightarrow-\frac{ch}{2\tilde{k}}\frac{\delta}{\delta\tilde{Q}^*(\mathbf{k})},\\
&\tilde{B}_0(\mathbf{k})\rightarrow-\frac{ch}{2\tilde{k}}\frac{\delta}{\delta\tilde{B}_0^*(\mathbf{k})}.
\end{aligned} \tag{2.4}$$

The auxiliary conditions, GE II, Eq. (5.8), can then be written in the form[6]

$$\begin{aligned}
&\frac{ch}{2k}\frac{\delta\Psi}{\delta Q^*(\mathbf{k})}-\phi(\mathbf{k})\Psi=0, \quad \frac{ch}{2\tilde{k}}\frac{\delta\Psi}{\delta\tilde{Q}^*(\mathbf{k})}+\tilde{\phi}(\mathbf{k})\Psi=0,\\
&\frac{ch}{2k}\frac{\delta\Psi}{\delta\phi(\mathbf{k})}-Q^*(\mathbf{k})\Psi=0, \quad \frac{ch}{2\tilde{k}}\frac{\delta\Psi}{\delta\tilde{\phi}(\mathbf{k})}+\tilde{Q}^*(\mathbf{k})\Psi=0.
\end{aligned} \tag{2.5}$$

The solution of these equations is

$$\Psi=\exp(\chi_0-\tilde{\chi}_0)\Omega_0, \tag{2.6}$$

where Ω_0 is a functional not containing $\phi(\mathbf{k})$, $Q^*(\mathbf{k})$, $\tilde{\phi}(\mathbf{k})$, and $\tilde{Q}^*(\mathbf{k})$; and

$$\chi_0=\frac{2}{ch}\int Q^*(\mathbf{k})\phi(\mathbf{k})k\,d\mathbf{k}, \quad \tilde{\chi}_0=\frac{2}{ch}\int\tilde{Q}^*(\mathbf{k})\tilde{\phi}(\mathbf{k})\tilde{k}\,d\mathbf{k}, \tag{2.7}$$

where $d\mathbf{k}$ stands for $dk_x dk_y dk_z$, the volume element in $\mathbf{k}$ space.

If there are charged particles in the field, the modified auxiliary conditions must be used.[7] If we put

$$\begin{aligned}
&f(\mathbf{r}_s,t_s)=(2\pi)^{-\frac{1}{2}}\sum_{s=1}^{n}\epsilon_s\exp i\varphi_s, \quad \varphi_s\equiv ckt_s-\mathbf{k}\cdot\mathbf{r}_s;\\
&\tilde{f}(\mathbf{r}_s,t_s)=(2\pi)^{-\frac{1}{2}}\sum_{s=1}^{n}\epsilon_s\exp i\tilde{\varphi}_s, \quad \tilde{\varphi}_s\equiv c\tilde{k}t_s-\mathbf{k}\cdot\mathbf{r}_s;
\end{aligned} \tag{2.8}$$

[5] For another representation, see C. Kikuchi, Thesis, University of Washington (1944).

[6] The wave functional Ψ used here is identical with Ψ' of Eq. (1.3). The prime has been omitted to simplify the notation. Similarly it is understood that all field operators are those of Eq. (1.2).

[7] Note that the f's defined here differ by a factor from those given earlier in GE II, Eq. (6.3).

Eqs. (6.4) GE II, become

$$\left[Q(\mathbf{k})-\phi(\mathbf{k})+\frac{1}{2k^2}f\right]\Psi=0, \qquad \left[\tilde{Q}(\mathbf{k})-\tilde{\phi}(\mathbf{k})-\frac{1}{2\tilde{k}^2}\tilde{f}\right]\Psi=0,$$
$$\left[Q^*(\mathbf{k})-\phi^*(\mathbf{k})+\frac{1}{2k^2}f^*\right]\Psi=0, \quad \left[\tilde{Q}^*(\mathbf{k})-\tilde{\phi}^*(\mathbf{k})-\frac{1}{2\tilde{k}^2}\tilde{f}^*\right]\Psi=0. \tag{2.9}$$

The wave functional satisfying these equations can be written

$$\Psi=\exp(\chi-\tilde{\chi})\Omega, \tag{2.10}$$

where Ω is again a functional independent of the functions occurring explicitly in Eq. (2.9);

$$\chi=\frac{2}{c\hbar}\int Q^*(\mathbf{k})\phi(\mathbf{k})k\,dk+\frac{1}{c\hbar}\int\phi(\mathbf{k})\frac{f^*}{k}d\mathbf{k}-\frac{1}{c\hbar}\int Q^*(\mathbf{k})\frac{f}{k}d\mathbf{k}+\chi',$$
$$\tilde{\chi}=\frac{2}{c\hbar}\int\tilde{Q}^*(\mathbf{k})\tilde{\phi}(\mathbf{k})\tilde{k}d\mathbf{k}-\frac{1}{c\hbar}\int\tilde{\phi}(\mathbf{k})\frac{\tilde{f}^*}{\tilde{k}}d\mathbf{k}+\frac{1}{c\hbar}\int\tilde{Q}^*(\mathbf{k})\frac{\tilde{f}}{\tilde{k}}d\mathbf{k}+\tilde{\chi}', \tag{2.11}$$

and χ' and $\tilde{\chi}'$ being arbitrary functions of the space-time coordinates of the particles.

As we wish to obtain a wave equation for Ω corresponding to Eq. (1.3) for Ψ we must replace each operator F by

$$\exp(-\chi+\tilde{\chi})F\exp(\chi-\tilde{\chi}).$$

The quantities $\phi(\mathbf{k})$, $Q^*(\mathbf{k})$, $\tilde{\phi}(\mathbf{k})$, $\tilde{Q}^*(\mathbf{k})$, and $\bar{B}_0^*(\mathbf{k})$ are invariant with respect to this transformation, but:

$$\exp(-\chi+\tilde{\chi})Q(\mathbf{k})\exp(\chi-\tilde{\chi})=Q(\mathbf{k})+\phi(\mathbf{k})-\frac{1}{2k^2}f,$$
$$\exp(-\chi+\tilde{\chi})\phi^*(k)\exp(\chi-\tilde{\chi})=\phi^*(\mathbf{k})+Q^*(\mathbf{k})+\frac{1}{2k^2}f^*,$$
$$\exp(-\chi+\tilde{\chi})\tilde{Q}(k)\exp(\chi-\tilde{\chi})=\tilde{Q}(\mathbf{k})+\tilde{\phi}(\mathbf{k})+\frac{1}{2\tilde{k}^2}\tilde{f}, \tag{2.12}$$
$$\exp(-\chi+\tilde{\chi})\tilde{\phi}^*(\mathbf{k})\exp(\chi-\tilde{\chi})=\tilde{\phi}^*(\mathbf{k})+\tilde{Q}^*(\mathbf{k})-\frac{1}{2\tilde{k}^2}\tilde{f}^*$$

and

$$\exp(-\chi+\tilde{\chi})\bar{B}_0(\mathbf{k})\exp(\chi-\tilde{\chi})=\bar{B}_0(\mathbf{k})-\frac{1}{a\tilde{k}}\tilde{\phi}(\mathbf{k})-\frac{1}{2a\tilde{k}^2}\tilde{f}. \tag{2.13}$$

To illustrate how these are calculated, consider the transform of $\bar{B}_0(\mathbf{k})$. From Eq. (2.4), if Λ is a functional of $\bar{B}_0^*(\mathbf{k})$,

$$\exp(-\chi+\tilde{\chi})\bar{B}_0(\mathbf{k})\exp(\chi-\tilde{\chi})\Lambda=-\exp(-\chi+\tilde{\chi})\left(\frac{c\hbar}{2\tilde{k}}\frac{\delta}{\delta\bar{B}_0^*(\mathbf{k})}\right)(\exp(\chi-\tilde{\chi})\Lambda)$$
$$=\frac{-c\hbar}{2\tilde{k}}\frac{\delta\Lambda}{\delta\bar{B}_0^*(\mathbf{k})}+\frac{c\hbar}{2\tilde{k}}\frac{\delta\tilde{\chi}}{\delta\bar{B}_0^*(\mathbf{k})}=\left[\bar{B}_0(\mathbf{k})+\frac{c\hbar}{2\tilde{k}}\frac{\delta\tilde{\chi}}{\delta\bar{B}_0^*(\mathbf{k})}\right]\Lambda.$$

Since from Eq. (2.11),

$$\frac{\delta\tilde{\chi}}{\delta\tilde{B}_0^*(\mathbf{k})}=-\frac{2\tilde{\phi}(\mathbf{k})}{ach}-\frac{\tilde{f}}{ach\tilde{k}^2},$$

Eq. (2.13) follows.

Next we shall show that the vector potentials $\mathbf{A}(\mathbf{k})$ and $\tilde{\mathbf{A}}(\mathbf{k})$ transform as follows:

$$\begin{aligned}\exp(-\chi+\tilde{\chi})\mathbf{A}(\mathbf{k})\exp(\chi-\tilde{\chi})&=\mathbf{A}(\mathbf{k})+\frac{\mathbf{k}}{k}\phi(\mathbf{k})-\frac{\mathbf{k}f}{2k^3},\\ \exp(-\chi+\tilde{\chi})\tilde{\mathbf{A}}(\mathbf{k})\exp(\chi-\tilde{\chi})&=\tilde{\mathbf{A}}(\mathbf{k})+\frac{\mathbf{k}}{\tilde{k}}\tilde{\phi}(\mathbf{k})+\frac{\mathbf{k}\tilde{f}}{2\tilde{k}^3}.\end{aligned}\tag{2.14}$$

Since χ and $\tilde{\chi}$ contain only the longitudinal component of the vector potentials, we have

$$\begin{aligned}\exp(-\chi+\tilde{\chi})\tilde{\mathbf{A}}(\mathbf{k})\exp(\chi-\tilde{\chi})&=\exp(-\chi+\tilde{\chi})(\tilde{\mathbf{A}}_T(\mathbf{k})+\tilde{\mathbf{A}}_L(k))\exp(\chi-\tilde{\chi})\\ &=\tilde{\mathbf{A}}_T(\mathbf{k})+\exp(-\chi+\tilde{\chi})\tilde{\mathbf{A}}_L(\mathbf{k})\exp(\chi-\tilde{\chi}),\end{aligned}\tag{2.15}$$

where the subscripts L and T indicate the longitudinal and transverse parts of $\tilde{\mathbf{A}}(\mathbf{k})$. From Eqs. (2.2) and (2.11) we further obtain

$$\begin{aligned}\exp(-\chi+\tilde{\chi})\tilde{\mathbf{A}}_L(\mathbf{k})\exp(\chi-\tilde{\chi})&\equiv\exp(-\chi+\tilde{\chi})\left[\mathbf{k}\frac{\mathbf{k}\cdot\tilde{\mathbf{A}}(\mathbf{k})}{k^2}\right]\exp(\chi-\tilde{\chi})\\ &=\frac{\mathbf{k}\mathbf{k}\cdot\tilde{\mathbf{A}}(\mathbf{k})}{k^2}+\frac{\mathbf{k}}{\tilde{k}}\tilde{\phi}(\mathbf{k})+\frac{\mathbf{k}}{2\tilde{k}^3}\tilde{f}.\end{aligned}$$

Substitution of this into Eq. (2.15) yields the desired result.

3. ELECTROSTATIC SELF-ENERGY

Let us transform back into coordinate space by means of the formula

$$F(\mathbf{r},t)=(2\pi)^{-4}\int\{F(\mathbf{k})\exp(-i\varphi)+F^*(\mathbf{k})\exp(i\varphi)+\tilde{F}(\mathbf{k})\exp(-i\tilde{\varphi})+\tilde{F}^*(\mathbf{k})\exp(i\tilde{\varphi})\}d\mathbf{k},\tag{3.1}$$

where

$$\varphi=ckt-\mathbf{k}\cdot\mathbf{r},\quad\tilde{\varphi}=c\tilde{k}t-\mathbf{k}\cdot\mathbf{r}.$$

We then obtain

$$\begin{aligned}\exp(-\chi+\tilde{\chi})\mathbf{A}(\mathbf{r}_s,t_s)\exp(\chi-\tilde{\chi})&=\mathbf{A}(\mathbf{r}_s,t_s)+(2\pi)^{-4}\int\frac{\mathbf{k}}{k}\phi(\mathbf{k})\exp(-i\varphi_s)d\mathbf{k}\\ &+(2\pi)^{-4}\int\frac{\mathbf{k}}{\tilde{k}}\tilde{\phi}(\mathbf{k})\exp(-i\varphi_s)d\mathbf{k}-\tfrac{1}{2}(2\pi)^{-4}\int\frac{\mathbf{k}}{k^3}f\exp(-i\varphi_s)d\mathbf{k}+\tfrac{1}{2}(2\pi)^{-4}\int\frac{\mathbf{k}}{\tilde{k}^3}\tilde{f}\exp(-i\varphi_s)d\mathbf{k},\end{aligned}\tag{3.2}$$

and

$$\begin{aligned}\exp(-\chi+\tilde{\chi})\phi(\mathbf{r}_s,t_s)\exp(\chi-\tilde{\chi})&=\phi(\mathbf{r}_s,t_s)+(2\pi)^{-4}\int Q^*(\mathbf{k})\exp(i\varphi_s)d\mathbf{k}+(2\pi)^{-4}\int\tilde{Q}^*(\mathbf{k})\exp(i\tilde{\varphi}_s)d\mathbf{k}\\ &+\tfrac{1}{2}(2\pi)^{-4}\int\frac{f^*}{k^2}\exp(i\varphi_s)d\mathbf{k}-\tfrac{1}{2}(2\pi)^{-4}\int\frac{\tilde{f}^*}{\tilde{k}^2}\exp(i\tilde{\varphi}_s)d\mathbf{k}.\end{aligned}\tag{3.3}$$

Furthermore

$$\exp(-\chi+\tilde{\chi})p_s^{(s)}\exp(\chi-\tilde{\chi})=p_s^{(s)}-i\hbar\frac{\partial}{\partial x_s}(\chi-\tilde{\chi}),$$

and

$$\exp(-\chi+\tilde{\chi})(i\hbar\partial/\partial t_s)\exp(\chi-\tilde{\chi})=i\hbar\partial/\partial t_s+i\hbar\frac{\partial}{\partial t_s}(\chi-\tilde{\chi}). \tag{3.4}$$

We are now ready to derive the transformation properties of

$$P_x^{(s)}\equiv -i\hbar\partial/\partial x_s-(\epsilon_s/c)A_x(\mathbf{r}_s,t_s)$$

and

$$T^{(s)}\equiv i\hbar\partial/\partial t_s-\epsilon_s\phi(\mathbf{r}_s,t_s) \tag{3.5}$$

occurring in Eq. (1.3).

For convenience, we shall introduce the quantities

$$\mathbf{D}(\mathbf{k})=\mathbf{A}(\mathbf{k})-\mathbf{k}\mathbf{k}\cdot\mathbf{A}(\mathbf{k})/k^2$$

and

$$\tilde{\mathbf{D}}(\mathbf{k})=\tilde{\mathbf{A}}(\mathbf{k})-\mathbf{k}\mathbf{k}\cdot\tilde{\mathbf{A}}(\mathbf{k})/\tilde{k}^2+\mathbf{k}\tilde{B}_0(\mathbf{k})/a\tilde{k}^2 \tag{3.6}$$

which satisfy the commutation rules

$$[D_i(\mathbf{k}),D_j^*(\mathbf{k}')]=\frac{ch}{2k}\left(\delta_{ij}-\frac{k_ik_j}{k^2}\right)\delta(\mathbf{k}-\mathbf{k}'),$$

and

$$[\tilde{D}_i(\mathbf{k}),\tilde{D}_j^*(\mathbf{k}')]=-\frac{ch}{2\tilde{k}}\left(\delta_{ij}-\frac{k_ik_j}{k^2}\right)\delta(\mathbf{k}-\mathbf{k}'). \tag{3.7}$$

We also need the relations:

$$\frac{\partial\chi}{\partial x_s}=\frac{i\epsilon_s}{ch}(2\pi)^{-\frac{1}{2}}\int\frac{k_x}{k}\phi(\mathbf{k})\exp(-i\varphi_s)d\mathbf{k}+\frac{i\epsilon_s}{ch}(2\pi)^{-\frac{1}{2}}\int\frac{k_x}{k}Q^*(\mathbf{k})\exp(i\varphi_s)d\mathbf{k}+\partial\chi'/\partial x_s,$$

$$-\frac{\partial\tilde{\chi}}{\partial x_s}=\frac{i\epsilon_s}{ch}(2\pi)^{-\frac{1}{2}}\int\frac{k_x}{\tilde{k}}\tilde{\phi}(\mathbf{k})\exp(-i\tilde{\varphi}_s)d\mathbf{k}+\frac{i\epsilon_s}{ch}(2\pi)^{-\frac{1}{2}}\int\frac{k_x}{\tilde{k}}\tilde{Q}^*(\mathbf{k})\exp(i\tilde{\varphi}_s)d\mathbf{k}-\partial\tilde{\chi}'/\partial x_s,$$

$$\frac{\partial\chi}{\partial t_s}=-\frac{i\epsilon_s}{ch}(2\pi)^{-\frac{1}{2}}\int\phi(\mathbf{k})\exp(-i\varphi_s)d\mathbf{k}-\frac{i\epsilon_s}{ch}(2\pi)^{-\frac{1}{2}}\int Q^*(\mathbf{k})\exp(i\varphi_s)d\mathbf{k}+\partial\chi'/\partial t_s,$$

and

$$-\frac{\partial\tilde{\chi}}{\partial t_s}=-\frac{i\epsilon_s}{ch}(2\pi)^{-\frac{1}{2}}\int\tilde{\phi}(\mathbf{k})\exp(-i\tilde{\varphi}_s)d\mathbf{k}-\frac{i\epsilon_s}{ch}(2\pi)^{-\frac{1}{2}}\int\tilde{Q}^*(\mathbf{k})\exp(i\tilde{\varphi}_s)d\mathbf{k}-\partial\tilde{\chi}'/\partial t_s. \tag{3.8}$$

Therefore, the transforms of Eq. (3.5) turn out to be

$$P_s'^{(s)}\equiv\exp(-\chi+\tilde{\chi})P_x^{(s)}\exp(\chi-\tilde{\chi})$$

$$=p_x^{(s)}-\frac{\epsilon_s}{c}D_x(\mathbf{r}_s,t_s)-i\hbar\frac{\partial}{\partial x_s}(\chi'-\tilde{\chi}')+\frac{\epsilon_s}{2c}(2\pi)^{-\frac{1}{2}}\int\left[\frac{k_xJ}{k^2}\exp(-i\varphi_s)-\frac{k_x\tilde{f}}{\tilde{k}^2}\exp(-i\tilde{\varphi}_s)\right]d\mathbf{k} \tag{3.9}$$

and similarly,

$$T'^{(s)}=ih\frac{\partial}{\partial t_s}+ih\frac{\partial}{\partial t_s}(\chi'-\tilde{\chi}')-\frac{\epsilon_s}{2}(2\pi)^{-1}\int\left[\frac{f^*}{k^2}\exp(i\varphi_s)-\frac{\tilde{f}^*}{\tilde{k}^2}\exp(i\tilde{\varphi}_s)\right]d\mathbf{k}. \tag{3.10}$$

In both Eqs. (3.9) and (3.10) the terms involving $Q(\mathbf{k})$, $\tilde{Q}(\mathbf{k})$, $\phi^*(\mathbf{k})$, $\tilde{\phi}^*(\mathbf{k})$ drop out because their argument functions have been eliminated from the wave functional; i.e.,

$$Q(\mathbf{k})\Omega=\tilde{Q}(\mathbf{k})\Omega=\phi^*(\mathbf{k})\Omega=\tilde{\phi}^*(\mathbf{k})\Omega=0.$$

Since χ' and $\tilde{\chi}'$ are arbitrary functions of the space-time coordinates, they can be chosen in such a way that their derivatives will just cancel the imaginary terms in Eqs. (3.9) and (3.10). The suitable choices are

$$\chi'=-\frac{1}{4ch}\int\frac{f^*f}{k^3}d\mathbf{k},\quad \tilde{\chi}'=-\frac{1}{4ch}\int\frac{\tilde{f}^*\tilde{f}}{\tilde{k}^3}d\mathbf{k}. \tag{3.11}$$

The real parts of these functions are:

$$-\frac{1}{4ch(2\pi)^3}\sum_{u,v}\epsilon_u\epsilon_v F(\varphi_u-\varphi_v)\quad\text{and}\quad -\frac{1}{4ch(2\pi)^3}\sum_{u,v}\epsilon_u\epsilon_v\tilde{F}(\tilde{\varphi}_u-\tilde{\varphi}_v), \tag{3.12}$$

where

$$F(\varphi_u-\varphi_v)=\int\frac{\cos\{ck(t_u-t_v)-\mathbf{k}\cdot(\mathbf{r}_u-\mathbf{r}_v)\}}{k^3}d\mathbf{k}$$

and (3.13)

$$\tilde{F}(\tilde{\varphi}_u-\tilde{\varphi}_v)=\int\frac{\cos\{c\tilde{k}(t_u-t_v)-\mathbf{k}\cdot(\mathbf{r}_u-\mathbf{r}_v)\}}{\tilde{k}^3}d\mathbf{k}.$$

Hence the operators $P_x'^{(s)}$ and $T'^{(s)}$ become

$$P_x'^{(s)}=p_x^{(s)}-\frac{\epsilon_s}{c}D_x(\mathbf{r}_s,t_s)+\frac{\epsilon_s}{2c(2\pi)^3}\sum_u'\epsilon_u\int\left[\frac{k_x}{k^3}\cos(\varphi_u-\varphi_s)-\frac{k_x}{\tilde{k}^3}\cos(\tilde{\varphi}_u-\tilde{\varphi}_s)\right]d\mathbf{k}$$

$$+\frac{\epsilon_s^2}{2c(2\pi)^3}\int\left[\frac{k_x}{k^3}-\frac{k_x}{\tilde{k}^3}\right]d\mathbf{k}, \tag{3.14}$$

and

$$T'^{(s)}=ih\frac{\partial}{\partial t_s}-\frac{\epsilon_s}{2(2\pi)^3}\sum_u'\epsilon_u\int\left[\frac{\cos(\varphi_u-\varphi_s)}{k^2}-\frac{\cos(\tilde{\varphi}_u-\tilde{\varphi}_s)}{\tilde{k}^3}\right]d\mathbf{k}-\frac{\epsilon_s^2}{2(2\pi)^3}\int\left[\frac{1}{k^2}-\frac{1}{\tilde{k}^2}\right]d\mathbf{k}. \tag{3.15}$$

The primes over the sigmas indicate that the terms $u=s$ are to be omitted in the summation. The last integral in Eq. (3.14) vanishes because the integrand is odd; the analogous term in Eq. (3.15) gives

$$\frac{1}{4\pi}\frac{\epsilon_s^2}{2a},$$

which can be interpreted as the electrostatic self-energy, and agrees with the earlier result calculated classically.[8]

[8] GE I, Eq. (5.4). There ϵ_s is in electrostatic units.

4. ELECTROSTATIC INTERACTION

It will be observed that Eqs. (3.14) and (3.15) can be somewhat simplified by writing

$$U_s=\sum_u{}' \frac{\epsilon_u}{(2\pi)^3}\int\left[\frac{\sin(\varphi_s-\varphi_u)}{k^3}-\frac{\sin(\tilde{\varphi}_s-\tilde{\varphi}_u)}{\tilde{k}^3}\right]d\mathbf{k}. \tag{4.1}$$

Accordingly,

$$P_x'^{(s)}=p_x^{(s)}-\frac{\epsilon_s}{c}D_x(\mathbf{r}_s,t_s)-\frac{\epsilon_s}{2c}\frac{\partial U_s}{\partial x_s}, \tag{4.2}$$

and

$$T'^{(s)}=i\hbar\frac{\partial}{\partial t_s}-\frac{\epsilon_s}{2c}\frac{\partial U_s}{\partial t_s}-\frac{1}{4\pi}\frac{\epsilon_s^2}{2a}. \tag{4.3}$$

It is possible to eliminate the last term in Eq. (4.2) by means of canonical transformation, i.e.,

$$P_x''^{(s)}\equiv\exp(-i\epsilon_s U_s/2ch)P_x'^{(s)}\exp(i\epsilon U_s/2ch)=p_x^{(s)}-\frac{\epsilon_s}{c}D_x(\mathbf{r}_s,t_s), \tag{4.4}$$

$$T''^{(s)}\equiv\exp(-i\epsilon_s U_s/2ch)T'^{(s)}\exp(i\epsilon_s U_s/2ch)=i\hbar\frac{\partial}{\partial t_s}-\frac{\epsilon_s}{c}\frac{\partial U_s}{\partial t_s}-\frac{\epsilon_s^2}{8\pi a}. \tag{4.5}$$

Substituting the above results into Eq. (1.3), we obtain the following for the relativistic wave equation of the sth particle:

$$[c\boldsymbol{\alpha}_s\cdot\mathbf{p}^{(s)}-\epsilon_s\boldsymbol{\alpha}_s\cdot\mathbf{D}(\mathbf{r}_s,t_s)+m_sc^2\alpha_s{}^4]\Omega=\left[i\hbar\frac{\partial}{\partial t_s}-\frac{\epsilon_s}{c}\frac{\partial U_s}{\partial t_s}-\frac{\epsilon_s^2}{8\pi a}\right]\Omega. \tag{4.6}$$

We note that the above equation differs from the usual wave equation in several respects. In the first place, it contains the self-energy term. Secondly, the term $\mathbf{D}(\mathbf{r}_s,t_s)$, which represents the interaction of the sth particle with the field, is not solenoidal but satisfies the more general equation

$$(1-a^2\Box)\operatorname{div}\mathbf{D}=0. \tag{4.7}$$

Finally, we shall show that $\partial U_s/\partial t_s$ gives the particle-particle electrostatic interaction function derived classically in GE I, Eq. (2.6).

Let

$$V_s=\frac{1}{c}\frac{\partial U_s}{\partial t_s}=\sum_u{}' V_{su},\quad V_{su}=V'_{su}-\tilde{V}'_{su}, \tag{4.8}$$

where

$$V'_{su}=\frac{\epsilon_u}{(2\pi)^3}\int\frac{\cos(\varphi_u-\varphi_s)}{k^2}d\mathbf{k}\quad\text{and}\quad\tilde{V}'_{su}=\frac{\epsilon_u}{(2\pi)^3}\int\frac{\cos(\tilde{\varphi}_u-\tilde{\varphi}_s)}{\tilde{k}^2}d\mathbf{k}. \tag{4.9}$$

The first integral can be evaluated very readily. Putting $T=t_u-t_s$, $R=|\mathbf{r}_u-\mathbf{r}_s|$, we get

$$\frac{\epsilon_u}{(2\pi)^3}\int\frac{\cos\{ckT-kR\cos\theta\}}{k^2}d\mathbf{k}=\begin{cases}\epsilon_u/4\pi R, & cT<R\\ 0, & cT>R.\end{cases} \tag{4.10}$$

For the integration in (4.9) we make use of the formula[9]

$$\int_0^\infty J_{\frac{1}{2}}(bk)\frac{J_{\frac{1}{2}}(a\tilde{k})}{\tilde{k}^{\frac{1}{2}}}k^{\frac{1}{2}}dk=\begin{cases}0, & \text{for } a<b\\ -\left(\frac{b}{a}\right)^{\frac{1}{2}}\dfrac{\lambda}{(a^2-b^2)^{\frac{1}{2}}}J_1[\lambda(a^2-b^2)^{\frac{1}{2}}], & \text{for } a>b\end{cases}$$

where $\tilde{k}=(k^2+\lambda^2)^{\frac{1}{2}}$. Multiply both sides by $a^{\frac{1}{2}}$ and integrate. Then, since

$$\int_0^a a^{\frac{1}{2}}J_{\frac{1}{2}}(a\tilde{k})da=\left(\frac{2}{\pi}\right)^{\frac{1}{2}}\tilde{k}^{-\frac{1}{2}}-\frac{a^{\frac{1}{2}}}{\tilde{k}}J_{-\frac{1}{2}}(a\tilde{k}),$$

we obtain, upon substituting the trigonometric equivalents of the half-integral Bessel functions, and finally replacing λ by $1/a$, the result

$$\int_0^\infty \frac{ka^2}{a^2k^2+1}\sin(kR)\cos\left[\frac{cT}{a}(a^2k^2+1)^{\frac{1}{2}}\right]dk$$

$$=\begin{cases}\dfrac{1}{8\pi R}\exp(-R/a) & \text{for } c|T|<R\\ \dfrac{1}{8\pi}\left[\exp(-R/a)/R+\dfrac{1}{a}\displaystyle\int_1^{cT/R}\frac{J_1[(R/a)(\xi^2-1)^{\frac{1}{2}}]}{(\xi^2-1)^{\frac{1}{2}}}d\xi\right] & \text{for } c|T|>R;\end{cases} \tag{4.11}$$

with the help of Eqs. (4.10) and (4.11), we finally obtain

$$V_{su}=\begin{cases}\dfrac{\epsilon_u}{4\pi R}[1-\exp(-R/a)] & \text{for } c|T|<R\\ -\dfrac{\epsilon_u}{4\pi}\left[\exp(-R/a)/R+\dfrac{1}{a}\displaystyle\int_1^{cT/R}\frac{J_1[R(\xi^2-1)^{\frac{1}{2}}/a]}{(\xi^2-1)^{\frac{1}{2}}}d\xi\right] & \text{for } c|T|>R.\end{cases} \tag{4.12}$$

But from the commutation rule, GE II Eqs. (1.7) to (4.10) we see that condition (B), discussed in the introduction, will not be satisfied unless $c|T|<R$. Therefore we shall have to discard that part of Eq. (4.12) for which $c|T|>R$. This does not constitute any limitation, since we are always interested in interactions for particles at the same common time. This would make $T=0<R$.

Our relativistic wave equation thus becomes

$$[c\boldsymbol{\alpha}_s\cdot\mathbf{p}^{(s)}-\epsilon_s\boldsymbol{\alpha}_s\cdot\mathbf{D}(\mathbf{r}_s,t_s)+m_sc^2\alpha_s{}^4]\Omega=\left[i\hbar\frac{\partial}{\partial t_s}-\frac{1}{4\pi}\sum_u{}'\frac{\epsilon_u\epsilon_s}{|\mathbf{r}_s-\mathbf{r}_u|}[1-\exp(-|\mathbf{r}_s-\mathbf{r}_u|/a)]-\frac{\epsilon_s{}^2}{8\pi a}\right]\Omega. \tag{4.13}$$

[9] G. N. Watson, *Theory of Bessel Function* (Cambridge University Press, 1922)— p. 415, Eq. (1), with $\mu=\nu=\frac{1}{2}$.

Letters to the Editor

PROMPT publication of brief reports of important discoveries in physics may be secured by addressing them to this department. The closing date for this department is the third of the month. Because of the late closing date for the section no proof can be shown to authors. The Board of Editors does not hold itself responsible for the opinions expressed by the correspondents. Communications should not in general exceed 600 words in length.

The Electron's Self-Energy

MARIO SCHÖNBERG
Department of Physics of the Faculdade de Filosofia, Ciencias e Letras, University of Sao Paulo, Brazil
February 1, 1945

IN a preceding letter, we have shown the possibility of building a satisfactory classical theory of a point-electron based on two principles:

(a) The total field created by a point charge results from the superposition of an attached field and a radiated one.

(b) Only the radiated field reacts on the emitting charge.

For the radiated field we had:

$$F^{\mu\nu}_{\text{rad}}=\tfrac{1}{2}(F^{\mu\nu}_{\text{ret}}-F^{\mu\nu}_{\text{adv}}). \tag{1}$$

Now we are going to indicate how the assumptions (a) and (b), together with Eq. (1), afford the basis for a satisfactory quantum theory without any self-energies or zero-point energy. Let us expand the potentials $\mathbf{A}_{\text{ret}}$ and ϕ_{ret} in Fourier series, using notations similar to those of Heitler's *Quantum Theory of Radiation* (Oxford, 1936):

$$\left.\begin{aligned}\mathbf{A}_{\text{ret}}&=\sum_\sigma(q_\sigma\mathbf{A}_\sigma+q_\sigma^*\mathbf{A}_\sigma^*)+\sum_\lambda(q_\lambda\mathbf{A}_\lambda+q_\lambda^*\mathbf{A}_\lambda^*),\\ \phi_{\text{ret}}&=\sum_\sigma(a_\sigma\phi_\sigma+a_\sigma^*\phi_\sigma^*).\end{aligned}\right\} \tag{2}$$

For the advanced potentials we have the expansions:

$$\left.\begin{aligned}A_{\text{adv}}&=i\sum_\sigma(\bar{q}_\sigma\mathbf{A}_\sigma-\bar{q}_\sigma^*\mathbf{A}_\sigma^*)+i\sum_\lambda(\bar{q}_\lambda\mathbf{A}_\lambda-\bar{q}_\lambda^*\mathbf{A}_\lambda^*),\\ \phi_{\text{ret}}&=i\sum_\sigma(\bar{a}_\sigma\phi_\sigma-\bar{a}_\sigma^*\phi_\sigma^*).\end{aligned}\right\} \tag{3}$$

The $(q_\sigma, q_\sigma^*; q_\lambda, q_\lambda^*; a_\sigma, a_\sigma^*)$ and $(\bar{q}_\sigma, \bar{q}_\sigma^*; \bar{q}_\lambda, \bar{q}_\lambda^*; \bar{a}_\sigma, \bar{a}_\sigma^*)$ are our field variables. We must find an hamiltonian $H=H_{\text{el}}+H_{\text{field}}$ such that the resulting Hamilton equations be equivalent to the Dirac wave equation for the electron and the inhomogeneous d'Alembert equations for the potentials. It is of capital importance that both the retarded and advanced potentials have the *same equations of motion*. From this it results that H_{field} is the sum of the energies of the various waves arising from $\mathbf{A}_{\text{ret}}$ and ϕ_{ret} *minus the energies of the waves* arising from $\mathbf{A}_{\text{adv}}$, and ϕ_{adv}, because the advanced and retarded potentials appear *with opposite signs* in H_{el}:

$$H_{\text{el}}=c\left(\mathbf{p}-\frac{e}{c}\mathbf{A}_{\text{rad}}\right)\cdot\boldsymbol{\alpha}+\beta mc^2+e\phi_{\text{rad}}. \tag{4}$$

The contributions of the advanced field behave as negative energy photons would do and the respective values of the frequencies in the matrix elements are negative, because of the factor i in expansions (3).

The longitudinal terms in H disappear when we apply Fermi's method of replacing them by Coulomb energies. The transverse self-energy results equal zero and the zero-point energy vanishes, because there are field oscillators with both positive and negative energies.

Similar considerations can be developed both in the meson and the positron theories, allowing one to eliminate difficulties, as will be shown elsewhere.

Part of the results of this letter were discussed at the meeting of the Brazilian Academy of Sciences, December 12, 1944.

High Energy Neutron-Proton Scattering and the Saturation Problem

LAMEK HULTHÉN
Institutionen för mekanik och matematisk fysik, Lund, Sweden
February 17, 1945

THE well-known property of heavy atomic nuclei called saturation—i.e., the fact that nuclear volume and binding energy are roughly proportional to the number of particles present, the mass number—is one of the most important empiric foundations of the theory of nuclear forces. Ever since the primary work of Heisenberg in 1932,[1] it has been regarded almost as an axiom that the saturation is to be explained as a pure exchange phenomenon analogous to the homopolar chemical binding. From a theoretical point of view this is a simple and attractive explanation, but it is very difficult to reconcile with the recent experiments on the angular distribution of fast neutrons scattered by protons.[2,3]

To illustrate this difficulty, let us consider the theory of Møller and Rosenfeld,[4] where the above-mentioned exchange character is particularly prominent. Neglecting the non-static effects which are of secondary importance in this connection, we find the interaction between two nucleons '1' and '2' can, according to the MR-theory, be written (cf. Ref. 4, p. 38):

$$V_{\text{MR}}(r)=(\boldsymbol{\tau}^{(1)}\boldsymbol{\tau}^{(2)})(g_1^2+g_2^2(\boldsymbol{\sigma}^{(1)}\boldsymbol{\sigma}^{(2)}))\frac{e^{-\varkappa r}}{4\pi r}.$$

From the Pauli principle (and the fact that the force is attractive in a ^1S-state) follows that this force is *repulsive* in all states of *odd* parity, the average of $V_{\text{MR}}(r)$ over the different possible spin and charge states being O. It is well-known that just this property of the force leads to saturation.

But this characteristic feature, that the force is attractive in S, D··· states but repulsive in P, F··· states also leads to a preferentially *backward* scattering of neutrons by protons, i.e., the intensity of the scattered neutrons (referred to the mass-center system of neutron and proton) has a maximum in a direction making 180° with the direction of incidence. It has already been pointed out that this theoretical prediction is inconsistent with the recent experiments.[6]

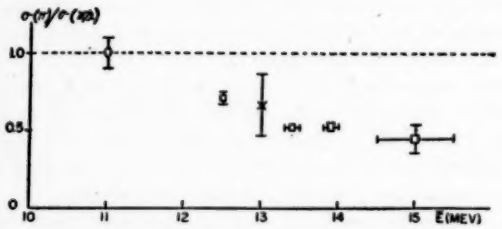

FIG. 1. Intensity ratio $\sigma(\pi)/\sigma(\pi/2)$ (=int. (180°)/int. (90°) in the mass-center system) for various high energies ($\bar{E}$=average energy of the incident neutrons in the laboratory system), according to different measurements; 0—Tatel, ×—Champion and Powell, □—Amaldi, Bocciarelli, Ferretti, and Trabacchi.

It may be of interest to note that the discrepancy becomes less striking if we turn to a pure pseudoscalar symmetrical theory. The interaction of dipole type ('tensor force'), which is of particular importance in this theory, has an angular effect opposite to that of the central force, and therefore the angular distribution is more uniform than in the MR-theory where the terms of dipole interaction type are entirely eliminated.[6] Thus, comparing different symmetrical theories, the pseudoscalar one seems to yield the least pronounced backward scattering. But the calculations give no ground for a hope that this theory might lead to an angular distribution with $\sigma(\pi)/\sigma(\pi/2)<1$ —although the dipole interaction is so dominant as to make it doubtful, according to Volkoff,[7] if such a theory leads to saturation at all.

Recent experiments on the scattering of high energy neutrons by protons indicate a fairly marked forward scattering, as appears from the diagram where the intensity ratio $\sigma(\pi)/\sigma(\pi/2)$ is plotted against the energy of the incident neutrons. (Tatel[8] measured the ratio for 148° and 90°, but the difference is immaterial.) The errors of $\sigma(\pi)/\sigma(\pi/2)$ are those assigned by the several authors themselves. For low energies theory and experiment both give a practically uniform distribution.

It should also be pointed out that these results seem to be qualitatively supported by the experiments of Barschall and Ladenburg on the scattering of 2.5 Mev neutrons by some heavier nuclei.[9] The manifest forward elastic scattering found in this case would be hard to understand theoretically, if the neutron-proton scattering were not of the same type.

Provided the experimental results concerning the neutron-proton scattering are correct, it seems necessary to re-examine the problem of the causes of the saturation and the charge-dependence of the nuclear forces. In this connection it should be mentioned that the non-symmetrical scalar-pseudoscalar theory[10] affords a rather simple possibility for reconciling the saturation properties of heavy nuclei with a neutron-proton scattering of the type indicated by the experiments.[11] At the same time the theory is able to account for the approximate equality of the neutron-proton and proton-proton forces in a ^1S-state. In this case the saturation is explained as a consequence of the repulsive forces with very short range which appear in the higher approximations of the perturbation theory.

In any case it is evident that the experiments in question are of fundamental importance for the further development of the theory, as has already been emphasized by Rarita and Schwinger.[6]

[1] W. Heisenberg, Zeits. f. Physik **77**, 1 (1932).
[2] E. Amaldi, D. Bocciarelli, B. Ferretti, G. C. Trabacchi, Naturwiss. **30**, 582 (1942); Ricerca Sci. **13**, 502 (1942).
[3] F. C. Champion, C. F. Powell, Proc. Roy. Soc. **A183**, 64 (1944).
[4] C. Møller, L. Rosenfeld, Danske Vidensk. Selsk. math.-fys. Medd. **17**, No. 8 (1940).
[5] L. Hulthén, Phys. Rev. **63**, 383 (1943). Formula (1) in this note should read:

$$I(\theta)=1-0.18\cos\theta+0.45\cos^2\theta-0.22\cos^3\theta+0.12\cos^4\theta;$$

thus $I(\pi)/I(\pi/2)=1.97$. A later calculation (Arkiv f. mat. astr. fysik **29A**, No. 33 (1943)) has shown that even F-states must be taken into account: for 14.5 Mev neutrons we then have $I(\pi)/I(\pi/2)\cong 2.2$.
[6] Arkiv **31A**, No. 15 (1944). Cf. also W. Rarita and J. Schwinger, Phys. Rev. **59**, 556 (1941).
[7] G. M. Volkoff, Phys. Rev. **62**, 134 (1942). It is, however, possible that this difficulty will disappear if the interactions of higher order in the perturbation theory are taken into account; cf. a remark on the non-symmetrical theory above.
[8] H. Tatel, Phys. Rev. **61**, 450 (1942).
[9] H. H. Barschall, R. Ladenburg, Phys. Rev. **61**, 129 (1942).
[10] L. Hulthén, K. Fysiograf. Sällsk. Lund Förhandl. **14**, Nr 2 (1944).
[11] Arkiv **31A**, No. 15 (1944).

Range of Light Variation in Cepheid Variables

P. L. BHATNAGAR
University of Delhi, India
February 18, 1945

THE beautiful investigation of Bethe[1] has shown that the energy output of the main sequence stars is satisfactorily accounted for in terms of the C-N cycle of nuclear reactions, whereby hydrogen is transformed into helium, the carbon-nitrogen content remaining unchanged. In the case of the giant stars, however, the observed luminosity is far greater than the computed value on the basis of the C-N cycle, and to explain the observed values, recourse must be had to protonic reactions with H^2, Li^6, Li^7, Be^9, B^{10}, B^{11}—unlike the C-N cycle in these reactions, the nuclei are consumed—which can take place rapidly enough at the comparatively low temperatures prevailing in the interiors of these stars. Gamow and Teller,[2] and also Greenfield,[3] have shown that the above reactions account broadly for the luminosities of the giants. It seems that the short-period group of cluster variables "live" probably on the B^{10} reaction; the Cepheid variables "live" on Li, Be, B^{11}; and the long-period variables, on H^2.

The present note is concerned with the range of light variation and its relation with the amplitude of pulsation. As the star pulsates, the temperature and density inside it undergo a periodic variation, and the rate of energy evolution, due to nuclear reactions at any stage of the pulsation, can be readily computed. If L_1 and L_2 denote the maximum and minimum rates of energy generation for a star of mass M and radius R, then, we find for the reaction $Li^7+H^1=2He^4$, using Eddington's solution[4] for the equation of pulsation,

$$\Delta m\equiv 2.5\log_{10}L_1/L_2\sim\frac{\Delta R}{R}\Big[0.25\{15-10(r'-1)\}+1.19\times10^9(r'-1)\Big(\frac{R}{M\beta\mu}\Big)^4\Big], \quad (1)$$

where the radius R oscillates between the limits $R+\Delta R$ and $R-\Delta R$; i.e., ΔR is the amplitude of pulsation; μ is

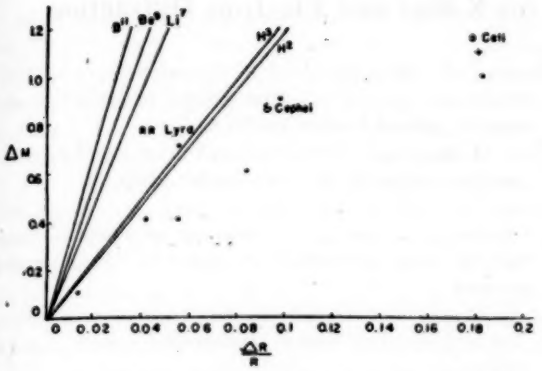

FIG. 1. Theoretical value of Δm for values of $\Delta R/R$. The observed values are shown for various stars.

the mean molecular weight; γ' is the effective ratio of specific heats; β denotes the ratio of gas pressure to total pressure; and its value is given by Eddington's quartic relation. Equation (1) holds practically as long as $\Delta R/R$ does not exceed about $\frac{1}{4}$. It will be observed that the ratio L_1/L_2 does not depend on the concentration of the reactants concerned and is practically insensitive to likely variations in M and R. Taking $M=1.75\times10^{34}$ g and $R=2.02\times10^{12}$ cm (these values correspond to δ Cephei), we have

$$\Delta m\sim2.4\Delta R/R. \tag{2}$$

The value of L_1/L_2 is not appreciably affected whether we take account of the variation of ϵ, the rate of energy generation per unit mass inside the star, or assume the central value ϵ_c to prevail throughout the stellar interior. The value given in Eq. (2) is based on the latter assumption. When the variation of ϵ is taken into account, we find, for example, for $\Delta R/R=0.1$, by a rapid numerical integration $\Delta m=2.5$, which may be compared with the value $\Delta m=2.4$ given by Eq. (2). In Table I, the relation between Δm and $\Delta R/R$ is given for the various reactions:

TABLE I. Variations of Δm and $\Delta R/R$ for various reactions.

$\Delta m\sim12(\Delta R/R)$,	$H^2+H^1=He^3$
$\Delta m\sim12(\Delta R/R)$,	$H^3+H^1=He^4$
$\Delta m\sim24(\Delta R/R)$,	$Li^7+H^1=2He^4$
$\Delta m\sim28(\Delta R/R)$,	$Be^9+H^1=Li^8+He^4$
$\Delta m\sim32(\Delta R/R)$,	$B^{11}+H^1=3He^4$

The observed light variation cannot be identified with Δm because the observed variation will depend on the extent to which the rate of flow of radiation is affected by the variations in temperature and density accompanying pulsation. The total energy generated during a period would, of course, be equal to the total energy radiated per period. As the nuclear processes are far more temperature sensitive than opacity, the observed light variation will not exceed Δm; i.e., Δm prescribes the upper limit to the observed light variation.

In the figure, the observed values for Δm and $\Delta R/R$ are exhibited for Cepheid variables with periods ranging from 0.5^d to 35^d. These values have been taken from Russell, Dugan, and Stewart.[5] The theoretical relationship between Δm and $\Delta R/R$ is also shown in the figure for the various reactions. It is interesting to find that the observed $(\Delta m, \Delta R/R)$ values lie below the theoretical lines for Li, Be, and B. This is, however, not true for the H^2 line, which is shown dotted in the figure, but as the Cepheids do not "live" on the H^2 reaction, the disposition of the H^2 line is not relevant for the Cepheids. The long-period variables, which presumably live on the H^2 reaction, should lie below the H^2 line, and this is the case for the typical long-period variable o Ceti for which the observed variation in radiometric magnitude is about 1.1^m and $\Delta R/R$ about 0.18. A detailed investigation will be published elsewhere.

[1] H. A. Bethe, Phys. Rev. **55**, 434 (1939).
[2] G. Gamow, and E. Teller, Phys. Rev. **55**, 791 (1939).
[3] M. A. Greenfield, Phys. Rev. **60**, 175 (1941).
[4] A. S. Eddington, *The Internal Constitution of Stars* (1926), p. 189.
[5] H. N. Russell, R. S. Dugan, and J. Q. Stewart, *Astronomy* (1938), p. 768.

Loss of Weight by Rotation

LEWI TONKS
General Electric Company, Research Laboratory, Schenectady, New York
February 14, 1945

IN an abstract of a paper[1] Charles T. Dozier analyzes the weight changes of an airplane in level flight according to whether it flies from west to east, or east to west at the equator, with valid conclusions. In view of his subsequent extension of the argument, it should be emphasized that level flight in this case is flight in a circular path —more particularly, a path whose projection on the equatorial plane of the earth is a circle. The particles of the rotating mass which he then envisages (a gyroscope at the equator with vertical axis) have, however, paths whose equatorial plane projections are not circles—they are straight lines! This makes quite a difference.

The astonishing conclusion reached by Dozier led me to set up and solve his problem. By writing down the Hamiltonian for a single particle of the rotating mass, and taking its derivative with respect to the distance from the center of the earth to the plane of rotation of the particle, I have calculated the instantaneous change in weight of the particle due to the combined earth and gyroscopic rotations. It consists of two terms. The first is the centrifugal force associated with the particle in its instantaneous position by virtue of the earth's rotation only, that is, as if the gyroscopic rotation were zero. The second term is dependent on the gyroscopic phase of the particle in a different way, but the variation is such, that in the course of one revolution of the gyroscope this term averages to zero.

It follows that the only loss of weight is the commonly accepted centrifugal one and that there is no such loss of weight by rotation as Dozier announces.

[1] C. T. Dozier, "Loss of Weight by Rotation," read by title at the January 19, 1945 meeting of the American Physical Society in New York City.

Report for 1944 of the American Society for X-Ray and Electron Diffraction

THE ASXRED held a joint meeting with the AAAS X-Ray Conference, at Gibson Island, Maryland, August 21–25, 1944. It was the only meeting of the year. The officers of the ASXRED were: L. H. Germer, president; W. H. Zachariasen, vice president; and J. D. H. Donnay, secretary-treasurer. Those of the conference were: L. H. Germer, chairman; P. P. Debye, vice-chairman.

The following papers were presented:

*Dorothy Wrinch, Smith College, Northampton, Massachusetts. **Fourier transforms and structure factor.**

*W. O. Milligan, Rice Institute, Houston, Texas. **X-rays and catalysis.**

Newell S. Gingrich, University of Missouri. Present address, 7903 Chicago Avenue, Silver Spring, Maryland. **Diffraction of x-rays by liquid elements.**

C. G. Shull, The Texas Company, Beacon, New York. **Some experimental studies of small angle scattering.**

*Richard S. Bear, Massachusetts Institute of Technology. **Small-angle diffraction studies on native protein fibers.**

E. J. Bicek, Illinois Institute of Technology. **Long spacing studies of high polymers.**

*Maurice L. Huggins, Kodak Research Laboratories, Rochester, New York. **Photography of crystal structures by optical Fourier synthesis.**

*J. C. M. Brentano, Northwestern University. **The comparative evaluation of x-ray powder patterns.**

James W. Ballard, Mine Safety Appliances Company, Pittsburgh, Pennsylvania. **Routine quantitative analysis by x-ray diffraction, photometric technique and method.**

M. J. Buerger, Massachusetts Institute of Technology. **The precession method of photographing the reciprocal lattice.**

*G. Tunell, Geophysical Laboratory, Washington, D. C. **The two-circle goniometer.**

F. E. Haworth, Bell Telephone Laboratories, Murray Hill, New Jersey. **Some new x-ray and electron diffraction techniques.**

*I. Fankuchen, Polytechnic Institute, Brooklyn, New York. **Microtechniques in x-ray diffraction.**

The council for 1945 is as follows: W. H. Zachariasen, president; David Harker, vice president; J. D. H. Donnay, secretary; C. C. Murdock, treasurer; L. H. Germer, past-president.

Abstracts of Papers

A1. Small-Angle Diffraction Studies on Protein Fibers. RICHARD S. BEAR.—A survey of the small-angle patterns of collagen (tendon), α-keratin (porcupine quill), β-keratin (feather) and clam muscle has disclosed the following: (1) As many as 20 to 40 or more layer lines are observable on the patterns of the fibers studied. The layer line positions lead to the following values for the fiber-axis periods: 95, 198, 640 and 725A, for feather, porcupine quill, collagen and clam muscle, respectively, and for normal dried materials. With collagen, appropriate treatments have succeeded in producing changes in the x-ray diagrams corresponding to period variations in the range 550–680A. (2) In most of the protein fiber diagrams, the larger part of the diffractions occur on the meridian of the pattern and on prominent row lines, one to each side of the meridian. The lateral spacings calculable from the row lines are 34, 83, and about 325A for feather, porcupine quill and clam muscle, respectively. Collagen patterns show no detectable large spacings other than those on the meridian, which appear to be solely the diffraction orders of the fiber-axis period. (3) Collagen is also distinctive in the manner of intensification of the meridional diffractions. The first order is predominant and corresponds to a slowly changing, longitudinal density variation extending over the entire 640A fiber period. This can be seen in electron microscope photographs of collagen fibrils as a banded structure of the same average period length. The other fibers yield patterns whose innermost intense meridional orders are higher than the first (the fourth, third, and fifth, respectively, for feather, porcupine quill and clam muscle). The clam muscle pattern is particularly interesting in this regard, emphasizing all meridional orders whose indices are multiples of five (to the fortieth). This feature is also recognizable in electron micrographs of clam muscle fibrils as a banded structure whose band period is 145A in longitudinal extension, representing a sub-pattern one-fifth the full 725A fiber period. (4) The diffuse wide-angle interferences are, in reality, clusters of very high orders of the large fundamental spacings. Though the wide-angle fine structure is only partially resolvable, it becomes more apparent the smaller are the large periods of a given material. (5) In other respects, the wide-angle and small-angle diffractions seem independent. The collagen large period can be varied 20 percent without detectable alteration in the positions of similarly oriented (meridional) wide-angle diffractions. Porcupine quill and clam muscle wide-angle patterns are, except for fine structure, very closely alike, but their small-angle diffractions are quantitatively very different. The electron microscope studies referred to are the work of F. O. Schmitt, C. E. Hall and M. A. Jakus.

* The papers marked by an asterisk are abstracted below.

A2. The Comparative Evaluation of X-ray Powder Patterns. J. C. M. BRENTANO.—Methods are discussed related to the evaluation of the individual line of a powder diffraction pattern (*a* and *c*), to "improving" the intensity distribution of a line (*b*) and to the way of utilizing the line groups of the chemical or morphological constituents of a mixed powder for evaluating the relative amounts present (*d*). In comparing x-ray diffraction lines of various constituents and at different angles, it is in a general way not justified to assume equal intensity distribution throughout the width of the lines. The typical case is that of lines with a comparatively narrow central peak region and a more-or-less extended low density foot or tail. (a) As a method for obtaining the integrated intensities of a line, it is proposed to measure the x-ray exposure by the intensity of the (111) reflection of the silver forming the photographic image. For not too high densities, this is proportionate to the exposure so that the integrated intensity can be obtained by a single measurement. This can be done by a counter. The characteristics of the method are similar to those of scatter densitometry,[1] but it can be applied in a higher density range and is not sensitive to surface scratches. (b) The uneven intensity distribution, which is unfavorable for evaluation by absorption densitometry requiring a point-to-point conversion, can be improved by recording the line pattern on a film rocked with uniform velocity through a range wider than the central dense part of the line, but smaller than its foot. The peak range of the line is thus broadened, and the ratio between densities in that range and the foot region is improved. The contour of the line is thus made more favorable for measurement with less increase of line width than by the use of wide slits or extra focal settings. (c) A rapid way of carrying out the actual point-to-point evaluation by absorption densitometry was found by superposing on the micro-densitometer tracing of the line pattern that of a stepped wedge, both recorded with the same densitometer setting. The tracing of the steps is used to correlate the densitometer record with a blackening curve by projecting the tracing on the curve. By combining (b) and (c) the point-to-point evaluation of each line can be done in one to two minutes. (d) To determine in the quantitative evaluation of the lines of a mixed powder which lines can be utilized and which are affected by superpositions, a separate pattern is taken for each constituent. The intensities of these lines should be proportionate to those of the corresponding line group of the mixed pattern; superpositions lead to departure from proportionality. A graphical method is given which shows up such lines and permits one to utilize all the remaining lines in evaluating the mass ratios of the constituents present in the powder. The method requires that the relative intensities should not be affected by absorption. This can be obtained with a powder rod of negligible absorption or a flat powder layer conforming with the focusing condition discussed by the speaker.[2]

[1] J. C. M. Brentano, Baxter and Cotton, Phil. Mag. **17**, 370 (1934).
[2] J. C. M. Brentano, Proc. Phys. Soc. **47**, 932 (1935) and **49**, 61 (1937).

A3. Some Techniques for the Growth and Preparation of Micro Specimens for X-ray Diffraction Studies. I. FANKUCHEN.—This paper presented techniques for the recrystallization on a micro scale of materials for x-ray study from both solution and the melt. Techniques were also presented for mounting such specimens both in air and sealed in capillary tubes. The use of a micro-camera for the study of local variation in structure was also discussed. The common feature of all apparatus and techniques was that preparation and mounting were all done under the microscope.

A4. Photography of Crystal Structures by Optical Fourier Synthesis. MAURICE L. HUGGINS.—Crystal structure analysts are making increasing use of electron density projections and Patterson vector projections obtained by Fourier series summations of the x-ray diffraction data. Since the direct summations are long and tedious, various methods have been developed for speeding up the summation process. One of these is a modification[1] of Sir Lawrence Bragg's[2] method of photographic superposition of patterns of light and dark bands, the orientation and spacing of the bands, and the times of exposure of the band patterns being determined by the x-ray data. A suitable set of band patterns for this purpose has been prepared on a roll of 35 mm film. With this, typical electron density and Patterson projections have been made in less than an hour. The electron density projections, so obtained, are true pictures of the unit of structure, magnified 100,000,000 or more times. The atoms are readily distinguished, as in the corresponding contour maps drawn from the results of the direct calculations. It is expected that copies of these rolls of band patterns will be made available soon, at a nominal cost, to others engaged in crystal structure work.

[1] M. L. Huggins, J. Am. Chem. Soc. **63**, 66 (1941).
[2] W. L. Bragg, Zeits. f. Krist. **A70**, 475 (1929); *The Crystalline State* (The Macmillan Company, New York and London, 1934), p. 229.

A5. A Review of the Application of X-Ray and Electron Diffraction Methods to Contact Catalysis. W. O. MILLIGAN.—The results of x-ray and electron diffraction examination of contact catalysts is reviewed from the point of view of (a) identification of compounds in catalysts; (b) compounds formed during treatment or use; (c) small angle scattering; and (d) relation between catalytic activity and (1) lattice constants, (2) intensities, (3) crystal size, (4) orientation. The mechanism of the formation of active catalyst is discussed from the point of view of (a) protective action, (b) solid solutions, (c) amorphous and crystalline states, (d) order and disorder, (e) distortion of crystal lattices. The state of absorbed substances and the potentialities of electron microscopic examination of catalysts are considered briefly. A bibliography of 135 references is included.

A6. The Two-Circle Goniometer in the X-ray Laboratory. G. TUNELL.—The principal uses of the two-circle goniometer in the x-ray laboratory are the orientation and

adjustment of faceted crystals for x-ray diffraction photographs and the preliminary determination of axial elements. Faceted crystals can be oriented and adjusted with the two-wide goniometer more rapidly and easily than any other way. Moreover, the adjustment is very flexible; it can be accomplished by a zone of faces, by a pole face alone, by a ring of faces, and in other ways. There are three types of two-circle goniometer: the Goldschmidt, the Czapski, and the Fedorov. None of these is available in the United States at the present time. If one is to be manufactured in this country, it is imperative that the adjustment head be made interchangeable with the Weissenberg, oscillation, and Laue cameras on the market. The method of measurement and calculation with the Goldschmidt goniometer, which is the most generally useful type in the x-ray laboratory, is described in the following works:

V. Goldschmidt, *Index der Krystallformen der Mineralien* (Verlagsbuchhandlung Julius Springer, Berlin, 1886).
V. Goldschmidt, *Krystallographische Winkeltabellen* (Verlagsbuchhandlung Julius Springer, Berlin, 1897).
E. T. Wherry and Charles Palache, "The Goldschmidt Two-circle Method," a collection of papers in *American Mineralogist*, Vol. 5 (1920).
V. Goldschmidt, *Kursus der Kristallometrie* (Gebrüder Borntraeger, Berlin, 1934).
A. Weissberger, "Laboratory Techniques of Organic Chemistry," Interscience (*in press*).

A7. Fourier Transforms and Structure Factor. DOROTHY WRINCH.—This paper summarizes the properties of Fourier transforms with special reference to their use in crystal analysis. Every distribution has its own characteristic Fourier transform and it is shown how, once it is recorded, it can be used for the determination of its contribution to the structure factor of any crystal in which it is part of the unit of pattern, since the Fourier transform of any lattice of points is also a lattice of points, namely the reciprocal lattice. Among those whose Fourier transforms are recorded are many simple point distributions, such as the vertices of a cube, a tetrahedron, an octahedron, finite point sets on a triangular or a hexagonal mesh, etc., which yield the Fourier transforms of like atoms placed at such point sets when multiplied by the atomic scattering factor. Fourier transforms are also recorded for a number of mega-distributions (comprising large numbers of points) including patterned cube and octahedral volumes and the corresponding shells and surfaces. The application of these transforms to the structure factors of small crystals is discussed. The Fourier transforms of a number of finite continuous distributions through cube and octahedral volumes and shells and on cube and octahedral surfaces are also included.

Proceedings of the American Physical Society

Meeting at New York, January 19 and 20, 1945

THE 265th meeting of the Americal Physical Society, being the 1944 Annual Meeting, was held conformably with the wartime practice at Columbia University in New York City on Friday and Saturday, January 19 and 20, 1945. Four hundred and eleven of our members registered, and another hundred and five who were nearly all members of the American Association of Physics Teachers which held meetings concurrently with ours. Columbia University treated us with its usual excellent hospitality, for which we are in particular debt to Messrs. H. W. Farwell and W. W. Havens of the Local Committee.

An outstanding feature of the meeting was the **Symposium on the Solid State** consisting of thirteen invited papers. This was arranged by a Committee of six composed of S. Dushman, T. A. Read, F. Seitz, W. Shockley, S. Siegel, and R. Smoluchowski acting by authorization of the Council. The names of the speakers and the titles of their papers are subjoined, as are those of two other invited papers by O. Beeck and by C. J. Davisson and L. E. Haworth, also the abstracts of twenty contributed papers of which three were read by title. During the symposium, time was set aside for a discussion of the proposal of a Division of the Physics of the Solid State in the Society. Marked differences of opinion were made manifest, and there was evident a strong feeling for continuing with the appointment of successive committees similar to the one which organized this symposium, without organizing a division. The decision was left to the Council.

At the business meeting held on Saturday morning were announced the names of the officers elected at the 1944 elections, the tellers having been M. W. Zemansky and W. E. Lamb. These officers are: *President*, Harvey Fletcher; *Vice President*, Edward U. Condon; *Secretary*, K. K. Darrow; *Treasurer*, G. B. Pegram; *Council members* (four-year term), I. I. Rabi and M. A. Tuve; and members of the *Board of Editors* (three-year term) J. B. Fisk, W. Pauli, and L. I. Schiff.

Following the business meeting the members of the Society were joined by the members of the American Association of Physics Teachers for the session devoted to the three annual events: the Retiring Presidential Address of the American Physical Society (**Twenty-five Years of Mass Spectroscopy** by A. J. Dempster), the Richtmyer Lecture of the Association (**Radiofrequency Spectroscopy** by I. I. Rabi) and the presentation of the Oersted Medal of the Association to H. L. Dodge, with presentation address by L. W. Taylor and response by Mr. Dodge.

The dinner of the Society and of the Association was held on the Friday evening at the Mens' Faculty Club of Columbia University, A. J. Dempster presiding. After-dinner talks were made by Harvey Fletcher, L. W. Taylor, R. C. Gibbs, R. Smoluchowski, W. F. G. Swann, and I. I. Rabi.

The Council of the American Physical Society met on the previous Thursday evening. It elected twenty-three candidates to fellowship and sixty-four to membership: their names follow. By rare good fortune, no names had to be added to the list of members lost through death.

Elected to Fellowship: Harvey Brooks, W. F. Busse, R. H. Cole, C. L. Critchfield, P. C. Cross, J. H. Dillon, Philipp Frank, K. L. Hertel, Cornelius Lanczos, J. L. Lawson, Melvin Mooney, S. H. Neddermeyer, Harry Nyquist, J. R. Pierce, George Placzek, N. Rashevsky, H. J. Reich, Arthur Roberts, Ragnar Rollefson, A. J. F. Siegert, Theodore Soller, L. A. Wood, and L. A. Young.

Elected to Membership: J. L. Barnes, Norman Bekkedahl, Frederick Bennington, Lucien Biberman, H. S. Brown, H. B. Callen, H. L. Cobb, Norman Elliott, Stephen Freeman, Jr., W. M. Good, W. M. Gootschalk, Arnold Graves, L. F. Green, B. S. Greensfelder, David Hagelbarger, R. N. Hall, J. G. Hamilton, Gladys Hargreaves, Mark Harrison, J. M. Hildt, B. G. Hurdle, J. V. Iribarne, D. E. Koshland, Jr., H. A. Levy, H. M. Linnette, R. C. Lord, P. R. Malmberg, Sister Cor Mariae, J. W. Marshall, G. D. Mason, D. R. McMillan, Jr., R. N. Moises, S. O. Morgan, Adair Morrison, F. J. Olmer,

D. W. Osborne, R. L. Rankin, C. H. Reich, H. K. Richards, J. L. Rood, Joseph Rotblat, H. M. Schwartz, Harold Sherman, J. P. Sinclair, G. F. Stockdale, R. W. Stoughton, W. E. Strimling, D. M. Studley, Otto Struve, J. E. Tompkins, D. D. Tunicliff, S. H. Turkel, J. K. Tyson, D. D. Van Horn, A. C. Vine, Roald Wangsness, Kyle Ward, Jr., Sydney Weinbaum, R. B. Wiley, Rosalyn S. Yalow, H. B. Yuen, J. L. Zar, and A. A. Zuehlke.

KARL K. DARROW, *Secretary*
American Physical Society
Columbia University
New York 27, N. Y.

SYMPOSIUM ON THE SOLID STATE

Whither American Physics? F. SEITZ, *Carnegie Institute of Technology.*

The Effect of High Hydrostatic Pressures on the Plastic Properties of Metals. P. W. BRIDGMAN, *Harvard University.*

Amplitude Dependence of Internal Friction of Metals. T. A. READ, *Frankford Arsenal.*

Virtues and Weaknesses of the Domain Concept. W. F. BROWN, JR., *Naval Ordnance Laboratory.*

The Fracture Stresses in Steels. C. M. ZENER, *Watertown Arsenal.*

Mechanical Properties and Structure of Alloys. M. GENSAMER, *Carnegie Institute of Technology.*

Some Aspects of the Theory of Ferromagnetism. J. H. VAN VLECK, *Harvard University.*

Creep of Metals as a Reaction Velocity. S. DUSHMAN, *General Electric Company.*

The Statistical Problem in Cooperative Phenomena. G. H. WANNIER, *University of Iowa.*

Effect of Small Stresses on Magnetic Properties. R. M. BOZORTH, *Bell Telephone Laboratories.*

Ferromagnetic Impurities in Solids. F. W. CONSTANT, *Duke University.*

Magnetization of Gold-Iron and Gold-Nickel Alloys. A. R. KAUFMANN, S. T. PAN, AND J. R. CLARK, *Massachusetts Institute of Technology.*

A Recording Fluxmeter of High Accuracy and Sensitivity. P. P. CIOFFI, *Bell Telephone Laboratories.*

ADDITIONAL INVITED PAPERS

Double Bragg Reflections in a Single Crystal. C. J. DAVISSON AND F. E. HAWORTH, *Bell Telephone Laboratories.*

Catalysis: A Challenge to the Physicist. O. BEECK, *Shell Development Company.*

ABSTRACTS OF CONTRIBUTED PAPERS

D1. Metallurgical Transformations in Metal Surfaces under Conditions of Boundary Lubrication. B. W. SAKMANN, *Massachusetts Institute of Technology.*—The surfaces of steel flats run-in on rotating cast-iron disks under lubricated conditions may show metallurgical transformations. The transformed material is considerably harder than the underlying steel and protrudes over initially smooth surfaces by several microns. The experiments which were made with the aim of identifying the nature of the transformations include etching tests, microhardness tests, x-ray diffraction pictures, different heat treatments of the transformations, and inspection of the microstructure of the transformed material and the transition region between the transformation and the bulk material of the steel. The results of some of the tests seem to indicate that one is dealing with a carbide rich phase. From the value of the friction force on the stationary flat and the linear velocity of the rotating disk it is possible to determine the heat produced during the running-in process. Heat conductivity calculations give an estimate of the temperature reached. The effect of different heat treatments on the etching characteristics of the transition region between transformed material and bulk steel confirms this estimate of the temperature.

D2. The Mechanics of the Metal Cutting Process. III. Plasticity Conditions in Oblique Cutting. M. EUGENE MERCHANT, *Cincinnati Milling Machine Company.*—Plasticity conditions have been investigated for the process of oblique cutting, which process was previously defined and analyzed in Part II of this series. The same simple case has been considered as that which yielded such a good approximation to experiment in the case of simple (orthogonal) cutting, described in Part I of this series—namely, the assumption that the shear strength of the material being cut is a function of the normal stress acting on the plane of shear. The application of the principle of minimum energy then results in a very simple major plasticity condition for the case of oblique cutting, also, namely, $2\phi'+\sigma'=C$, where ϕ' and σ' are angles defining the geometry of the process of chip formation and its accompanying force

system, and C is a constant derivable from the relationship found between shear strength and normal stress for the particular material being cut. This relationship is found to be in good agreement with experiment.

D3. Resistance of Carbon to Carbon Contact. W. B. PIETENPOL AND F. C. WALZ, *University of Colorado.*—The contact resistance of plane carbon surfaces was measured at constant temperature over a pressure range of 78.88 to 31803.6 grams per sq. cm. A potentiometer method was used with current approximately 0.1 ampere. Corrections were made for the resistance of solid carbon and resistances were measured to four significant figures with pressures determined to 0.1 gram per sq. cm. After pressures are increased the contact resistances decrease with time and at low pressures do not reach equilibrium values until approximately 24 hours have elapsed. When pressures are decreased contact resistances increase with smaller time lags. The equilibrium contact resistance-pressure curves are in good agreement with the theory summarized by Windred* where the values are expressed by the equation $R=k/P^n$ and the constants differ for increasing and decreasing pressures.

* G. Windred, J. Frank. Inst. 231, 547 (1941).

D4. Low Angle Scattering of X-Rays. M. H. JELLINEK, *M. W. Kellogg Company* AND I. FANKUCHEN, *Polytechnic Institute of Brooklyn.*—Recently there has been increased interest in the low angle scattering of x-rays. All studies to date have used photographic methods for recording the scattered radiation. Where discrete maxima, whose location is to be determined, are concerned, this is no handicap but for some studies a continuous scattering must be studied over an intensity range of over 1000 to 1. We have used a Geiger counter and amplifier to measure this sort of low angle scattering. The intensities available are easily within the range of this instrument.

D5. Low Angle X-Ray Scattering. I. FANKUCHEN, *Polytechnic Institute of Brooklyn* AND M. H. JELLINEK, *M. W. Kellogg Company.*—In published work on low angle scattering, use has always been made of sharply defined beams of essentially monochromatic x-rays and long specimen-to-film distances. We have tried another entirely different method which seems to hold some promise. This utilizes two good single crystals, one as a monochromator and the other as an analyzer. The specimen is placed between the two crystals and a Geiger counter circuit is used to record the x-ray intensity as a function of the setting of the analyzing crystal. We have used the second crystal in the anti-parallel position and later as suggested to us by Dr. H. Friedman* in the parallel position.

* Naval Research Laboratory, Anacostia Station.

D6. Molecular Theory of the Scattering of Light in Fluids. BRUNO H. ZIMM, *Columbia University (Introduced by M. Goeppert-Mayer).*—A direct molecular theory of the scattering of light by fluids of isotropic molecules is developed utilizing recent advances in the statistical mechanics of condensed phases. The extent of the interference between the wave trains scattered from different molecules of the fluid is calculated with the aid of spatial molecular distribution functions. The integrals of these functions which are encountered are simply related to the concentration and volume derivatives of the free energy. The results are the same in first approximation as those of the continuous theory based on fluctuations originally proposed by Smoluchowski and Einstein. Higher approximations of the molecular theory are especially suitable for the study of critical opalescence and scattering by fluids consisting of very large molecules.

D7. The Continuum at the Mercury Arc Cathode. CHARLES G. SMITH. *Raytheon Manufacturing Company, Newton, Massachusetts.**—Micro-photographs of the arc spot on a quiescent mercury surface were secured by employing an arc gliding lengthwise over a long bead of mercury held between magnetic poles in a vacuum. The arc moved in the characteristic retrograde direction. The motion of the generated vapor being opposite to that of the arc, and the rapid progress of the cathode spot, prevented both the moving vapor and the arc pressure from disturbing the surface. The photographs show a well delineated source of light in the mercury surface or within 0.0005 cm of it, the intensity of which greatly exceeds that anywhere in the plasma. The continuous spectrum originates only at the cathode and doubtless comes from within the liquid from the electronically excited region that gives rise to the electron emission of the apparently cool mercury in accordance with the author's emission theory[1] of the mercury arc.

* Experiments performed at Harvard University.
[1] C. G. Smith, Phys. Rev. 62, 48 (1942).

D8. Motion of Electrolytes in a Magnetic Field. CLIFFORD E. SWARTZ, *University of Rochester (Introduced by W. van der Grinten).*—Investigation of the rotation of certain electrolytes ($FeCl_3$, HCl, $SnCl_2$) between and in contact with magnetic poles, has been carried out with many variations on the original Ehrenhaft experiments.[1] These variations do not differ fundamentally from the original experiments because the rotation and sense of rotation are unaffected by some inhomogeneity of the field. Ferromagnetic substances need not be used; the rotation is dependent on a chemical reaction. These rotations can be explained by assuming potential differences throughout the solution caused by the presence of the metal. This assumption has been verified by means of a special potentiometer and probe arrangement.

[1] F. Ehrenhaft, Bull. Am. Phys. Soc. 19, 3, 10 (June 23, 1944).

D9. The Measurement of Single Magnetic Charges and the Electrostatic Field around the Permanent Magnet. FELIX EHRENHAFT, *New York City.*—It has been observed in the microscopic dark field that in a magnetic condenser with horizontal homogeneous field established by an Alnico 5 permanent magnet test bodies of various substances fall vertically and undeflected in gases, or are deflected at various measurable angles to either condenser plate, their paths crossing the center line. Observing these falling

bodies, the north or south magnetic charge of a single test body can be measured, applying the method of the author[1] in determining the positive or negative electric charge on a single particle. Applying a horizontal inhomogeneous axially symmetrical magnetic field, it has been observed that the force of charge qH exceeds the force of polarization so that even diamagnetic particles (e.g., Sb, Cu, C) move to the denser lines of force. A new fact added to past experience[2] is that the general path of a body bearing simultaneously electric and magnetic charges is a helix (spiral) in the constant field of a permanent magnet. The region of observation is shielded electrostatically. The electric field is created by the permanent magnet. Electricity and magnetism are aspects of a single phenomenon. Demonstrations will be provided at Manhattan College, New York City.

[1] F. Ehrenhaft, Anz. d. Wien. Akad. d. Wiss. No. VII (Mar. 4, 1909)
[2] F. Ehrenhaft, Nature 154, 426 (1944); Phys. Rev. 65, 287 (1944).

D10. Theoretical Implications of the Magnetic Current. GABRIEL KANE, *Manhattan College.*—The symmetrical form of Maxwell's field equations containing terms with magnetic charge and magnetic current is already in the literature.[1] The wave equations for electromagnetic waves traveling in a conducting medium may be deduced from these field equations. It is found that such wave equations contain terms in E and H in addition to the usual first and second derivatives of E and H with respect to time. The theoretical necessity of a magnetic current can be demonstrated by a process of reasoning similar to that which led Maxwell to the hypothesis of a displacement current. The nature of the magnetostatic potential will be discussed and the essential differences between the field of a permanent magnet and that of a steady current indicated.[2] The influence of magnetic current and magnetic charge on the concepts of the vector potential and the Hertzian vector will be considered.

[1] Page and Adams, *Electrodynamics* (D. Van Nostrand Company, New York, 1940), p. 160.
[2] Abraham and Becker, *Classical Electricity and Magnetism* (Blackie & Sons, London, 1943), p. 131.

D11. The Action of a Magnetic Field on Ferric Hydroxide. CHARLES B. REYNOLDS, *Hearst Radio, Inc., New York.*—A solution of ferric hydroxide was prepared for study of its action under the influence of a magnetic field. Upon application of a magnetic field the solution was observed to clear, a deposit appearing on the north pole of the electromagnet. The action was immediate and violent. It was found that reversal of the field reversed the deposit and that reversal could be accomplished three or four times. The composition of the deposit will be discussed. It was noted that the action was a function of the amount and concentration of the base used to form the hydroxide,[1] the nature of the base as well as the nature of the iron salt from which the hydroxide was precipitated.[2] It further appears that the ferric hydroxide is ferromagnetic since the action is also a function of magnetic field intensity.[3] The foregoing seems to offer some support to Ehrenhaft's claims as to the polar nature of magnetism.[4]

[1] R. Chevallier and S. Mathieu, Comptes rendus 206, 1469, 1955 (1938).
[2] A. Quartaroli, Gazz. Chim. Ital. 64, 161 (1934).
[3] P. Selwood, *Magnetochemistry* (Interscience Publishers, Inc., New York, 1943), p. 226.
[4] F. Ehrenhaft, Phys. Rev. 65, 287 (1944).

E1. The Application of Network Analysis to Some Electron Optical Problems. ALBERT F. PREBUS AND IGNACE ZLOTOWSKI, *Ohio State University and* GABRIEL KRON, *General Electric Company.*—By suitable correlation of the variables, the trajectory equation

$$\phi(z)\cdot\frac{d^2r}{dz^2}+\tfrac{1}{2}\phi'(z)\cdot\frac{dr}{dz}+\tfrac{1}{4}\left[\phi''(z)+\frac{e}{2mc^2}H^2(z)\right]\cdot r=0$$

of an electron lens may be identified with the differential equation describing the dependence of the voltage distribution upon the impedance characteristics of a simple type of ideal inhomogeneous transmission line. By choosing the specific impedances as functions of the independent variable z [distance along the axis of symmetry] and the parameters $H(z)$ and $\phi(z)$ [z component of the magnetic field and electrostatic potential, respectively, on the axis], the values of the dependent variable $r(z)$ [radial displacement of the electron] correspond to voltages along the line. The equivalent network provides a rapid means of obtaining accurate numerical solutions of the trajectory equation. Application of this method is demonstrated for the case of a strong magnetic lens by comparing the results with the exact solutions given by Glaser.[1] The usefulness of a two-dimensional network for determining the electrode configuration of an electrostatic lens from a given axial potential distribution is discussed.

[1] W. Glaser, Zeits. f. Physik. 117, 285 (1941).

E2. Capture Cross Section of Hydrogen for Slow Neutrons. LEROY G. SCHULZ* AND M. GOLDHABER, *University of Illinois.*—The capture cross section of hydrogen for slow neutrons is of great theoretical interest. The most accurate experimental method for its determination is probably that devised by Frisch, v. Halban, and Koch,[1] who determined this cross section by measuring the ratio of the capture cross section of boron to that of hydrogen. As later measurements made by various other methods did not agree well with their result, it seemed worth while to repeat their experiment with some modifications and increased accuracy. We find for the ratio of the capture cross section of B to that of H the value 1954 ± 24, in good agreement with the value 1940 ± 100, obtained by Frisch, v. Halban, and Koch. If we assume for B a capture cross section of 600×10^{-24} cm^2 we obtain for H a capture cross section of 0.307×10^{-24} cm^2, which should be compared with the theoretical value of 0.302×10^{-24} cm^2 given by Rarita and Schwinger.[2]

* Now at the Haskins Laboratories, New York, New York.
[1] O. R. Frisch, H. v. Halban, and J. Koch, Proc. Danish Acad. 15, 10 (1938).
[2] W. Rarita and J. Schwinger, Phys. Rev. 59, 436 (1941).

E3. Evidence for the Production of a Non-Ionizing Radiation other than Neutrons and Gamma-Rays by 10-Mev Deuterons. GERHART GROETZINGER, P. GERALD KRUGER, AND LLOYD SMITH, *University of Illinois.*—An arrangement of two Geiger-Mueller counters in coincidence shielded by various thicknesses of lead up to 19-cm thickness has been used to investigate non-ionizing radiations produced by a cyclotron. The cyclotron was enclosed by watertanks of 120-cm thickness. Electrons have been

found of energies greater than 5 Mev; their number as a function of the lead thickness indicates that they are produced by a radiation far more penetrating than gamma-rays. The water in the tanks close to the counters was later saturated with boric acid and the leadhouse surrounded by enough cadmium and paraffin to eliminate a large fraction of both fast and slow neutrons, which might have penetrated the watertanks. No appreciable effect on the counting rate was noticed. Various external targets (P, Mn, Sb, and W) were used in the cyclotron. A slight dependence of the number of counts on the target material was observed.

E4. *K* to *L* Conversion Ratio. I. S. LOWEN, *New York University*.—The relative proportions of electric and magnetic-multipole radiation occurring in nuclear transitions may be determined with the aid of the K to L conversion ratio and the absolute values of the internal conversion coefficients.[1,2] Theoretical calculations which have served as the basis for such evaluations have been presented in the case of light nuclei ($Z<50$) for two circumstances: (*a*) for the electric multipole case using Schrodinger non-relativistic theory, (*b*) for the magnetic multipole case such that the binding energy of the ejected electron may be neglected.[1,3] For those energies such that the assumption of negligible binding energy is not a good one, it is desirable to have estimates for the K to L ratio for magnetic multipole radiation valid over the same range of energies as (*a*). Such estimates have been obtained for nuclei with $Z<50$ with the aid of the Pauli theory and will be presented in the form of curves suited for the estimation of relative proportions of magnetic and electric multipole radiation in those cases where the binding energy of the electron may not be neglected.

[1] Hebb and Nelson, Phys. Rev. **58**, 486 (1940).
[2] A. C. Helmholz, Phys. Rev. **60**, 415 (1941).
[3] Dancoff and Morrison, Phys. Rev. **55**, 122 (1939).

E5. Magnetic Multipole Conversion for *K* Electrons. G. GOERTZEL AND I. S. LOWEN, *New York University*.—Formulae for internal conversion coefficients for K electrons in light nuclei have been derived for two different approximations: (*a*) Non-relativistic using Schrodinger hydrogen-like wave functions;[1,2] (*b*) relativistic but restricted to low binding energies.[2] In approximation (*a*), where the spin of the electron is neglected, the magnetic multipole conversion vanishes as a consequence of the parity selection rules.[2] However, when the electron spin is taken into account through the use of the Pauli theory, the interaction of the magnetic moment of the electron with the magnetic field of the radiation leads to a finite non-vanishing conversion coefficient for 2^l magnetic multipole radiation given by

$$\beta_{K^l}=\frac{l}{2l+1}\left(\frac{\nu}{2}\right)^2\left[\frac{l+1}{l-1}\alpha_{K^{l-1}}+\frac{l+2}{l+1}\alpha_{K^{l+1}}\right]$$

where α_{K^l} is the 2^l electric multipole coefficient (non-relativistic)[2] and ν is the γ-ray energy in units of mc^2. This result is restricted to elements with $Z<50$ and γ-ray energies not greater than about 3×10^6 volts.

[1] M. H. Hebb and G. E. Uhlenbeck, Physica **5**, 605 (1938).
[2] S. M. Dancoff and P. Morrison, Phys. Rev. **55**, 122 (1939).

E6. Charge Neutralization by Atmospheric Ions. W. G. POLLARD, *University of Tennessee*.*—The neutralization of an insulated, charged, conducting object immersed in a neutral ion atmosphere in which the mobilities of both ions are constant and independent of the field is considered. The object becomes surrounded by an opposite ion sheath whose volume increases exponentially with time to a limiting value just sufficient to have contained a charge at the original plasma density equal and opposite to that initially carried by the object. The total charge in the sheath increases to a maximum and then drops to zero. The sum of the sheath and object charges decays exponentially but individually they are more complex functions of time. In the plasma the density of both kinds of ion remains constant at its initial value and the field is that which would be produced by the object if it carried the sheath charge in addition to its own. A general solution for the field and charge density in the sheath as functions of position and time which join continuously with the plasma values over the moving sheath boundary is obtained. The character of this solution will be discussed at the meeting.

* This work was done for The Chicopee Manufacturing Corporation, Chicopee Falls, Massachusetts.

T1. Computation of Electron Trajectories in Electrostatic Lenses of Rotational and Plane Symmetry. IGNACE ZLOTOWSKI AND ALBERT F. PREBUS, *Ohio State University*.—Network analysis is applied to the specification of the cardinal points of electrostatic lenses. The advantages of this method of numerical integration of the lens trajectory equation are shown by comparing it with other methods currently in use. The requisite axial potential distributions of the lenses are obtained from accurate electrolytic trough measurements. Data of practical value are provided which show the dependence of optical properties on electrode parameters of some familiar types of electrostatic lenses. The inverse problem of determining the axial potential distributions corresponding to a given trajectory is investigated.

T2. Loss of Weight by Rotation. CHARLES T. DOZIER, *San Diego*.—From consideration of the earth as an astronomical body with sidereal period of rotation about its polar axis, the weight of a mass at rest on the earth's equator is the resultant of the full gravitational attractive force between mass and earth diminished by the centrifugal force acting on the mass. If the mass has horizontal translation along the equator, the gravitational attractive force, so far as is known, will remain constant, but the centrifugal force acting on the mass will increase during easterly and decrease during westerly translation. A forty-thousand-pound airplane in level flight at three hundred miles per hour along the equator near sea level is 160 pounds lighter in easterly than in westerly flight. Now consider a mass rotating about a vertical axis through its center, fixed in longitude and altitude. The easterly-moving half of the mass loses weight and simultaneously the westerly-moving half gains in weight, within limits, but the loss exceeds the gain, without limits. The net loss in

weight is proportional to the square of the angular velocity of rotation of the mass about its axis. Appropriate factors are introduced for other latitudes and altitudes.

T3. Gravitational Ground Speed Indicator. CHARLES T. DOZIER, *San Diego.*—Reference is made to the current abstract, "Loss of weight by rotation," by this author. The effect of torque developed by the difference in weight of the easterly- and westerly-moving halves of a mass rotating about a vertical axis through its center and mounted in an airplane is found to be proportional to the east-west component of level flight ground speed of the plane. The mass rotates at constant angular velocity. Two such masses rotating in opposite directions are connected by linkage in such a manner as to indicate the torque and thus the east-west component of ground speed directly on a calibrated scale. Latitude and altitude factors are introduced. The full ground speed of the plane is derived by vector methods from this component and the known direction of flight. Patent rights are assigned by the author to Consolidated Vultee Aircraft Corporation, San Diego, California.